

1 Impact of PØD NuMu Samples in BANFF

2 Hogan, Matthew¹ and Toki, Walter¹

3 June 9, 2019

4 ¹Colorado State University, Fort Collins, USA

5 **Abstract**

6 This is the abstract

7 **Contents**

8	1	Introduction	10
9	1.1	ND280	10
10	1.1.1	The PØD	11
11	1.2	Usage of ND280 Psyche Software	12
12	2	ND280 Binned Likelihood	14
13	2.1	Motivation	14
14	2.2	Introduction to Conditional PDFs and Likelihoods	15
15	2.3	BANFF Fit Test Statistic	16
16	2.3.1	Flux, Cross Section, and Detector Systematics	20
17	3	PØD Selections and Data Samples	23
18	3.1	Global Reconstruction	23
19	3.2	PØD Selection Cuts	25
20	3.2.1	Pre-Selection Cuts	25
21	3.2.2	ν_μ CC Inclusive in FHC Cut	27
22	3.2.3	$\bar{\nu}_\mu$ CC Inclusive in RHC Cuts	27
23	3.2.4	ν_μ Background CC Inclusive in RHC Cuts	29
24	3.3	Sample Kinematics and Validation	29
25	3.4	PØD Water-Out Samples	30
26	3.4.1	CC Inclusive	31
27	3.4.1.1	ν_μ Selection in FHC Mode:	31
28	3.4.1.2	$\bar{\nu}_\mu$ Selection in RHC Mode:	38
29	3.4.1.3	ν_μ Background Selection in RHC Mode:	45
30	3.4.2	CC 1-Track (CCQE Enhanced)	52

31	3.4.2.1	ν_μ Selection in FHC Mode:	52
32	3.4.2.2	$\bar{\nu}_\mu$ Selection in RHC Mode:	59
33	3.4.2.3	ν_μ Background Selection in RHC Mode:	66
34	3.4.3	CC N-Tracks (CCnQE Enhanced)	66
35	3.4.3.1	ν_μ Selection in FHC Mode:	66
36	3.4.3.2	$\bar{\nu}_\mu$ Selection in RHC Mode:	73
37	3.4.3.3	ν_μ Background Selection in RHC Mode:	80
38	3.5	PØD Water-In Samples	80
39	3.5.1	CC Inclusive	81
40	3.5.1.1	ν_μ Selection in FHC Mode:	81
41	3.5.1.2	$\bar{\nu}_\mu$ Selection in RHC Mode:	88
42	3.5.1.3	ν_μ Background Selection in RHC Mode:	95
43	3.5.2	CC 1-Track (CCQE Enhanced)	95
44	3.5.2.1	ν_μ Selection in FHC Mode:	95
45	3.5.2.2	$\bar{\nu}_\mu$ Selection in RHC Mode:	102
46	3.5.2.3	ν_μ Background Selection in RHC Mode:	109
47	3.5.3	CC N-Tracks (CCnQE Enhanced)	109
48	3.5.3.1	ν_μ Selection in FHC Mode:	109
49	3.5.3.2	$\bar{\nu}_\mu$ Selection in RHC Mode:	110
50	3.5.3.3	ν_μ Background Selection in RHC Mode:	110
51	3.5.4	Differences Between Water-Out and Water-In Samples	110
52	4	PØD-Only BANFF Parameterization	111
53	4.1	PØD Samples Fit Binning	111
54	4.1.1	Fit Binning Determination	112
55	5	Detector Systematics	115

56	6 Fitter Validation	116
57	7 Fitter Results	117
58	8 Discussion	118
59	References	119
60	Nomenclature	121

61 **List of Figures**

62 1.1	Exploded view of the off-axis detectors of ND280	10
63 1.2	Cartoon of the PØD	11
64 1.3	Cartoon of an Individual PØDule	12
65 1.4	Fluxing Tuning Histogram for FHC Events	13
66 2.1	BANFF Pre-fit Flux Covariance Matrix	20
67 2.2	BANFF ND280 NuMu and ANuMu Flux Binning Parameters	21
68 2.3	Cross Section Parameters Pre-fit Correlation Matrix	21
69 3.1	PØD Air FHC ν_μ CC Inc. Lepton Cand. Reco. Momentum by True Particle	32
70 3.2	PØD Air FHC ν_μ CC Inc. Lepton Cand. Reco. $\cos\theta$ by True Particle . . .	33
71 3.3	PØD Air FHC ν_μ CC Inc. Lepton Cand. Reco. Momentum by NEUT Mode	34
72 3.4	PØD Air FHC ν_μ CC Inc. Lepton Cand. Reco. $\cos\theta$ by NEUT Mode . . .	35
73 3.5	PØD Air FHC ν_μ CC Inc. Lepton Cand. Reco. Momentum by True Topology	36
74 3.6	PØD Air FHC ν_μ CC Inc. Lepton Cand. Reco. $\cos\theta$ by True Topology . . .	37
75 3.7	PØD Air FHC ν_μ CC Inc. Lepton Cand. True E_ν by NEUT Mode	38
76 3.8	PØD Air RHC $\bar{\nu}_\mu$ CC Inc. Lepton Cand. Reco. Momentum by True Particle	39
77 3.9	PØD Air RHC $\bar{\nu}_\mu$ CC Inc. Lepton Cand. Reco. $\cos\theta$ by True Particle . . .	40
78 3.10	PØD Air RHC $\bar{\nu}_\mu$ CC Inc. Lepton Cand. Reco. Momentum by NEUT Mode	41
79 3.11	PØD Air RHC $\bar{\nu}_\mu$ CC Inc. Lepton Cand. Reco. $\cos\theta$ by NEUT Mode . . .	42
80 3.12	PØD Air RHC $\bar{\nu}_\mu$ CC Inc. Lepton Cand. Reco. Momentum by True Topology	43
81 3.13	PØD Air RHC $\bar{\nu}_\mu$ CC Inc. Lepton Cand. Reco. $\cos\theta$ by True Topology . . .	44
82 3.14	PØD Air FHC $\bar{\nu}_\mu$ CC Inc. Lepton Cand. True E_ν by NEUT Mode	45
83 3.15	PØD Air RHC ν_μ CC Inc. Lepton Cand. Reco. Momentum by True Particle	46
84 3.16	PØD Air RHC ν_μ CC Inc. Lepton Cand. Reco. $\cos\theta$ by True Particle . . .	47
85 3.17	PØD Air FHC ν_μ CC Inc. Lepton Cand. Reco. Momentum by NEUT Mode	48

86	3.18 PØD Air FHC ν_μ CC Inc. Lepton Cand. Reco. $\cos\theta$ by NEUT Mode	49
87	3.19 PØD Air FHC ν_μ CC Inc. Lepton Cand. Reco. Momentum by True Topology	50
88	3.20 PØD Air FHC ν_μ CC Inc. Lepton Cand. Reco. $\cos\theta$ by True Topology	51
89	3.21 PØD Air FHC ν_μ CC Inc. Lepton Cand. True E_ν by NEUT Mode	52
90	3.22 PØD Air FHC ν_μ CC Inc. Lepton Cand. Reco. Momentum by True Particle	53
91	3.23 PØD Air FHC ν_μ CC Inc. Lepton Cand. Reco. $\cos\theta$ by True Particle	54
92	3.24 PØD Air FHC ν_μ CC Inc. Lepton Cand. Reco. Momentum by NEUT Mode	55
93	3.25 PØD Air FHC ν_μ CC Inc. Lepton Cand. Reco. $\cos\theta$ by NEUT Mode	56
94	3.26 PØD Air FHC ν_μ CC Inc. Lepton Cand. Reco. Momentum by True Topology	57
95	3.27 PØD Air FHC ν_μ CC Inc. Lepton Cand. Reco. $\cos\theta$ by True Topology	58
96	3.28 PØD Air FHC ν_μ CC Inc. Lepton Cand. True E_ν by NEUT Mode	59
97	3.29 PØD Air RHC $\bar{\nu}_\mu$ CC Inc. Lepton Cand. Reco. Momentum by True Particle	60
98	3.30 PØD Air RHC $\bar{\nu}_\mu$ CC Inc. Lepton Cand. Reco. $\cos\theta$ by True Particle	61
99	3.31 PØD Air RHC $\bar{\nu}_\mu$ CC Inc. Lepton Cand. Reco. Momentum by NEUT Mode	62
100	3.32 PØD Air RHC $\bar{\nu}_\mu$ CC Inc. Lepton Cand. Reco. $\cos\theta$ by NEUT Mode	63
101	3.33 PØD Air RHC $\bar{\nu}_\mu$ CC Inc. Lepton Cand. Reco. Momentum by True Topology	64
102	3.34 PØD Air RHC $\bar{\nu}_\mu$ CC Inc. Lepton Cand. Reco. $\cos\theta$ by True Topology	65
103	3.35 PØD Air FHC $\bar{\nu}_\mu$ CC Inc. Lepton Cand. True E_ν by NEUT Mode	66
104	3.36 PØD Air FHC ν_μ CC N-Tracks Lepton Cand. Reco. Momentum by True Particle	67
105		
106	3.37 PØD Air FHC ν_μ CC N-Tracks Lepton Cand. Reco. $\cos\theta$ by True Particle	68
107	3.38 PØD Air FHC ν_μ CC N-Tracks Lepton Cand. Reco. Momentum by NEUT Mode	69
108		
109	3.39 PØD Air FHC ν_μ CC N-Tracks Lepton Cand. Reco. $\cos\theta$ by NEUT Mode	70
110	3.40 PØD Air FHC ν_μ CC N-Tracks Lepton Cand. Reco. Momentum by True Topology	71
111		

112	3.41 PØD Air FHC ν_μ CC N-Tracks Lepton Cand. Reco. $\cos\theta$ by True Topology	72
113	3.42 PØD Air FHC ν_μ CC N-Tracks Lepton Cand. True E_ν by NEUT Mode . . .	73
114	3.43 PØD Air RHC $\bar{\nu}_\mu$ CC N-Tracks Lepton Cand. Reco. Momentum by True	
115	Particle	74
116	3.44 PØD Air RHC $\bar{\nu}_\mu$ CC N-Tracks Lepton Cand. Reco. $\cos\theta$ by True Particle .	75
117	3.45 PØD Air RHC $\bar{\nu}_\mu$ CC N-Tracks Lepton Cand. Reco. Momentum by NEUT	
118	Mode	76
119	3.46 PØD Air RHC $\bar{\nu}_\mu$ CC N-Tracks Lepton Cand. Reco. $\cos\theta$ by NEUT Mode .	77
120	3.47 PØD Air RHC $\bar{\nu}_\mu$ CC N-Tracks Lepton Cand. Reco. Momentum by True	
121	Topology	78
122	3.48 PØD Air RHC $\bar{\nu}_\mu$ CC N-Tracks Lepton Cand. Reco. $\cos\theta$ by True Topology	79
123	3.49 PØD Air FHC $\bar{\nu}_\mu$ CC N-Tracks Lepton Cand. True E_ν by NEUT Mode . .	80
124	3.50 PØD Water FHC ν_μ CC Inc. Lepton Cand. Reco. Momentum by True Particle	82
125	3.51 PØD Water FHC ν_μ CC Inc. Lepton Cand. Reco. $\cos\theta$ by True Particle .	83
126	3.52 PØD Water FHC ν_μ CC Inc. Lepton Cand. Reco. Momentum by NEUT Mode	84
127	3.53 PØD Water FHC ν_μ CC Inc. Lepton Cand. Reco. $\cos\theta$ by NEUT Mode .	85
128	3.54 PØD Water FHC ν_μ CC Inc. Lepton Cand. Reco. Momentum by True Topology	86
129	3.55 PØD Water FHC ν_μ CC Inc. Lepton Cand. Reco. $\cos\theta$ by True Topology .	87
130	3.56 PØD Water FHC ν_μ CC Inc. Lepton Cand. True E_ν by NEUT Mode . . .	88
131	3.57 PØD Water RHC $\bar{\nu}_\mu$ CC Inc. Lepton Cand. Reco. Momentum by True Particle	89
132	3.58 PØD Water RHC $\bar{\nu}_\mu$ CC Inc. Lepton Cand. Reco. $\cos\theta$ by True Particle .	90
133	3.59 PØD Water RHC $\bar{\nu}_\mu$ CC Inc. Lepton Cand. Reco. Momentum by NEUT Mode	91
134	3.60 PØD Water RHC $\bar{\nu}_\mu$ CC Inc. Lepton Cand. Reco. $\cos\theta$ by NEUT Mode .	92
135	3.61 PØD Water RHC $\bar{\nu}_\mu$ CC Inc. Lepton Cand. Reco. Momentum by True	
136	Topology	93
137	3.62 PØD Water RHC $\bar{\nu}_\mu$ CC Inc. Lepton Cand. Reco. $\cos\theta$ by True Topology .	94

138	3.63 PØD Water FHC $\bar{\nu}_\mu$ CC Inc. Lepton Cand. True E_ν by NEUT Mode	95
139	3.64 PØD Water FHC ν_μ CC 1-Track Lepton Cand. Reco. Momentum by True	
140	Particle	96
141	3.65 PØD Water FHC ν_μ CC 1-Track Lepton Cand. Reco. $\cos\theta$ by True Particle	97
142	3.66 PØD Water FHC ν_μ CC 1-Track Lepton Cand. Reco. Momentum by NEUT	
143	Mode	98
144	3.67 PØD Water FHC ν_μ CC 1-Track Lepton Cand. Reco. $\cos\theta$ by NEUT Mode	99
145	3.68 PØD Water FHC ν_μ CC 1-Track Lepton Cand. Reco. Momentum by True	
146	Topology	100
147	3.69 PØD Water FHC ν_μ CC 1-Track Lepton Cand. Reco. $\cos\theta$ by True Topology	101
148	3.70 PØD Water FHC ν_μ CC 1-Track Lepton Cand. True E_ν by NEUT Mode . .	102
149	3.71 PØD Water RHC $\bar{\nu}_\mu$ CC Inc. Lepton Cand. Reco. Momentum by True Particle	103
150	3.72 PØD Water RHC $\bar{\nu}_\mu$ CC Inc. Lepton Cand. Reco. $\cos\theta$ by True Particle . .	104
151	3.73 PØD Water RHC $\bar{\nu}_\mu$ CC Inc. Lepton Cand. Reco. Momentum by NEUT Mode	105
152	3.74 PØD Water RHC $\bar{\nu}_\mu$ CC Inc. Lepton Cand. Reco. $\cos\theta$ by NEUT Mode . .	106
153	3.75 PØD Water RHC $\bar{\nu}_\mu$ CC Inc. Lepton Cand. Reco. Momentum by True	
154	Topology	107
155	3.76 PØD Water RHC $\bar{\nu}_\mu$ CC Inc. Lepton Cand. Reco. $\cos\theta$ by True Topology .	108
156	3.77 PØD Water FHC $\bar{\nu}_\mu$ CC Inc. Lepton Cand. True E_ν by NEUT Mode	109
157	4.1 PØD Momenta Resolutions Used for Fit Binning	113
158	4.2 PØD Angular Residuals Used for Fit Binning	114

159 **List of Tables**

160 3.1 PØD WT FV and Corridor Definition	27
161 3.2 POT Used in This Analysis	30

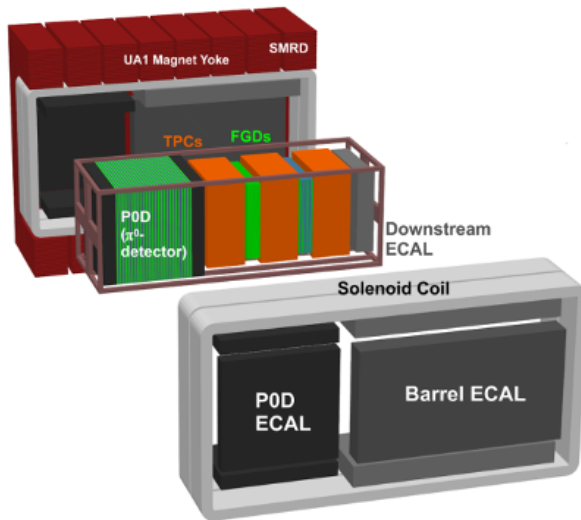


Figure 1.1: Exploded view of the off-axis detectors of ND280. The neutrino beam is directed from left to right along the figure.

162 1 Introduction

163 The primary goal of an oscillation experiment is to measure the parameters in a neutrino
 164 mixing matrix. All other parameters, with some having some theoretical importance to
 165 fundamental physics, are nuisance parameters. To understand the methodology of Beam
 166 and Near detector Flux task Force (BANFF) fit, it is relevant to understand how likelihood
 167 fitting works.

168 1.1 ND280

169 The T2K near detector (ND) complex consists of on-axis and off-axis detectors at 280m away
 170 from the secondary beamline proton target. The off-axis detector is used in this analysis
 171 which consists of several subdetectors housed inside the UA1/NOMAD magnet yoke as
 172 shown in figure 1.1. A similar analysis was also performed with the on-axis detector and is
 173 available in T2K-TN-335[13]. . The magnet provides a 0.2T magnetic field which is designed
 174 to provide momentum and particle identification for the tracker region.

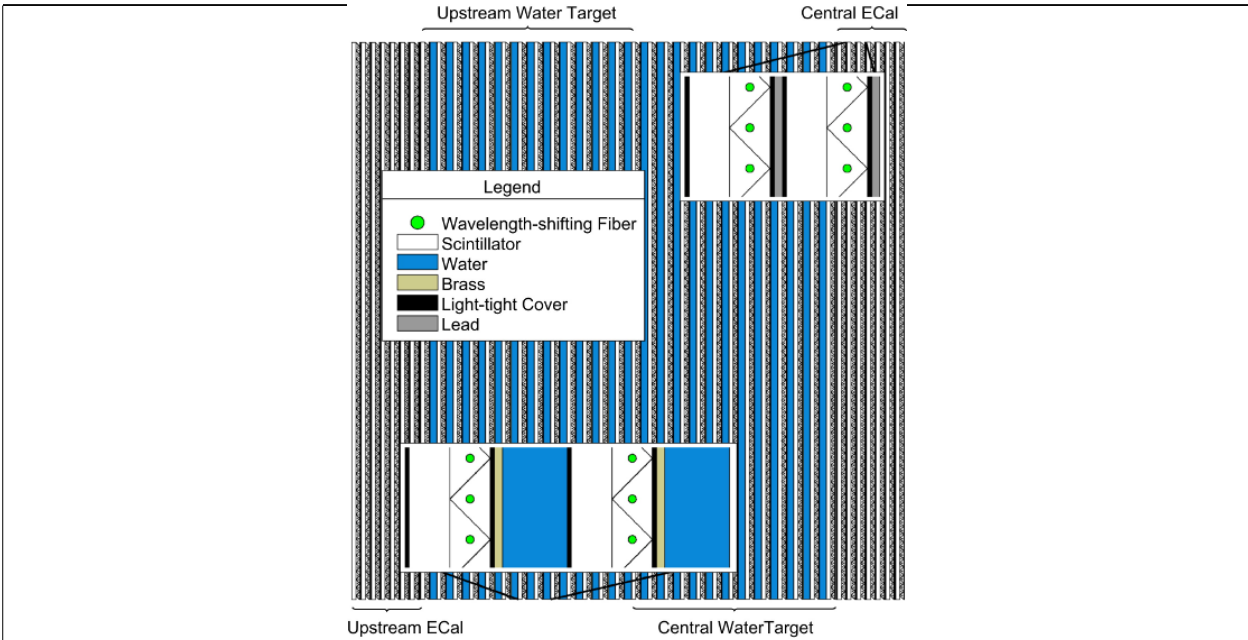


Figure 1.2: This cartoon illustrates the concept design of the PØD where the neutrino beam is approaching from the left.

¹⁷⁵ 1.1.1 The PØD

¹⁷⁶ The PØD, short for π^0 Detector, is a plastic scintillator based tracking calorimeter inside the
¹⁷⁷ ND280 basket. The PØD is constructed as many sandwiches of active and inactive materials
¹⁷⁸ designed to fully contain π^0 decay photons. The four primary regions inside the PØD in
¹⁷⁹ order of upstream to downstream of the neutrino beam are the upstream ECal (USECal),
¹⁸⁰ upstream water target (WT), central WT, and central ECal (CECal). A representation of
¹⁸¹ the entire PØD can be seen in Figure 1.2. Each active module, also called a PØDule, consists
¹⁸² of two orthogonally oriented sheets of triangular, scintillator-doped plastic bars as shown in

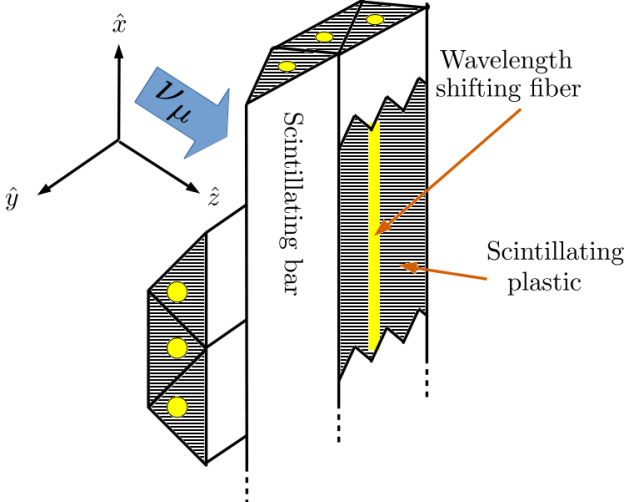


Figure 1.3: This cartoon illustrates the design of a PØDule with orthogonal layers of scintillating, triangular bars. When a charged particle travels through the bar such as a muon from CC interaction, the scintillation light is captured and wavelength shifted inside a fiber bored in the center of each bar. The wavelength shifted light is later observed by a photon counter.

183 Figure 1.3. The ECal regions are designed to contain decay photons inside the PØD by
 184 alternating the scintillator planes with lead sheets. The WT regions, as compared to the lead
 185 sheets in the ECals, alternate a thin brass sheet and water filled bags between the PØDules.
 186 A unique feature of the PØD is that the water can be drained out resulting in two detector
 187 configurations: water-in and water-out.

188 1.2 Usage of ND280 Psyche Software

189 Psyche is a general framework for data handling, event selections, and systematic evaluations
 190 with toy experiments. Psyche is a “lean” package from the perspective of analyzing MC
 191 events since that functionality is built heavily into Highland2. The analysis performed in
 192 this technical note required making additions to psyche in order replicate features available
 193 in Highland2. It would be wise for future analyses to build a selection in Highland2 and
 194 migrate that psyche once mature.

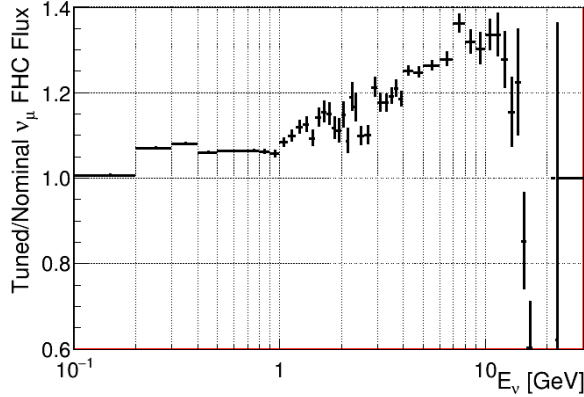


Figure 1.4: Fluxing tuning histogram for ν_μ FHC events taken from the 13av3 flux release.

BANFF uses a psyche package called psycheSteering that interfaces with all the psyche tools to manage the migration of samples into its analysis code. New PØD selections were added to the psycheSelections package and validated using the psycheSteering AnalysisManager class. The AnalysisManager provides the functionality to get the true and reconstructed detector observables from each reconstructed event along with the flux tuning and detector systematic weights.

Flux tuning is the process of applying an event weight based on the true neutrino energy, flavor, and run period. Since the ND280 MC uses a series of models to describe the expected neutrino flux, it cannot perfectly model the true flux nor know the beam conditions at run time. The beam group is responsible for releasing the expected and measured neutrino flux in order to account for these differences. To flux tune an event, the relevant neutrino flavor flux histogram must be referenced. The weight is extracted by taking the ratio of the tuned flux to the nominal flux in the MC for a given neutrino energy. As an example Figure 1.4 shows the flux tuning weights for true ν_μ FHC events.

209 **2 ND280 Binned Likelihood**

210 The BANFF likelihood maximization procedure is a binned likelihood maximization of the
211 ND280 data. In a ND280 and Super-Kamiokande (SK) joint fit, the measurements from both
212 detectors are considered along with their respective nuisance parameters. This approach
213 is more computationally expensive compared to the Markov Chain Monte Carlo analysis
214 (MaCh3) which will not be explained here. The BANFF likelihood maximization, hitherto
215 referred to as the “BANFF-fit”, includes nuisance parameters that affect the measurement of
216 the oscillation parameters, but are not physics goals of the T2K experiment. The BANFF-
217 fit parameters and their respective covariances are then used as inputs in the oscillation
218 analysis. This “divide-and-conquer” approach allows for more rapidly completed studies
219 on the effects of model parameters and biases present. Also this approach should provide
220 the same result with a joint ND280 and SK analysis as is performed in MaCh3. However,
221 information encoded in the ND280 measurements for shared nuisance parameters like the
222 neutrino flux is inevitably lost in the BANFF-fit.

223 The modern BANFF-fit likelihood is described in detail in TN-220[10]. It uses a fre-
224 quentist approach to find the best nuisance parameter set to maximize a binned likelihood.
225 Subsequent updates to the BANFF analysis[11, 4, 3] increase the sample sizes and systematic
226 parameterizations.

227 **2.1 Motivation**

228 Curve fitting is commonly found in the particle physics community literature due to the
229 need to compare two models or constrain unknown model parameters using one or more
230 histograms. For the first case, this involves two competing models, H_0 and H_1 , in order to
231 establish if the data supports new Physics (H_1) not predicted in the Standard Model (H_0).
232 The second case finds the “best” set of the model predictions, θ , that match the data as is the

233 case for the BANFF-fit. In both cases, chi-squared tests are performed to provide goodness
234 of fit, parameter estimation (also referred to as “best fit parameters”), and error/confidence
235 estimation.

236 2.2 Introduction to Conditional PDFs and Likelihoods

237 Consider the problem of extracting physics parameters \vec{y} given some data vector \vec{N} . The
238 conditional probability density function (PDF) \mathcal{P} to measure these parameters is given as

$$\mathcal{P}(\vec{y}|\vec{N}) = \frac{\mathcal{L}(\vec{N}|\vec{y})\mathcal{P}(\vec{y})}{\int \mathcal{L}(\vec{N}|\vec{x})\mathcal{P}(\vec{x})d\vec{x}}, \quad (2.1)$$

239 where anything right of a vertical line represents a condition on the probability, $\mathcal{L}(\vec{N}|\vec{y})$
240 is the likelihood of the model with parameters \vec{y} , $\mathcal{P}(\vec{y})$ is the probability for the model,
241 and the denominator is the normalization over all possible constraints on the observations.
242 A frequentist interpretation of a PDF is a proportion of outcomes of repeated trials or
243 experiments. A likelihood function is an expression of the probability of observing data as a
244 function of the model parameters in their appropriate ranges.

245 One arrives at (2.1) by using the definition of compound probabilities

$$\mathcal{P}(A, B) = \mathcal{P}(B|A)\mathcal{P}(A) \quad (2.2)$$

246 to evaluate $\mathcal{P}(\vec{y}|\vec{N})$ as

$$\mathcal{P}\left(\underbrace{\vec{y}}_B \middle| \underbrace{\vec{N}}_A\right) = \frac{\mathcal{P}(\vec{N}, \vec{y})}{\mathcal{P}(\vec{N})} \quad (2.3)$$

247 with the denominator here is recognized as the normalization of the PDF. The compound

248 PDF $\mathcal{P}(\vec{N}, \vec{y})$ can expanded using Bayes' theorem which states

$$\mathcal{P}(A|B)\mathcal{P}(B) = \mathcal{P}(B|A)\mathcal{P}(A), \quad (2.4)$$

249 and combined with (2.2) yielding

$$\mathcal{P}\left(\underbrace{\vec{N}}_A, \underbrace{\vec{y}}_B\right) = \mathcal{P}(\vec{N}|\vec{y}) \times \mathcal{P}(\vec{y}), \quad (2.5)$$

250 where the PDFs to the left and right of the \times operator are recognized as the likelihoods and
251 priors, respectively. Combining resulting in (2.3) and (2.5) reproduces the original expression
252 of (2.1).

253 2.3 BANFF Fit Test Statistic

254 For the BANFF fit, one considers the problem of trying to maximize the agreement between
255 measured and predicted data histograms. This is equivalent to maximizing a binned likeli-
256 hood function \mathcal{L} of the data given the a set of parameters that predict the measured rate.
257 The use of likelihood functions in fits to histogram is explained further in reference [2] and
258 the PDG review on Statistics. By invoking Wilks' theorem, also known as the likelihood ratio
259 theorem, the likelihood maximization procedure is converted into a minimization problem
260 involving a test statistic denoted as a chi-squared. Below is an explanation of the BANFF
261 test statistic, $\Delta\chi^2$, and its systematic model terms.

262 Consider many binned samples that select different charged current topologies. A conve-
263 nient choice of observables for all the samples are the outgoing charged lepton l momentum P_l
264 and angle $\cos\theta_l$ as measured in ND280. Much of this is also documented in TN-220[10] where
265 additional details can be found. For each $(P_l, \cos\theta_l)$ analysis bin $i = 1, 2, \dots, M - 1, M$, the

266 likelihood is given by

$$\mathcal{L}(\vec{N}^d | \vec{N}^p) = \left(\prod_{i=1}^M \left(\vec{N}_i^p \right)^{\vec{N}_i^d} \frac{e^{-\vec{N}_i^p}}{\vec{N}_i^d!} \right) \quad (2.6)$$

267 where \vec{N}_i^d is the number of observed data events in the i th bin and \vec{N}_i^p is the number of
 268 predicted events as a function of nuisance parameters in the i th bin. One recognizes the
 269 likelihood function in (2.6) as a product of Poisson distributions with each corresponding
 270 to bins $i = 1, 2, \dots, M - 1, M$. The sets of dependent nuisance parameters, also sometimes
 271 called systematics, that affect the predicted event rate are

- 272 • cross section physics models, labeled as “xsec”,
- 273 • neutrino flux, and
- 274 • detector biases and inefficiencies.

275 Given these three sets of systematics, the number of predicted CC events from any neutrino
 276 flavor ν_l at ND280 is calculated using the general formula

$$N_{\nu_l} = \Phi_{\nu_l} \times \sigma_{\nu_l}^T \times T_N \times \epsilon_{\nu_l}, \quad (2.7)$$

277 where Φ_{ν_l} is the flux of l flavor neutrinos, $\sigma_{\nu_l}^T$ is the cross section of the interaction for
 278 neutrino flavor l on target T , T_N is the number of T targets, and ϵ_{ν_l} is the total efficiency
 279 to reconstruct and properly identify the event as ν_l CC interactions. Each term in (2.7) is
 280 modeled carefully and the efficiency term is estimated using Monte Carlo (MC) simulations
 281 and control samples. The number of predicted events from the MC for a given analysis bin
 282 i is given by

$$\vec{N}_i^p(\vec{b}, \vec{x}, \vec{d}) = w_i^{\text{POT}}(\vec{d})_i^{\text{Det}} \sum_{j=1}^{N_i^{\text{MC}}} \left[\sum_{k=1}^{N^{\text{Flux}}} \left(\delta_{j,k}^{\text{Flux}} (\vec{b})_k^{\text{Flux}} \right) \prod_{l=1}^{N^{\text{xSyst}}} w_{j,l}((\vec{x})_l^{\text{xsec}}) \right]. \quad (2.8)$$

283 Here w_i^{POT} is the protons on target (POT) weight for the i th analysis which normalizes
 284 the MC statistics to expected data statistics. To account for the detector inefficiencies, the
 285 $(\vec{d})_i^{\text{Det}}$ parameters are normalization parameters that vary the total number of predicted
 286 events in the i th bin. Each $(\vec{d})_i^{\text{Det}}$ is determined prior to the fit by surveying over a large
 287 number of toy experiments with the detector systematics varied in each. The sum over
 288 $j = 1, 2, \dots, N_i^{\text{MC}} - 1, N_i^{\text{MC}}$ considers the contribution of all MC events in the i th analysis
 289 bin. The $(\vec{b})_k^{\text{Flux}}$ parameters, out of a total of N^{Flux} , are flux normalization systematics
 290 for each flux bin. Since the flux bins are categorized not only by neutrino energy, but also
 291 by flavor and horn current, the $\delta_{j,k}^{\text{Flux}}$ term in the sum over k selects the correct flux bin.
 292 The parameters $w_{j,l}$ are pre-calculated weights as a function for the l th cross section model,
 293 $(\vec{x})_l^{\text{xsec}}$, with a total of N^{xSyst} cross section model terms. Different T target materials have
 294 separate cross section parameters and also the number of targets is constant.

295 Using the likelihood ratio test theorem, a test statistic is defined as taking -2 times the
 296 natural logarithm of the ratio of predicted to observed likelihoods

$$\Delta\chi_{\text{LLR}}^2 = -2 \log \frac{\mathcal{L}(\vec{N}^d | \vec{N}^p)}{\mathcal{L}(\vec{N}^d | \vec{N}^d)}, \quad (2.9)$$

297 where this test statistic $\Delta\chi_{\text{LLR}}^2$ obeys a true chi-squared distribution for asymptotically
 298 large statistics and the likelihood functions are of the form (2.6). The denominator in (2.9)
 299 is the MC predicted probability which assumes the best maximum likelihood estimate is
 300 the number of observed events. Penalty terms from the cross section, flux, and detector
 301 systematics are included in order to prevent overfitting of the data. The new test statistic

302 for all of ND280, $\Delta\chi^2_{\text{ND280}}$, is given by

$$\Delta\chi^2_{\text{ND280}} = \Delta\chi^2_{\text{LLR}} + \Delta\chi^2_{\text{xsec}} + \Delta\chi^2_{\text{Flux}} + \Delta\chi^2_{\text{Det}} \\ - 2 \left(\log \frac{\mathcal{L}(\vec{N}^d | \vec{N}^p)}{\mathcal{L}(\vec{N}^d | \vec{N}^d)} + \underbrace{\log \pi(\vec{x})}_{\text{xsec}} + \underbrace{\log \pi(\vec{b})}_{\text{Flux}} + \underbrace{\log \pi(\vec{d})}_{\text{Det}} \right), \quad (2.10)$$

303 where each of the PDFs $\pi(\vec{y} = \vec{x}, \vec{b}, \vec{d})$ are assumed multivariate normal distributions

$$\pi(\vec{y}) = C_y e^{\left(-\frac{1}{2}\Delta\vec{y} \cdot V_y^{-1} \cdot \Delta\vec{y}^T\right)}, \quad (2.11)$$

304 $\Delta\vec{y}$ is a vector with the difference between the current/explored and nominal set of vector
305 parameters \vec{y} , T corresponds to the transpose operator, and the normalization is given by

$$C_y = ((2\pi)^{k_y} \det(V_y))^{-\frac{1}{2}} \quad (2.12)$$

306 with V_y being the covariance matrix for a vector \vec{y} with k_y rows. The expanded form of the
307 test statistic $\Delta\chi^2_{\text{ND280}}$ is given by

$$\Delta\chi^2_{\text{ND280}} = 2 \sum_{i=1}^M \left[\vec{N}_i^p - \vec{N}_i^d + \vec{N}_i^d \log \left(\frac{\vec{N}_i^d}{\vec{N}_i^p} \right) \right] \\ + \Delta\vec{x} \cdot (V_x^{-1}) \cdot \Delta\vec{x}^T + \Delta\vec{b} \cdot (V_b^{-1}) \cdot \Delta\vec{b}^T + \Delta\vec{d} \cdot (V_d^{-1}) \cdot \Delta\vec{d}^T \quad (2.13)$$

308 where the “ \cdot ” is the matrix multiplication operator. It must be stated that the test statistic
309 (2.13) purposefully *excludes normalization terms*. Once the global minimum of the test
310 statistic is found, the postfit covariance matrix V is calculated as the inverse of the Hessian
311 matrix H

$$V_{i,j}(\hat{\vec{y}}) = (H_{i,j})^{-1} = \left(\frac{\partial^2}{\partial y_i \partial y_j} (\Delta\chi^2_{\text{ND280}}) \Big|_{\vec{y}=\hat{\vec{y}}} \right)^{-1} \quad (2.14)$$

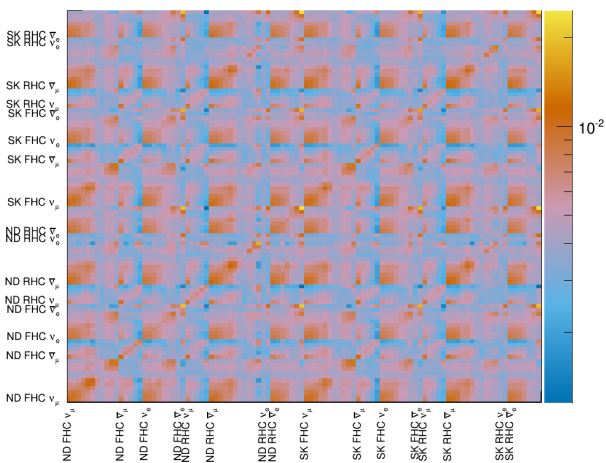


Figure 2.1: BANFF pre-fit flux covariance matrix shown with respective detector, horn current, and neutrino flavor.

312 where $y_i, y_j \in \vec{y}$ and $\hat{\vec{y}}$ is the maximum likelihood estimate for the parameters \vec{y} .

313 2.3.1 Flux, Cross Section, and Detector Systematics

314 Below is a description for each of the systematics in the BANFF likelihood and test statistic
 315 penalty terms. First is a description of flux, followed by the cross section, and finally the
 316 detector systematics.

317 **Flux:** The flux weight is binned as a function of neutrino energy, horn current/polarity
 318 (FHC and RHC), and neutrino flavor (ν_μ , $\bar{\nu}_\mu$, ν_e , and $\bar{\nu}_e$). There are 50 ND280 and 50 SK
 319 parameters with an associated covariance matrix as shown in Figure 2.1. The binning and
 320 covariance matrix is provided by the T2K flux group prior to the BANFF analysis. Each
 321 flux bin is assigned a normalization parameter with initial value of one (1) for all events in
 322 that neutrino energy bin. A value of 1.1 indicates that any event in that energy bin has an
 323 additional weight of 1.1, or 10% increase in events. An example of the flux normalizations
 324 and uncertainties used in the 2017 analysis are shown in Figure 2.2.

325 **Cross Section:** There are a number of cross section model systematics implemented in
 326 BANFF to account for the uncertainties in cross section measurements. The cross section

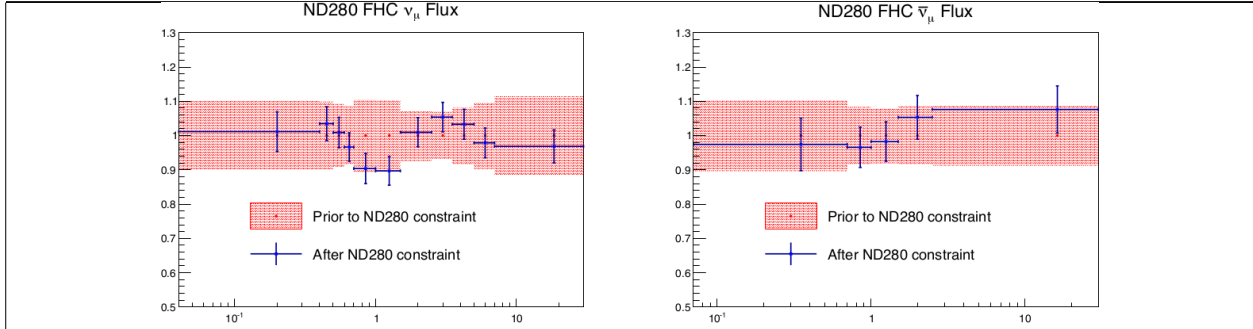


Figure 2.2: BANFF ND280 flux ν_μ and $\bar{\nu}_\mu$ binning parameters from T2K-TN-324 data post-fit results. The uncertainties are extracted from the pre-fit and post-fit covariance matrices.

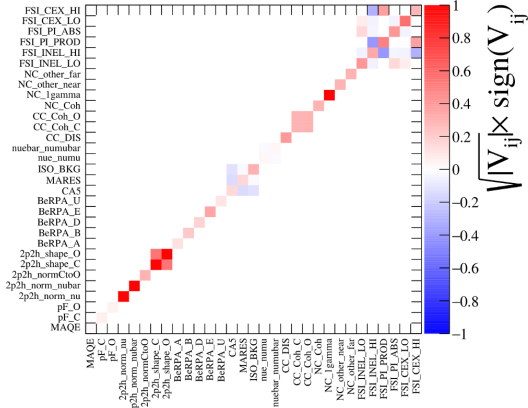


Figure 2.3: Cross section parameters pre-fit correlation matrix from the 2017 BANFF analysis.

models used in this analysis are the 2017 Neutrino Interactions Working Group (NIWG) parameterization, which is a canonical set of parameters and covariance matrix shared among all analyses in T2K. A technical description of the 2017 parameterization is given in TN-315[5] and TN-307[14]. There are a total of 25 cross section parameters for interactions like meson exchange current that affect the shape and normalization of the cross section. The cross section correlation matrix is shown in Figure 2.3[4].

333 Detector Systematic Errors: Detector systematics are implemented in BANFF to
334 account for uncertainties in detector efficiencies. Since neutrino interaction events can mi-
335 grate from sample-to-sample, bin-to-bin, or both depending on the relevant systematics,
336 numerous toy experiments are performed by varying parameters that model known detector

337 systematics. After many toy experiments, a covariance matrix is constructed as

$$\sigma_{\text{Det}}^2(x, y) = \left(\frac{1}{xy}\right)_{\text{Nom}} \sum_{i=1}^{N_{\text{Toy}}} \sum_{j=1}^{N_{\text{Toy}}} (x_i - \bar{x})(y_j - \bar{y}), \quad (2.15)$$

338 where “Nom” refers to the nominal MC prediction for bins x/y , N_{Toy} is the number of toy
339 experiments, and \bar{x}/\bar{y} is the mean of all the toy experiments. While there could be
340 one detector systematic normalization for each analysis bin, also called a observable normal-
341 ization, a single one can be assigned to multiple analysis bins to reduce the number of fit
342 parameters. This procedure requires careful consideration of the shared detector systematics
343 among analysis bins. A considerable drawback to designing normalizations in this way is that
344 not all detector systematics are Gaussian with respect to the observables $(P_l, \cos \theta_l)$, and so
345 the covariance matrix may not be an accurate representation of the detector systematics.

346 **3 PØD Selections and Data Samples**

347 This section describes the development of ν_μ and $\bar{\nu}_\mu$ CC Inclusive selections in both FHC
348 and RHC beam configuration for PØD-based analyses. These selections are the continuation
349 of previous works that developed ν_μ CC Inclusive selections between the PØD and TPC1.
350 The first such analyses were T2K-TN-80 and T2K-TN-100 which described the ν_μ CC In-
351 clusive event selection and, later, cross-section analysis using ND280 Production 5 software,
352 respectively[7, 8]. These analyzes relied on each sub-detector’s reconstruction software and
353 developed a track matching algorithm since the ND280 “Global” reconstruction matching
354 was problematic in Production 5. As the inter-detector matching reconstruction improved in
355 “Global”, two CC-0 π cross section analyzes, T2K-TN-258 and T2K-TN-328, were developed
356 that also used the CC Inclusive selection as pre-selection cuts[16, 6]. The selections described
357 in this technical note also employ the same pre-selection cuts. What follows from here in
358 this section is a layout of the following topic discussions.

359 The first topic discussed in this section is a description of the π^0 Detector (PØD). The
360 next topic is the event reconstruction using the “Global” reconstruction software. Following
361 that is the pre-selection cut flow. With the pre-selection cuts established, each of the three
362 CC Inclusive selection’s cut flow is described. Concluding this section is a discussion of the
363 three samples in the following order: ν_μ in FHC mode, $\bar{\nu}_\mu$ in RHC, and ν_μ background in
364 RHC.

365 **3.1 Global Reconstruction**

366 The task of the Global reconstruction is to combine all the ND280 information into a com-
367 bined reconstructed object. It was originally designed to analyze “CCQE-like” events in the
368 Tracker region and has been extended to operate with all of ND280. A brief description
369 of the Global reconstruction is described below. First the specific detector technologies and

370 electronics of ND280 are explained. That is followed by the calibration procedure to properly
371 tune each detector’s response. And finally a general outline of the reconstruction algorithms
372 to form tracks and vertices in ND280 is presented.

373 ND280 events are first collected in the form of electronic signals from either multipixel
374 photon counters (MPPCs) in the scintillator-based sub-detectors or charge collection planes
375 of the time projection chambers (TPCs). MPPCs were chosen for the scintillator-based sub-
376 detectors since they are insensitive to the strong 0.2T magnetic field present in ND280. The
377 PØD, ECals, and SMRD all share the same “Trip-T” frontend board (TFB) electronics of
378 which collect the photoelectrons released when photons interact with a pixel in the MPPCs.
379 The FGDs operate with the same MPPC technology while using different frontend electron-
380 ics. The TPCs utilize a locally strong electric field to collect ionization electrons from an
381 Argon-based gas. Collected charge in the TPCs are collected and enhanced using micromega
382 technology[1]. With the collected information from each sub-detector, the next step is the
383 data calibration.

384 Data calibration in ND280 is the process where the charge and timing information col-
385 lected from each sub-detector is adjusted to match with expected parameters. This is an
386 important process that takes into account environmental changes, aging effects, and other
387 behavior that might be present. Calibration data is collected frequently before and during
388 operational runtime and is stored in a database for later use. A common calibration is to
389 measure the detector’s cosmic ray response since most cosmic rays deposit the same energy
390 per unit length. After the data has been calibrated, reconstruction algorithms now attempt
391 to find charged particle tracks in the data.

392 The Global reconstruction is a software package that attempts to recognize patterns of
393 data to form tracks and find vertices for those tracks. Particle shower reconstruction in
394 Global will not be discussed in this TN since no shower objects are used. Each sub-detector
395 reconstruction is run to seeds Global’s track matching algorithms. Global attempts to then

396 re-fit sub-detector tracks using a Kalman filter while correcting for particle energy loss as a
397 function of length (dE/dx) and multi-scattering processes. A vertex is then associated with
398 the re-fit track using another Kalman filter algorithm. A further detailed description of the
399 track matching and vertex finding algorithms for Global is described in T2K-TN-46[15].

400 **3.2 PØD Selection Cuts**

401 The selection of CC Inclusive events use a series of cuts to select the primary lepton. The
402 pre-selection cuts (“precuts”) are applied first to extract events that start in the PØD FV.
403 A MIP is more likely to reach TPC1 from the PØD FV since the PØD is constructed out
404 of heavy materials especially in the CECal. So the main track each selection is designed to
405 select a muon.

406 This following sections will describe the precuts common to all CC Inclusive selections
407 and the branching of different cuts, after the precuts, to select the main track.

408 **3.2.1 Pre-Selection Cuts**

409 The pre-selection (“precuts”) were initially developed to select ν_μ CC Inclusive using the PØD
410 and TPC sub-detector reconstruction softwares separately[7]. They were then used with the
411 Global reconstruction software for the ν_μ CC-0 π selection in the FHC beam configuration as
412 described in technical note T2K-TN-258[16]. The description and flow of the precuts are
413 described here as well since there is an incomplete description of the selection precuts.

414 The precuts are performed on each bunch per beam spill as follows

- 415 1. The event has a “good” data quality flag.
 - 416 • An event is rejected if any sub-detector or electronics in ND280 reported as “bad”
417 during that bunch.
- 418 2. There is at least one (1) track reconstructed in TPC1.

- 419 • There are no restrictions on the number of tracks fully contained in the PØD or
420 existing into other sub-detectors.

421 3. The track in TPC1 must have more than 18 nodes.

- 422 • The TPC reconstruction gathers vertical and horizontal hits into clusters of hits.
423 The charge distribution of the cluster is used to get a vertical (horizontal) position
424 that is more accurate than the individual readout pads. A node is constructed
425 out of each cluster with associated track state information. The set of nodes are
426 used to fit the track helix[12].

427 4. The reconstructed vertex is within the PØD WT FV.

- 428 • The PØD FV is defined to include as much as the WT regions as possible. Its
429 X and Y borders are 25 cm away from the PØDule edges while its Z borders
430 intersect the last and first half downstream PØDule in the USECal and CECal,
431 respectively. The enumerated volume edges are shown in table 3.1. This volume,
432 while used for track-based analyzes in the past, was optimized for π^0 and ν_e
433 analyzes[9].

434 5. All tracks that enter TPC1 pass the veto cut

- 435 • An event is rejected if any PØD track enters TPC1 from outside the “corridor”
436 volume. This cut was designed to eliminate broken tracks between the PØD and
437 TPC1 when the separate sub-detector reconstructions were used[7]. In practice,
438 this cut ensures that Global tracks entering TPC1 away from its X and Y edges.
439 The corridor definition is the same as defined in T2K-TN-208 and shown in Ta-
440 ble 3.1.

PØD WT FV			Corridor Volume		
-836	< X <	764	-988	< X <	910
-871	< Y <	869	-1020	< Y <	1010
-2969	< Z <	1264	-3139	< Z <	-900

Table 3.1: The PØD WT FV (left) and veto corridor volume (right) in the ND280 coordinate system. The corridor spans from the 5th (8th) to 40th (80th) PØDule (scintillator layer). All the units are given in millimeters.

After passing all the precuts, a single, global track, which is observed in TPC1, is assigned as the “main track” of a selection. The main track for ν_μ selections is the highest momentum, negatively-charged track (HMNT). Similarly the highest momentum, positively-charged track (HMPT) is assigned the main track for $\bar{\nu}_\mu$ selections.

This concludes the application of precuts to all the CC Inclusive selections. The following subsubsections describe the CC Inclusive selection cuts, first in FHC mode and then RHC mode.

3.2.2 ν_μ CC Inclusive in FHC Cut

- The highest momentum negatively charged track (HMNT) is the lepton candidate

As discussed in Section section 3.2.1 on page 25, this selection is the basis for the ν_μ CC-0 π PØD+TPC1 analysis. In FHC mode, the vast majority of neutrino interactions are ν_μ CC events producing an outgoing, negatively charged muon. So if there is no negatively charged track in the TPC, the event is rejected.

3.2.3 $\bar{\nu}_\mu$ CC Inclusive in RHC Cuts

- The highest momentum positively charged track (HMPT) is the lepton candidate
- The HMPT must be the highest momentum track (HMT)

457 In RHC, the majority of neutrinos in the beam is $\bar{\nu}_\mu$ since the horn focuses negatively charged
 458 pions. To select $\bar{\nu}_\mu$ CC interaction events by selecting positively charged muons, the lepton
 459 candidate is the HMPT in the TPC. The event is rejected if there is no positively charged
 460 track. However, since the RHC mode beam is not as $\bar{\nu}_\mu$ pure as the FHC beam, another cut
 461 was added to reduce this effect.

462 Since RHC neutrino beam can be described as a $\bar{\nu}_\mu$ -enhanced beam, the HMPT must
 463 also be the HMT due to the significant “wrong-sign” ν_μ background. This effect is two
 464 fold due to the nature of the neutrino source and the cross section between neutrinos and
 465 antineutrinos.

466 Firstly the neutrino flux is larger in RHC mode due to neutrino production at the tar-
 467 get. The source of neutrinos are from protons, which have positive charge, on a graphite
 468 target. This method is more likely to produce positively charged pions in the target than
 469 negatively charged one. While the horns are designed to select the negatively charged pions
 470 in RHC mode, the excess amount of positively charged pions will penetrate the horns’ filter.
 471 Therefore there are many more $\pi^+ \rightarrow \mu^+ + \nu_\mu$ decays in RHC compared to FHC mode.

472 Secondly, antineutrino interactions on matter are suppressed compared to neutrinos due
 473 to helicity considerations. Consider neutrino-electron scattering, the cross section for $\nu_e + e^-$
 474 is given by

$$\frac{d\sigma}{d\Omega} = \frac{G^2 s}{4\pi^2}, \quad (3.1)$$

475 where G is the Fermi constant and s is the center of mass energy squared. The outgoing
 476 particles are isotropic since the initial and final spin state of the system is $J = 0$. Compare
 477 (3.1) with the cross section for $\bar{\nu}_e + e^-$

$$\frac{d\sigma}{d\Omega} = \frac{G^2 s}{16\pi^2} (1 - \cos \theta)^2, \quad (3.2)$$

478 where θ is the observed scattering angle of the electron. Since the total spin of the $\bar{\nu}_e + e^-$

479 system is $J = 1$ with the $J_z = 1$, the antineutrino is preferentially forward scattered.

480 Integrating over all angles, the cross sections come out to

$$\sigma(\bar{\nu}_e + e^-) = \frac{1}{3}\sigma(\nu_e + e^-).$$

481 The factor $1/3$ arises from the fact that angular momentum conservation forbids the $J_z = -1$

482 and 0 states for $\bar{\nu}_e + e^-$ scattering. The same $1/3$ factor arises with e^- replaced with quarks.

483 Therefore the cross sections for neutrinos are larger than antineutrinos.

484 3.2.4 ν_μ Background CC Inclusive in RHC Cuts

- 485 • The highest momentum negative track (HMNT) is the lepton candidate
- 486 • The HMNT must be the highest momentum track (HMT)

487 As discussed in section 3.2.3 on page 27, the RHC neutrino beam has a significant wrong-sign ν_μ background. The selection of the HMNT is designed to select the negatively charged muons. To prevent selecting the antineutrino events, the HMNT must also be the HMT.

490 The event is rejected if there is no negatively charged track. If there are both positively and negatively charged tracks, the HMT cut discriminates if the event originates from a ν_μ or

492 $\bar{\nu}_\mu$.

493 3.3 Sample Kinematics and Validation

494 This section examines the kinematics for each of selections while differentiating between water-in and water-out mode. The selection cuts were implemented in Psyche which is the software interface that BANFF uses to select events. An analysis of the kinematics are carefully cross validated with the same selection cuts in the T2K high level analysis framework called Highland. Comparing the results between Highland and Psyche is important since

Run Period	Horn Current	PØD Status	Data POT ($\times 10^{20}$)	MC POT ($\times 10^{20}$)
2	+250 kA	Water	0.4339	12.03
		Air	0.3591	9.239
3b	+205 kA		0.2172	4.478
3c	+250 kA		1.364	26.32
4			1.782	34.99
		Water	1.642	34.97
5c	-250 kA		0.4346	22.77
6b		Air	1.288	14.17
6c			0.5058	5.275
6d			0.7753	6.884
6e			0.8479	8.594
7b		Water	2.436	33.70
8	+250 kA		1.580	26.46
		Air	4.148	36.06
Sand	FHC		-	11.19
Sand	RHC		-	12.92
2, 3b, 3c, 4, 8	FHC	Air	7.872	79.18
		Water	3.657	73.47
6b, 6c, 6d, 6e	RHC	Air	3.417	34.92
		Water	2.871	56.48

Table 3.2: T2K MC and data POT divided by run periods. The bottom four rows are the aggregated periods grouped by horn current and PØD status which is how the data analysis is performed.

499 they are complementary frameworks within T2K. The data sets used in this analysis are
500 runs 2-8 in both PØD water-in and water-out (air) modes as shown in Table 3.2.

501 3.4 PØD Water-Out Samples

502 This section shows the kinematic distributions for the PØD water-out samples. First an
503 examination of the CC Inclusive samples and the effects of the systematic weights will be
504 explored. The samples are then examined as CC 1-track and CC N-tracks.

505 **3.4.1 CC Inclusive**

506 The CC Inclusive sample cuts are discussed 3.2.1. Since both flux and systematic weights
507 are applied to all MC events in BANFF, it is important to validate the event weights. Using
508 neither set of weights is referred to as the nominal MC.

509 **3.4.1.1 ν_μ Selection in FHC Mode:** Shown in Figures 3.1 to 3.7 are the momentum
510 and $\cos\theta$ distributions for ν_μ CC Inclusive events in FHC mode. There are three pairs of
511 P, θ figures with the same truth information break down accompanied by one of neutrino
512 energy. The truth information categories are lepton candidate particle, NEUT reaction, and
513 topology. Each figure consists of a set of four sub-figures which illustrate the application of
514 flux and detector systematic weights.

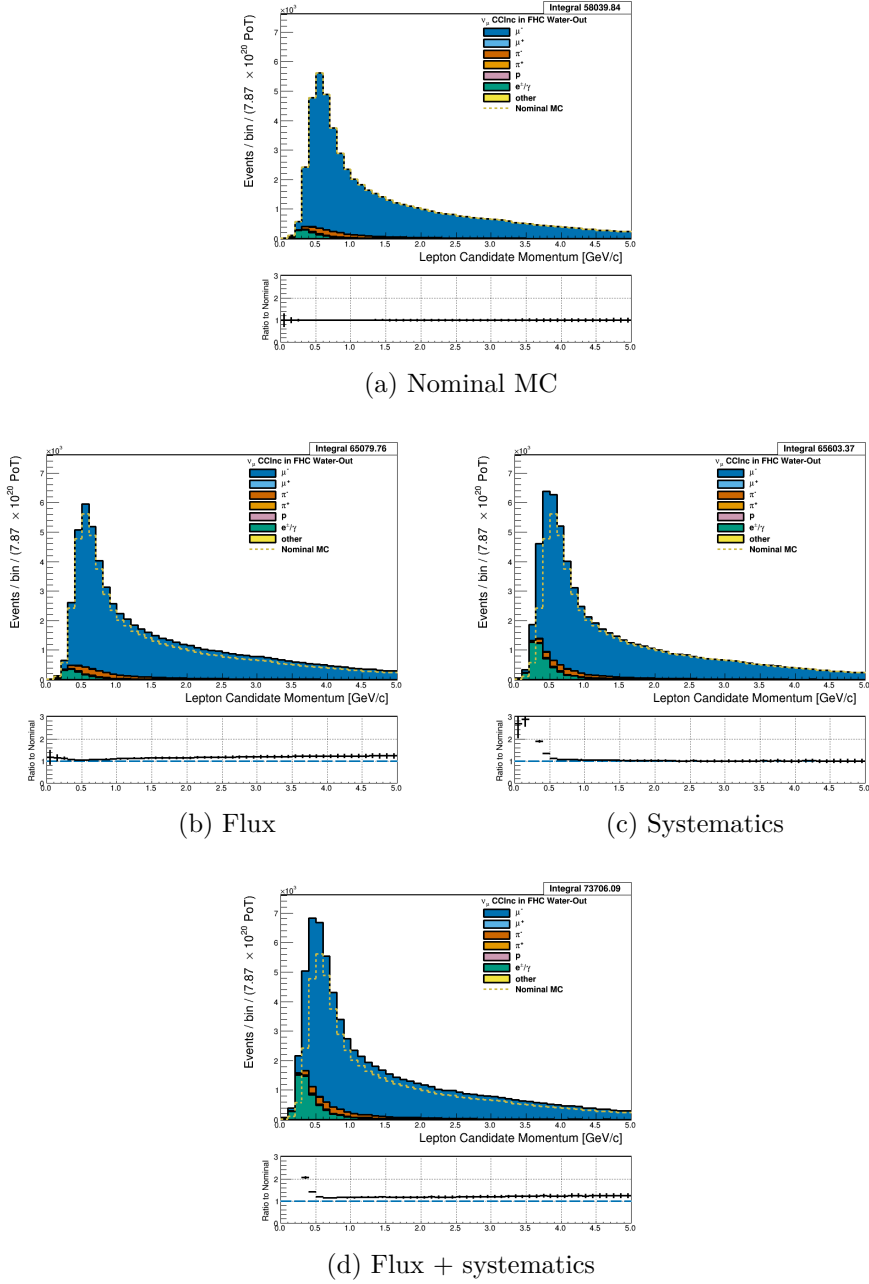


Figure 3.1: Reconstructed lepton candidate momentum separated by true particle species for FHC ν_μ CC Inc. events occurring in the PØD in water-out mode. (a) The nominal MC prediction without any weights applied. (b) The flux tuning are applied. (c) The systematic weighting are applied. (d) Both flux and systematic weighting are applied.

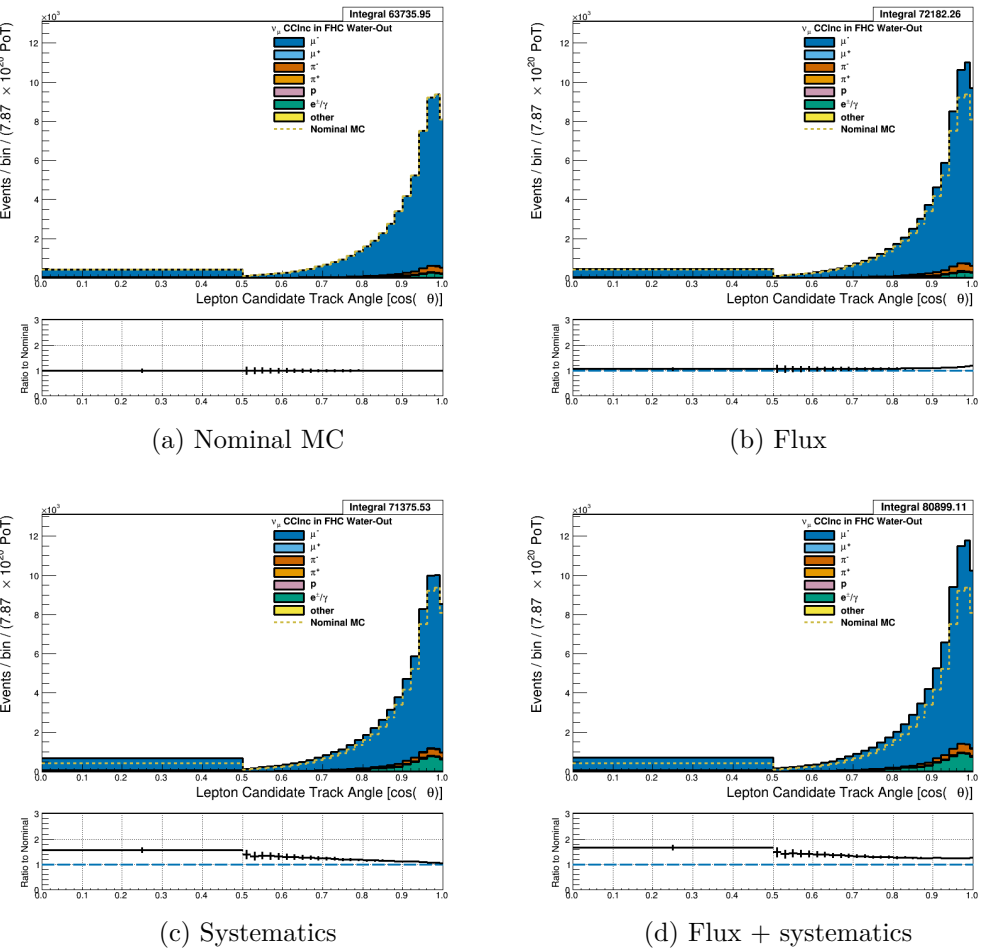


Figure 3.2: Reconstructed lepton candidate angle separated by true particle species for FHC ν_μ CC Inc. events occurring in the PØD in water-out mode. (a) The nominal MC prediction without any weights applied. (b) The flux tuning are applied. (c) The systematic weighting are applied. (d) Both flux and systematic weighting are applied.

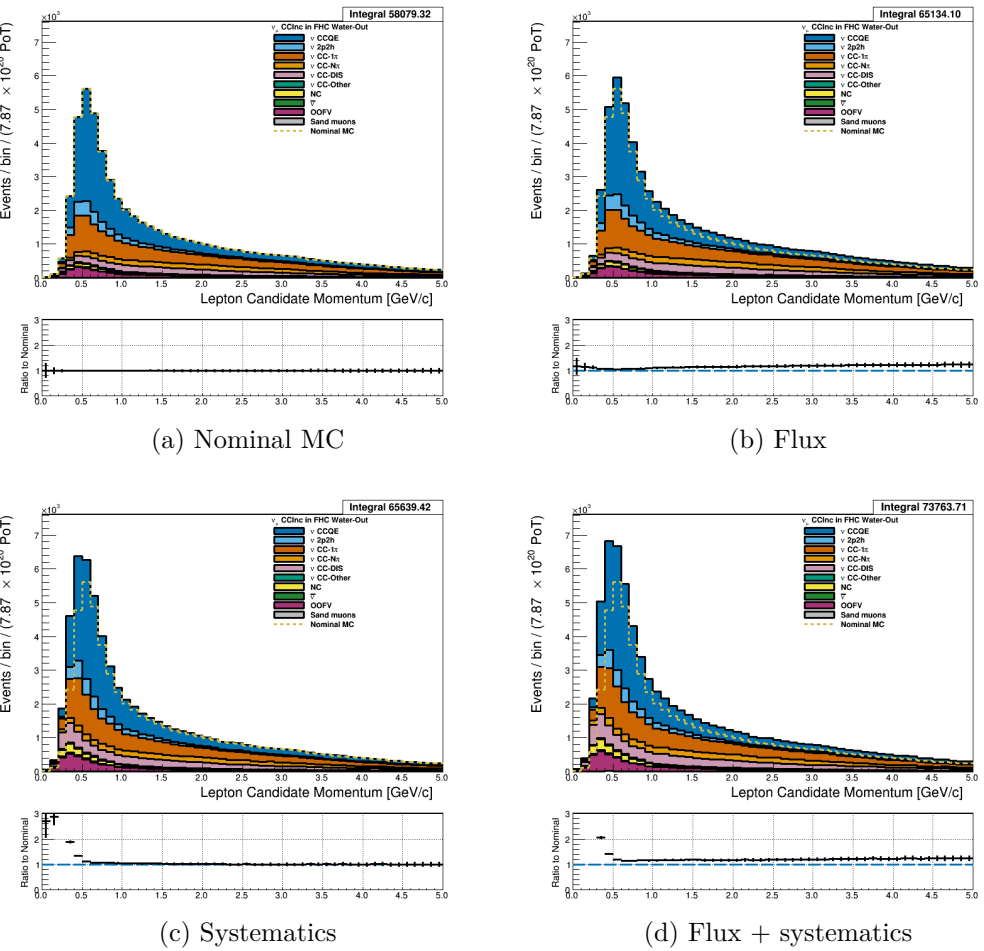


Figure 3.3: Reconstructed lepton candidate momentum separated by NEUT model interaction mode for FHC ν_μ CC Inc. events occurring in the PØD in water-out mode. (a) The nominal MC prediction without any weights applied. (b) The flux tuning are applied. (c) The systematic weighting are applied. (d) Both flux and systematic weighting are applied.

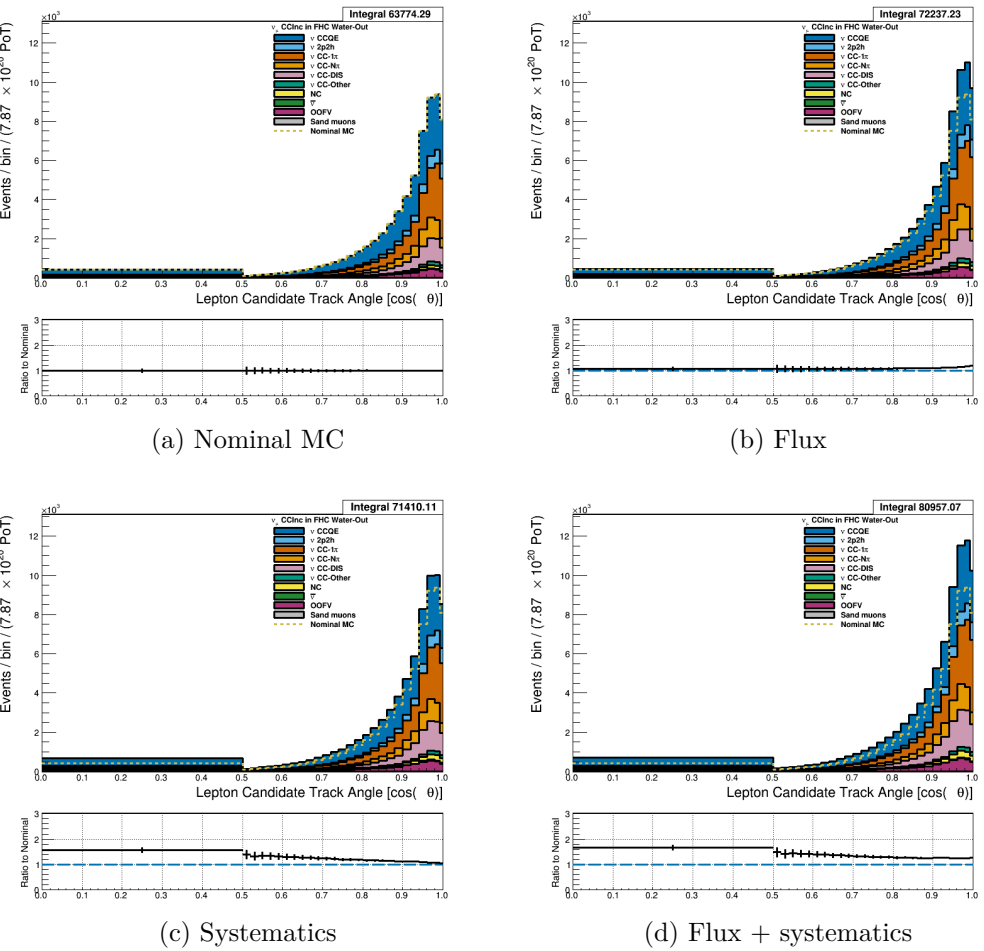


Figure 3.4: Reconstructed lepton candidate $\cos\theta$ separated by NEUT model interaction mode for FHC ν_μ CC Inc. events occurring in the PØD in water-out mode. (a) The nominal MC prediction without any weights applied. (b) The flux tuning are applied. (c) The systematic weighting are applied. (d) Both flux and systematic weighting are applied.

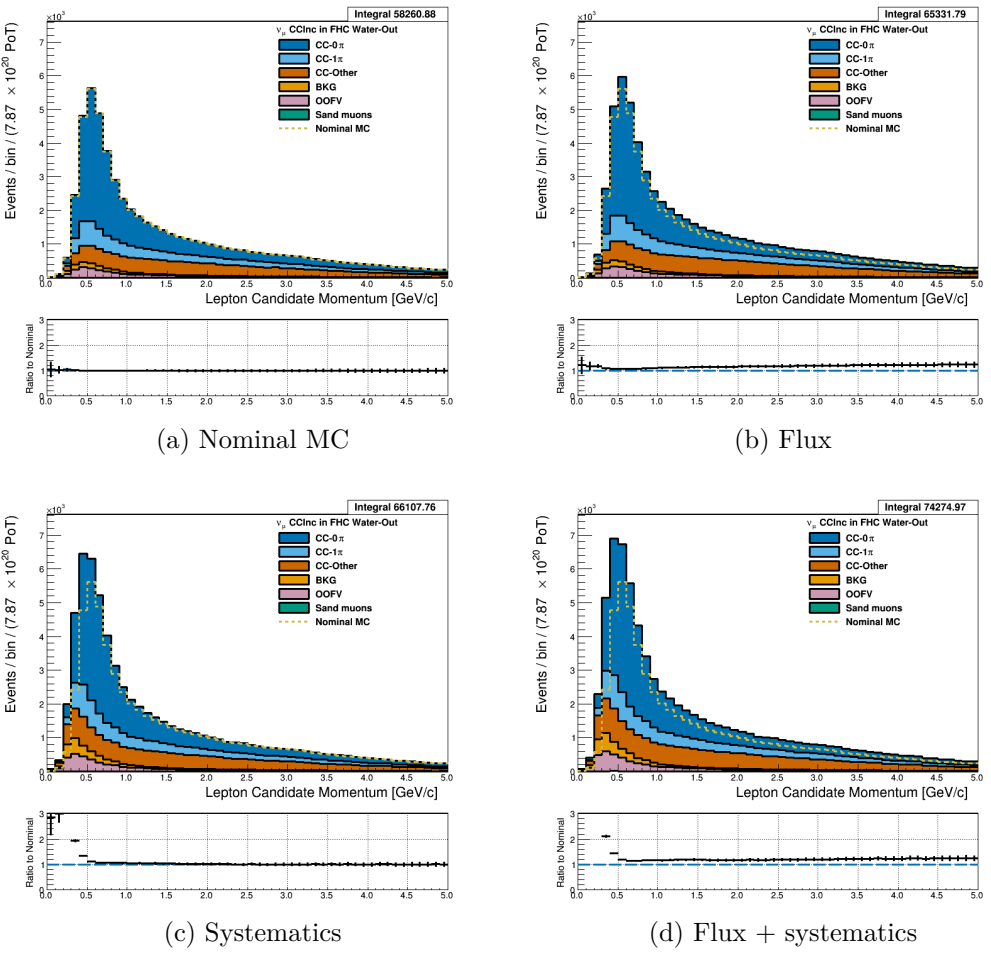


Figure 3.5: Reconstructed lepton candidate momentum separated by topology for FHC ν_μ CC Inc. events occurring in the PØD in water-out mode. (a) The nominal MC prediction without any weights applied. (b) The flux tuning are applied. (c) The systematic weighting are applied. (d) Both flux and systematic weighting are applied.

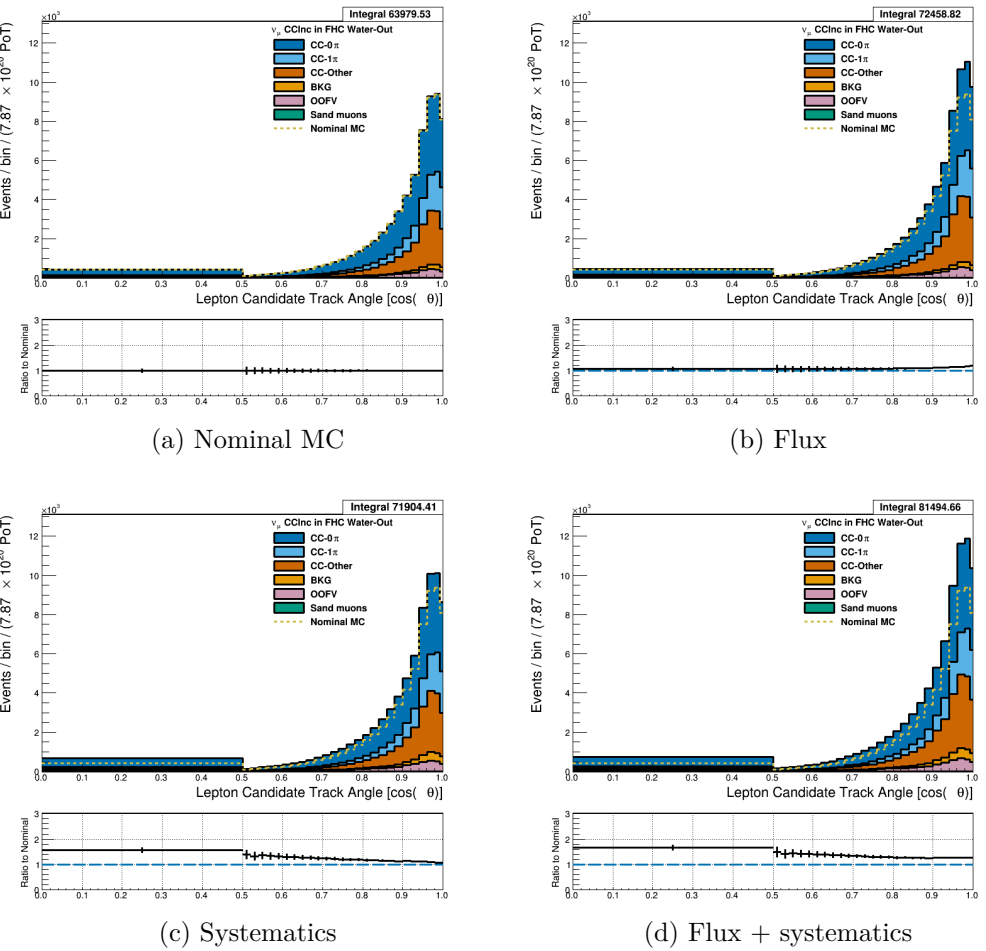


Figure 3.6: Reconstructed lepton candidate $\cos \theta$ separated by topology for FHC ν_μ CC Inc. events occurring in the PØD in water-out mode. (a) The nominal MC prediction without any weights applied. (b) The flux tuning are applied. (c) The systematic weighting are applied. (d) Both flux and systematic weighting are applied.

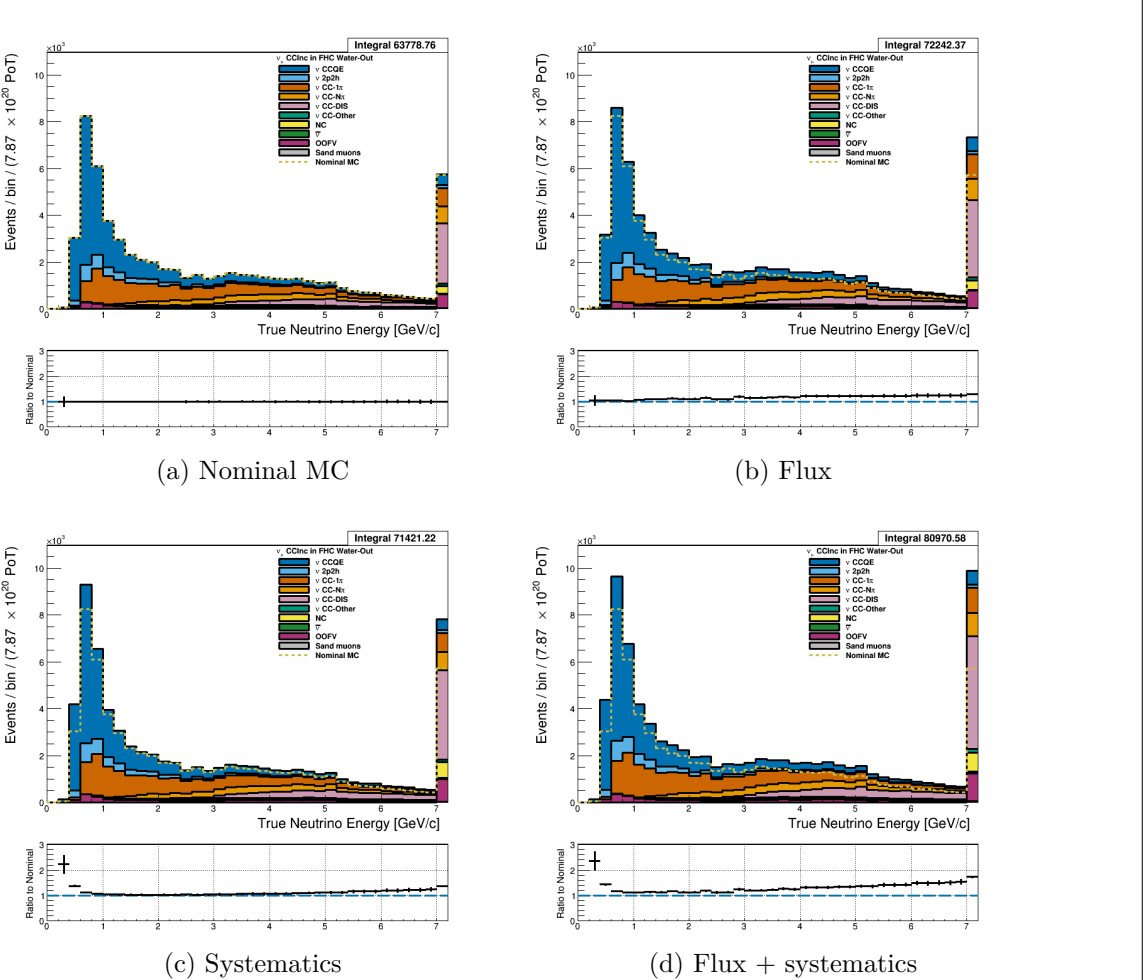


Figure 3.7: True neutrino energy associated with the lepton candidate separated by NEUT model interaction mode for FHC ν_μ CC Inc. events occurring in the PØD in water-out mode. (a) The nominal MC prediction without any weights applied. (b) The flux tuning are applied. (c) The systematic weighting are applied. (d) Both flux and systematic weighting are applied.

3.4.1.2 $\bar{\nu}_\mu$ Selection in RHC Mode: Shown in Figures 3.8 to 3.14 for $\bar{\nu}_\mu$ CC Inclusive events in RHC mode. There are three pairs of P, θ figures with the same truth information break down accompanied by one of neutrino energy. The truth information categories are lepton candidate particle, NEUT reaction, and topology. Each figure consists of a set of four sub-figures which illustrate the application of flux and detector systematic weights.

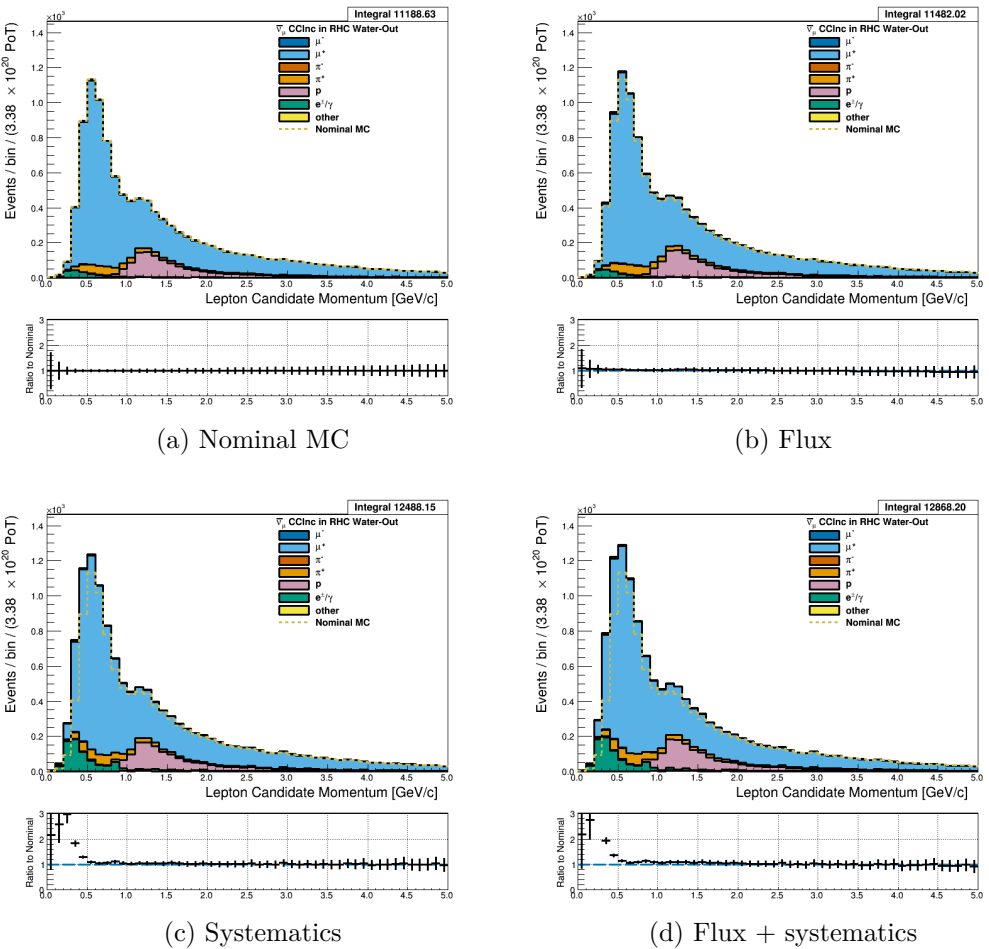


Figure 3.8: Reconstructed lepton candidate momentum separated by true particle species for RHC $\bar{\nu}_\mu$ CC Inc. events occurring in the PØD in water-out mode. Reconstructed lepton candidate angle separated by true particle species for RHC $\bar{\nu}_\mu$ CC Inc. events occurring in the PØD in water-in mode. (a) The nominal MC prediction without any weights applied. (b) The flux tuning are applied. (c) The systematic weighting are applied. (d) Both flux and systematic weighting are applied.

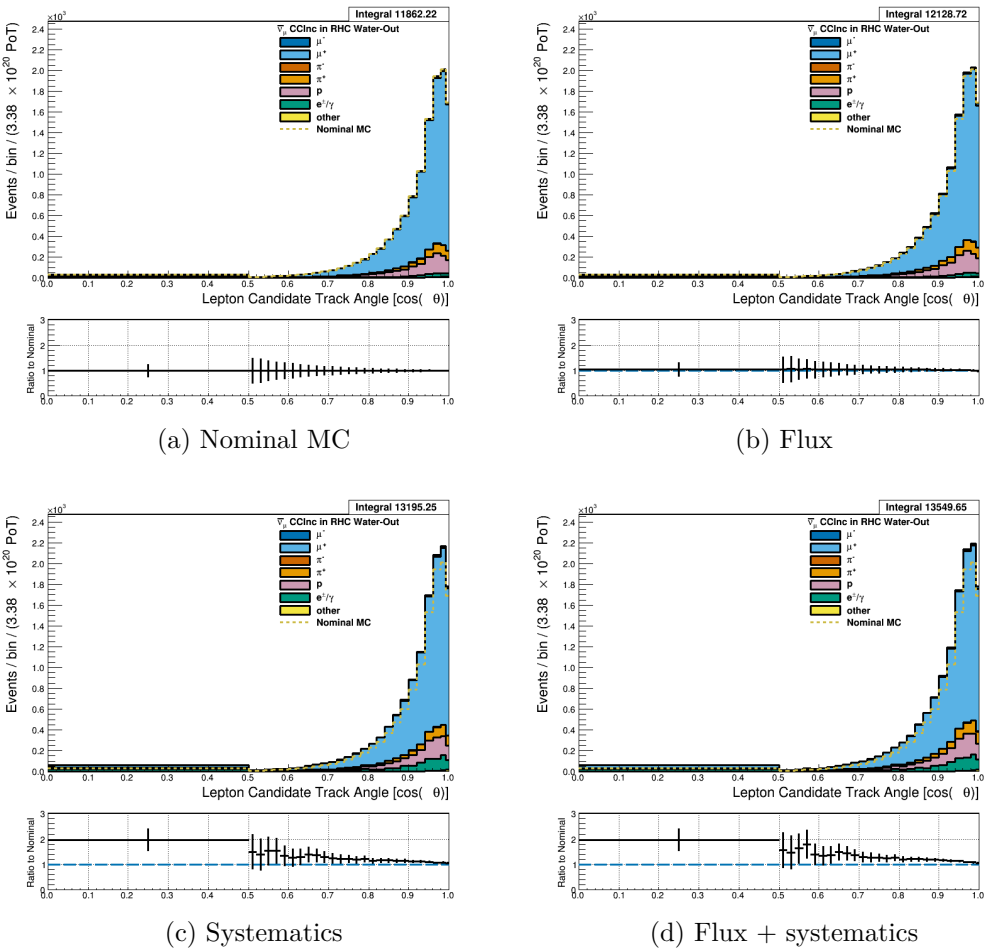


Figure 3.9: Reconstructed lepton candidate angle separated by true particle species for RHC $\bar{\nu}_\mu$ CC Inc. events occurring in the PØD in water-out mode. (a) The nominal MC prediction without any weights applied. (b) The flux tuning are applied. (c) The systematic weighting are applied. (d) Both flux and systematic weighting are applied.

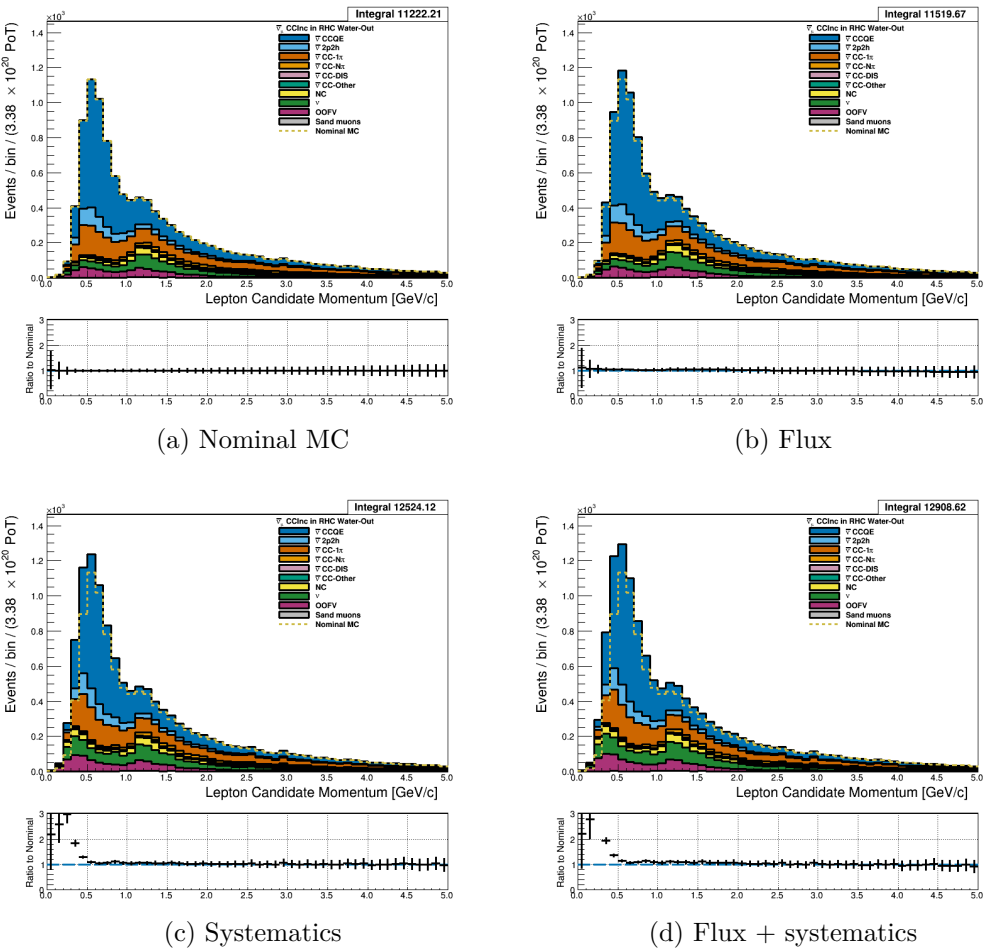


Figure 3.10: Reconstructed lepton candidate momentum separated by NEUT model interaction mode for RHC $\bar{\nu}_\mu$ CC Inc. events occurring in the P̄OD in water-out mode. (a) The nominal MC prediction without any weights applied. (b) The flux tuning are applied. (c) The systematic weighting are applied. (d) Both flux and systematic weighting are applied.

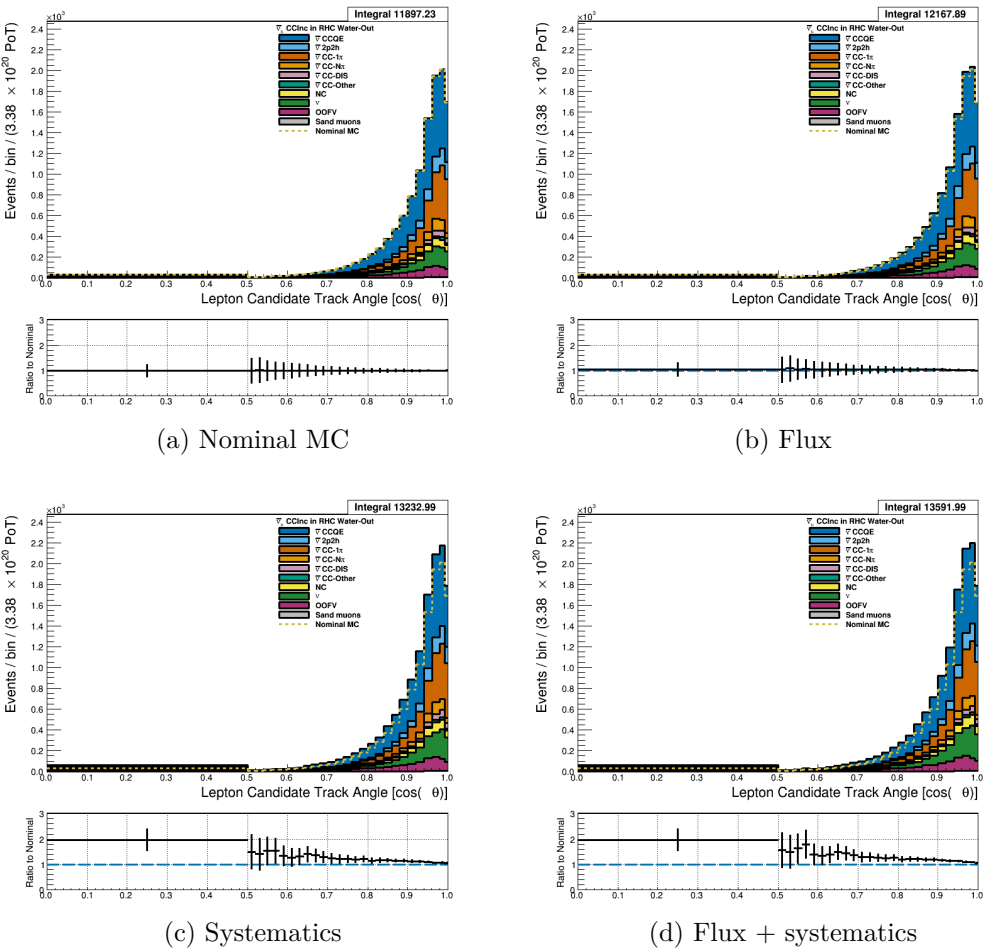


Figure 3.11: Reconstructed lepton candidate $\cos \theta$ separated by NEUT model interaction mode for RHC $\bar{\nu}_\mu$ CC Inc. events occurring in the PØD in water-out mode. (a) The nominal MC prediction without any weights applied. (b) The flux tuning are applied. (c) The systematic weighting are applied. (d) Both flux and systematic weighting are applied.

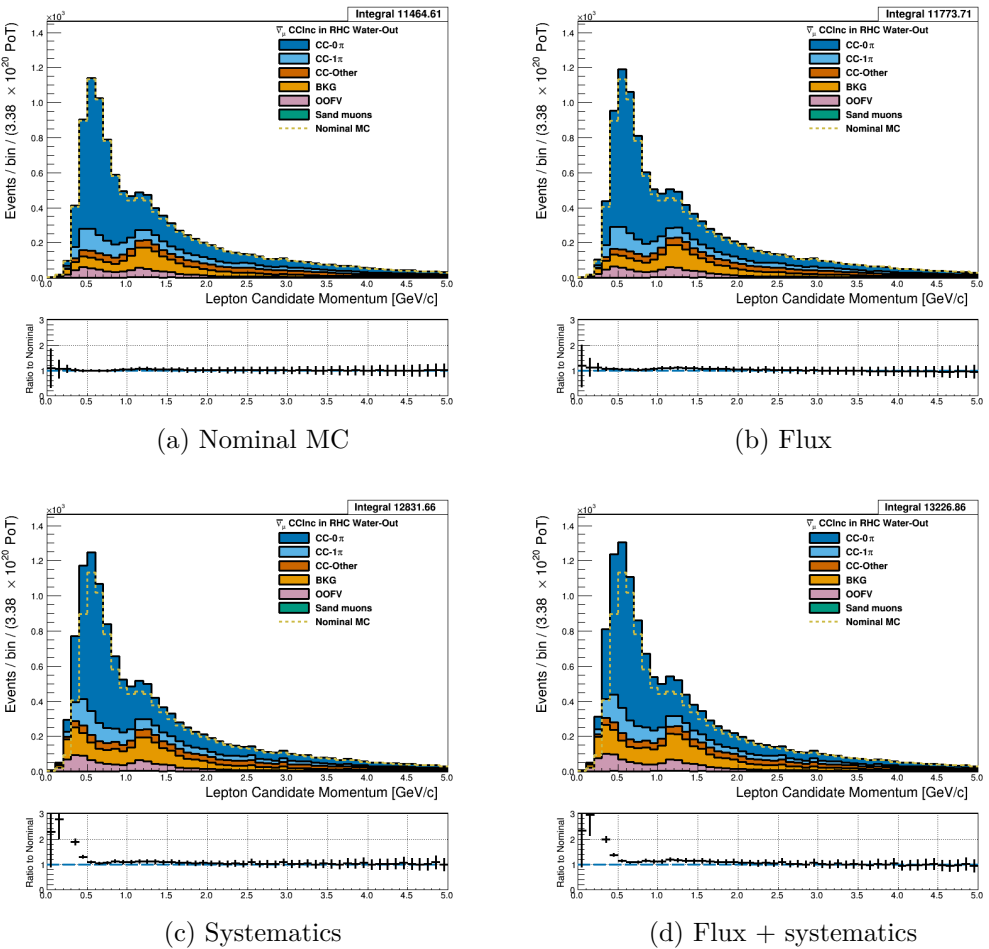


Figure 3.12: Reconstructed lepton candidate momentum separated by topology for RHC $\bar{\nu}_\mu$ CC Inc. events occurring in the PØD in water-out mode. (a) The nominal MC prediction without any weights applied. (b) The flux tuning are applied. (c) The systematic weighting are applied. (d) Both flux and systematic weighting are applied.

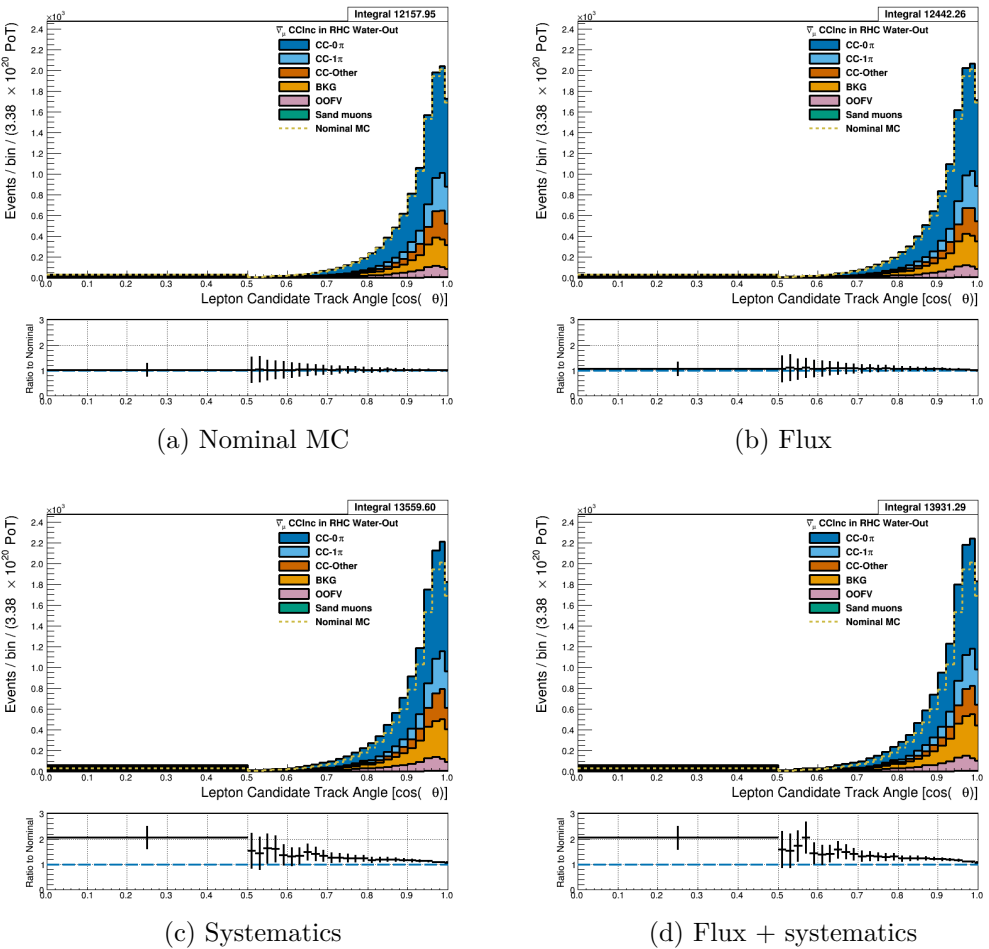


Figure 3.13: Reconstructed lepton candidate $\cos \theta$ separated by topology for RHC $\bar{\nu}_\mu$ CC Inc. events occurring in the PØD in water-out mode. (a) The nominal MC prediction without any weights applied. (b) The flux tuning are applied. (c) The systematic weighting are applied. (d) Both flux and systematic weighting are applied.

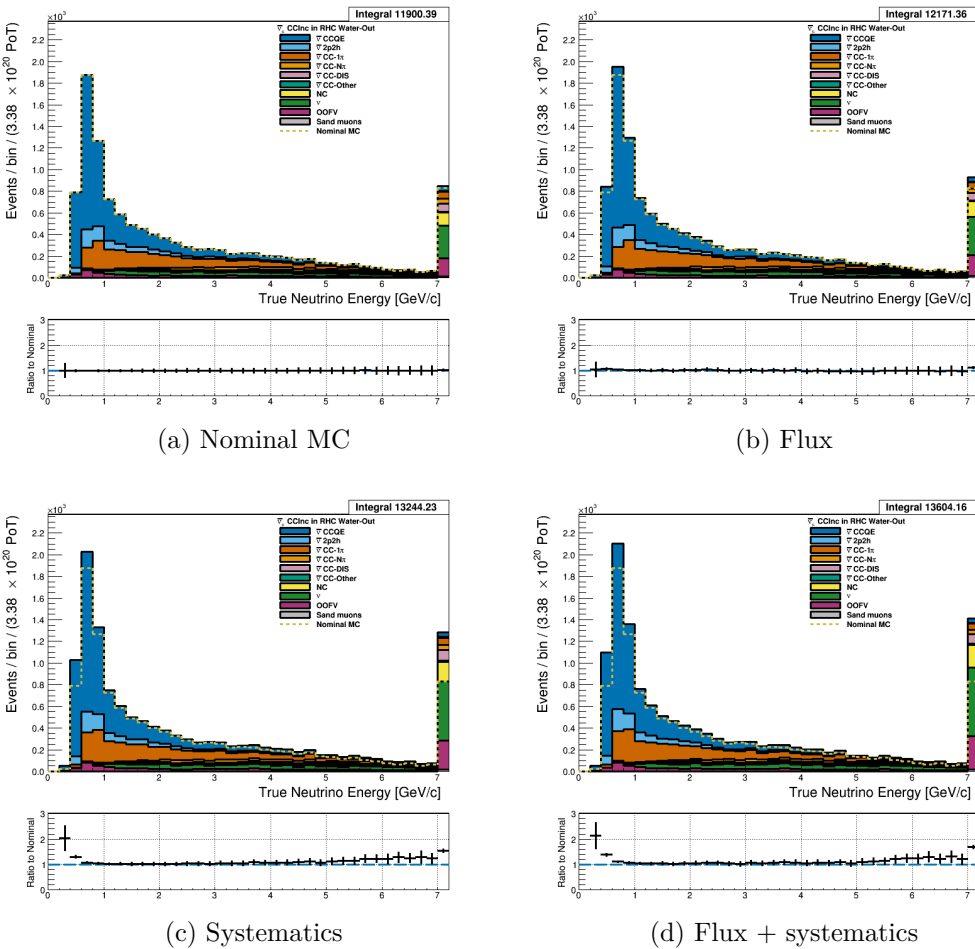


Figure 3.14: True neutrino energy associated with the lepton candidate separated by NEUT model interaction mode for RHC $\bar{\nu}_\mu$ CC Inc. events occurring in the PØD in water-out mode. (a) The nominal MC prediction without any weights applied. (b) The flux tuning are applied. (c) The systematic weighting are applied. (d) Both flux and systematic weighting are applied.

520 **3.4.1.3 ν_μ Background Selection in RHC Mode:** Shown in Figures 3.15, 3.16 and 3.19
521 to 3.21 and ????

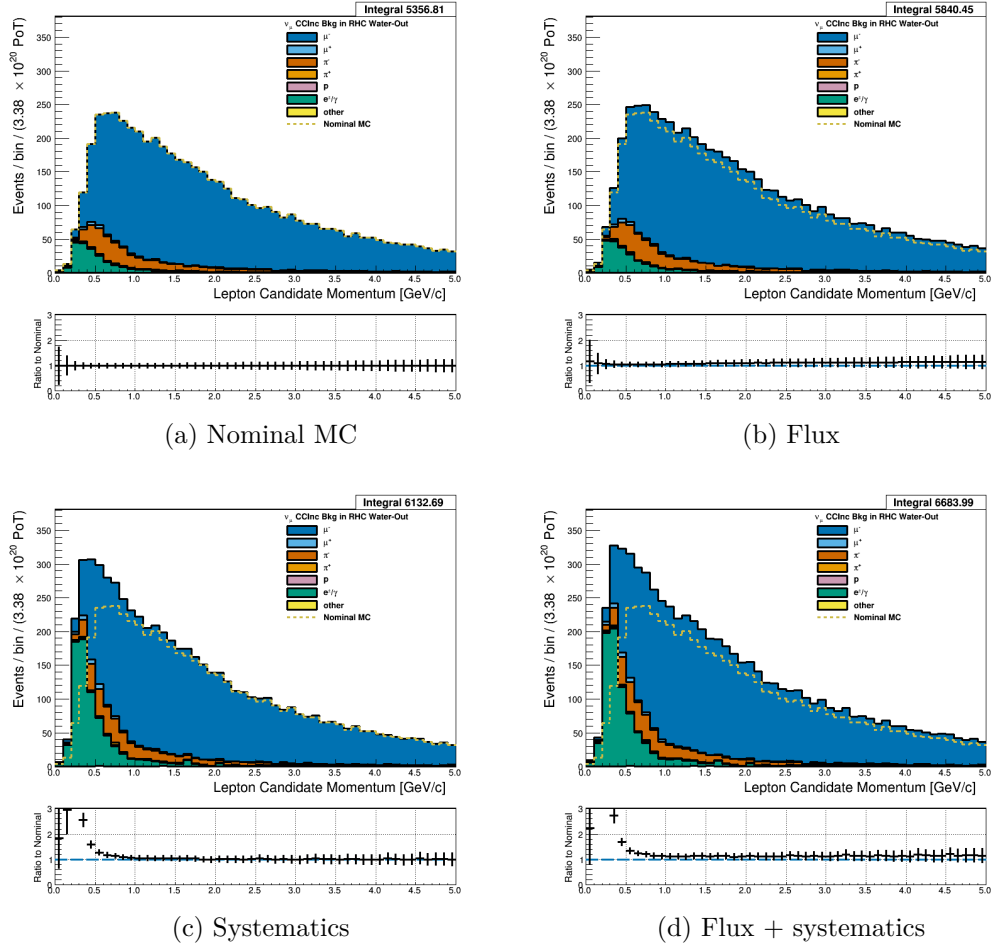


Figure 3.15: Reconstructed lepton candidate momentum separated by true particle species for RHC ν_μ CC Inc. events occurring in the PØD in water-out mode. (a) The nominal MC prediction without any weights applied. (b) The flux tuning are applied. (c) The systematic weighting are applied. (d) Both flux and systematic weighting are applied.

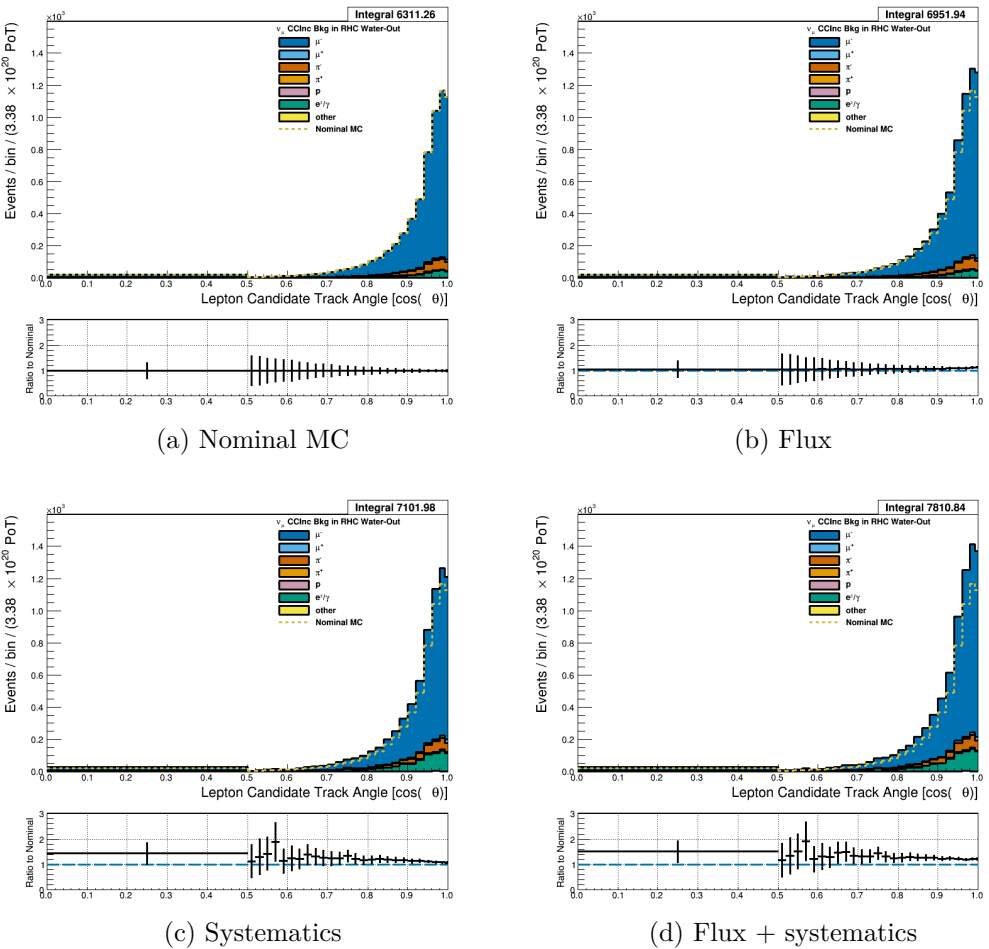


Figure 3.16: Reconstructed lepton candidate angle separated by true particle species for RHC ν_μ CC Inc. events occurring in the PØD in water-out mode. (a) The nominal MC prediction without any weights applied. (b) The flux tuning are applied. (c) The systematic weighting are applied. (d) Both flux and systematic weighting are applied.

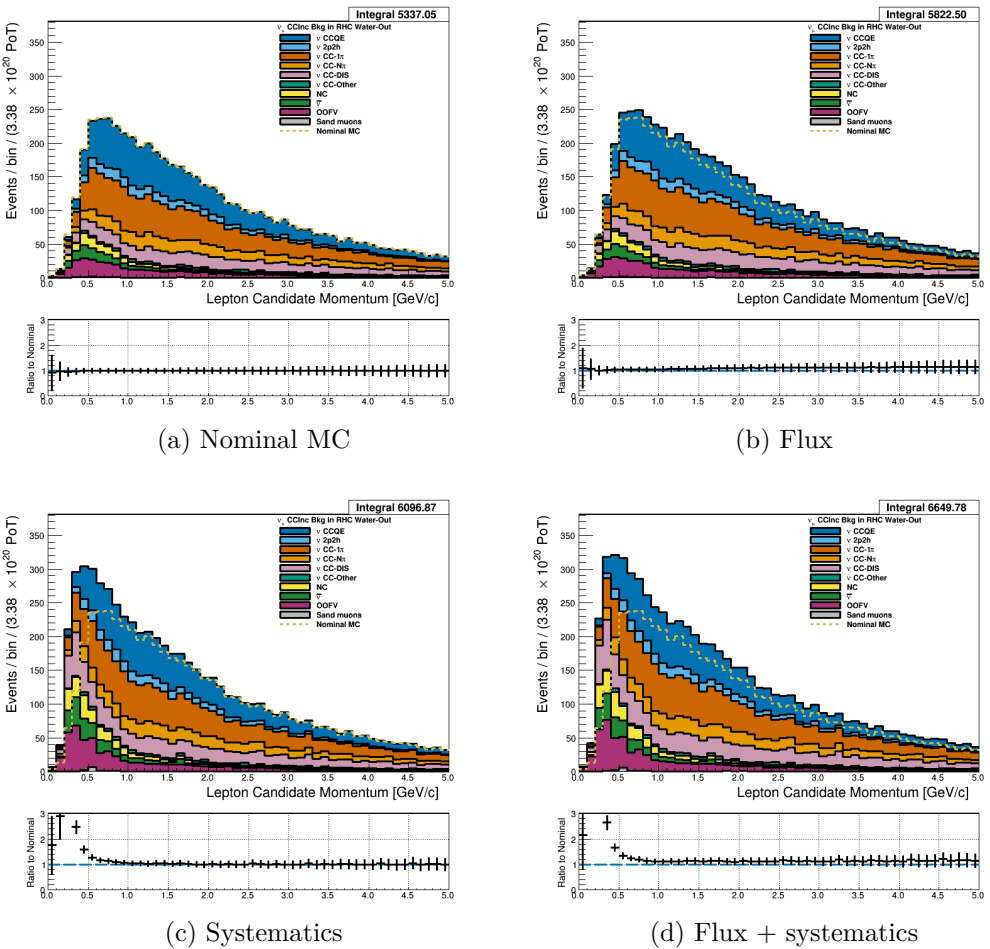


Figure 3.17: Reconstructed lepton candidate momentum separated by NEUT model interaction mode for RHC ν_μ CC Inc. events occurring in the PØD in water-out mode. (a) The nominal MC prediction without any weights applied. (b) The flux tuning are applied. (c) The systematic weighting are applied. (d) Both flux and systematic weighting are applied.

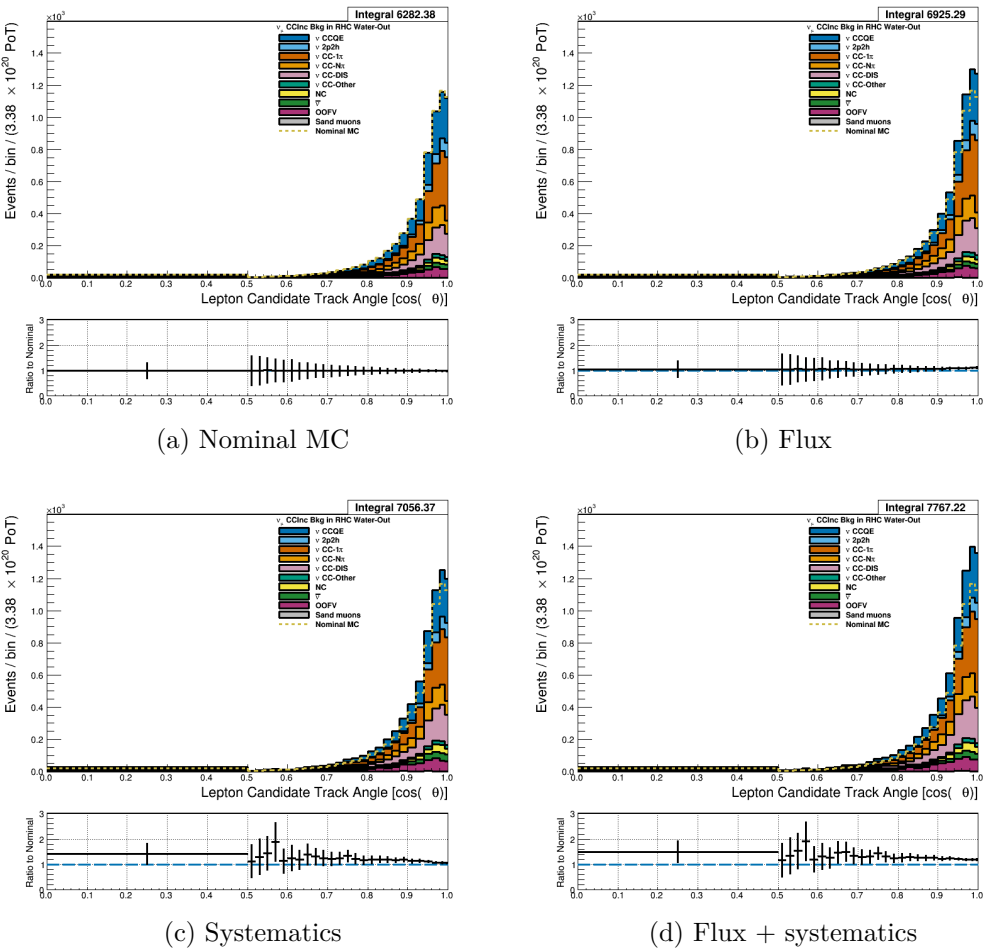


Figure 3.18: Reconstructed lepton candidate $\cos \theta$ separated by NEUT model interaction mode for FHC ν_μ CC Inc. events occurring in the PØD in water-out mode. (a) The nominal MC prediction without any weights applied. (b) The flux tuning are applied. (c) The systematic weighting are applied. (d) Both flux and systematic weighting are applied.

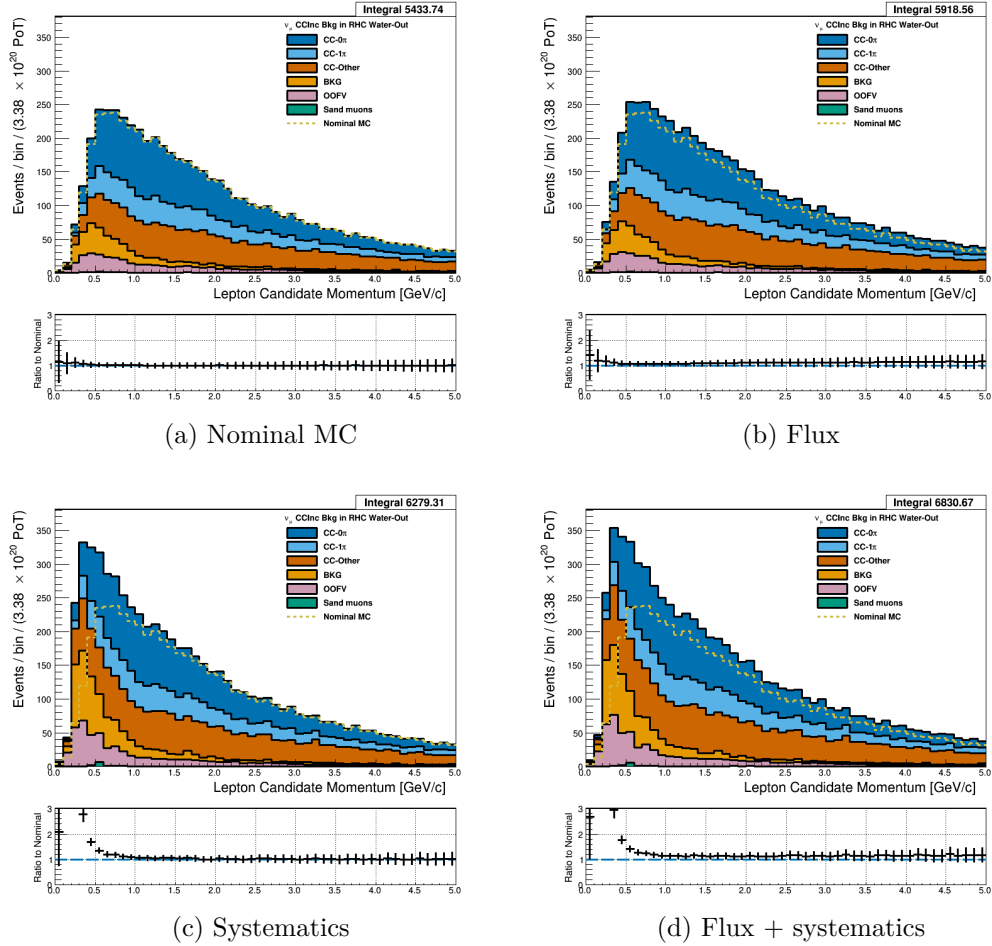


Figure 3.19: Reconstructed lepton candidate momentum separated by topology for FHC ν_μ CC Inc. events occurring in the PØD in water-out mode. (a) The nominal MC prediction without any weights applied. (b) The flux tuning are applied. (c) The systematic weighting are applied. (d) Both flux and systematic weighting are applied.

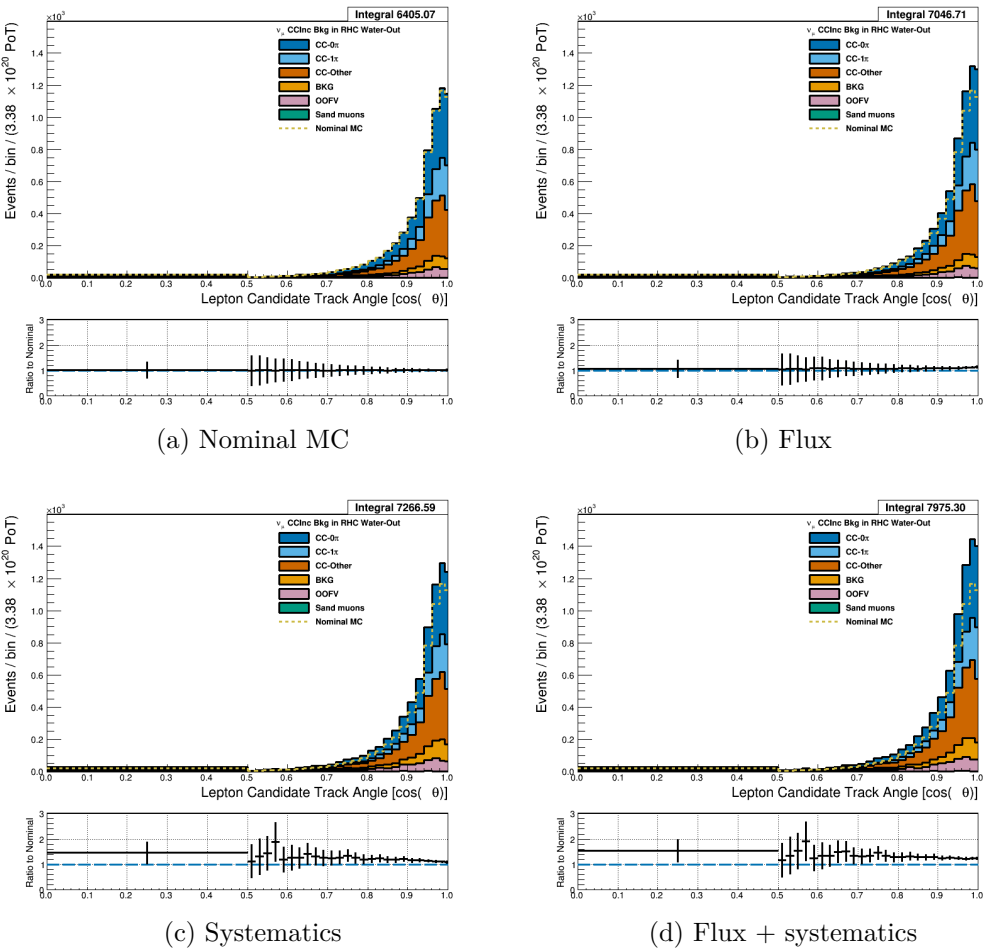


Figure 3.20: Reconstructed lepton candidate $\cos \theta$ separated by topology for FHC ν_μ CC Inc. events occurring in the PØD in water-out mode. (a) The nominal MC prediction without any weights applied. (b) The flux tuning are applied. (c) The systematic weighting are applied. (d) Both flux and systematic weighting are applied.

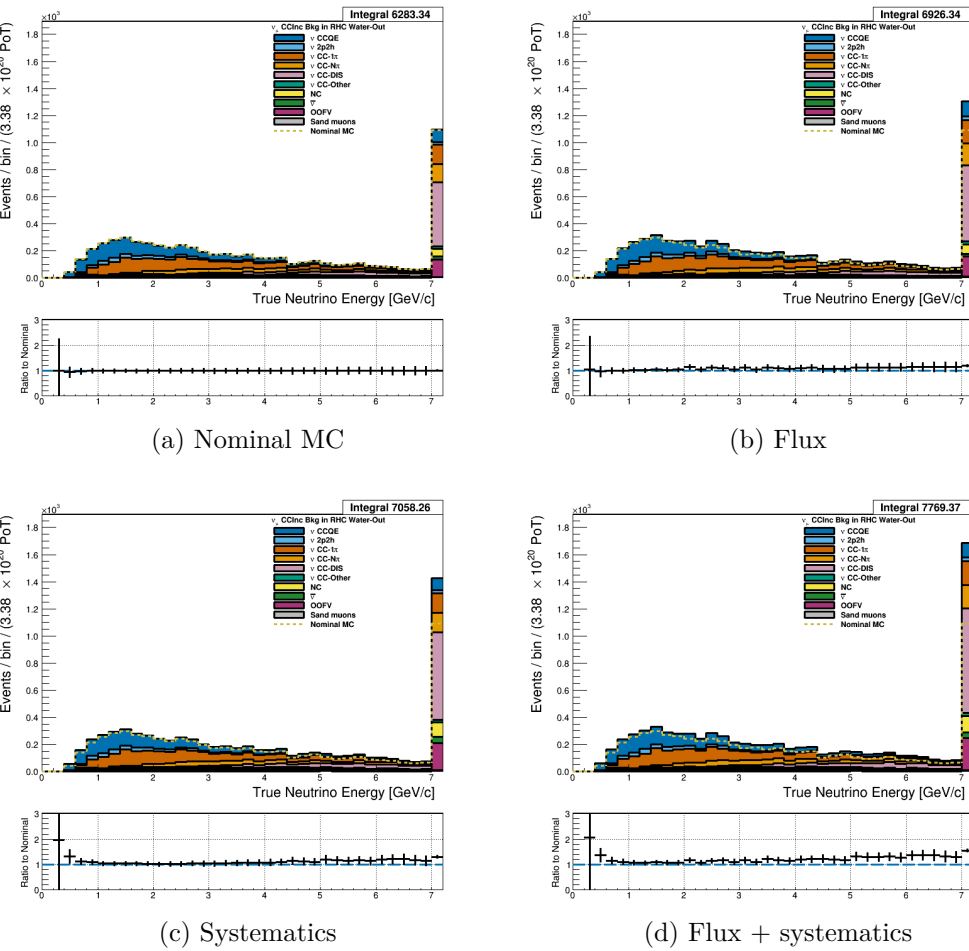


Figure 3.21: True neutrino energy associated with the lepton candidate separated by NEUT model interaction mode for FHC ν_μ CC Inc. events occurring in the PØD in water-out mode. (a) The nominal MC prediction without any weights applied. (b) The flux tuning are applied. (c) The systematic weighting are applied. (d) Both flux and systematic weighting are applied.

522 3.4.2 CC 1-Track (CCQE Enhanced)

523 **3.4.2.1 ν_μ Selection in FHC Mode:** Shown in

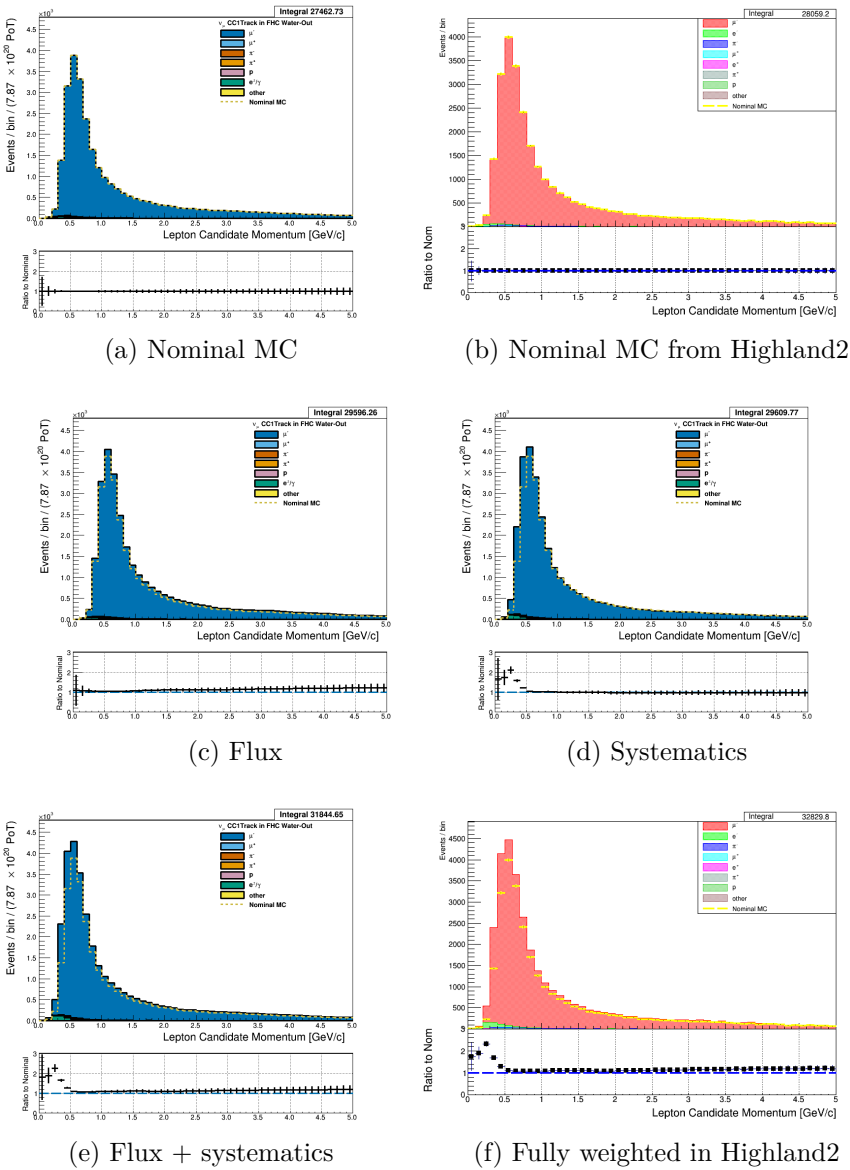


Figure 3.22: Reconstructed lepton candidate momentum separated by true particle species for FHC ν_μ CC 1-Track events occurring in the PØD in water-out mode. (a) The nominal MC prediction without any weights applied. (b) The same POT-normalized plot as (a) using a subset of the water-out MC in Highland. (c) The flux tuning are applied. (d) The systematic weighting are applied. (e) Both flux and systematic weighting are applied. (f) The same POT-normalized plot as (e) using a subset of the water-out MC in Highland. There is a $\sim 1\%$ difference between Highland2 and BANFF since a subset of the MC was used to generate Highland plots.

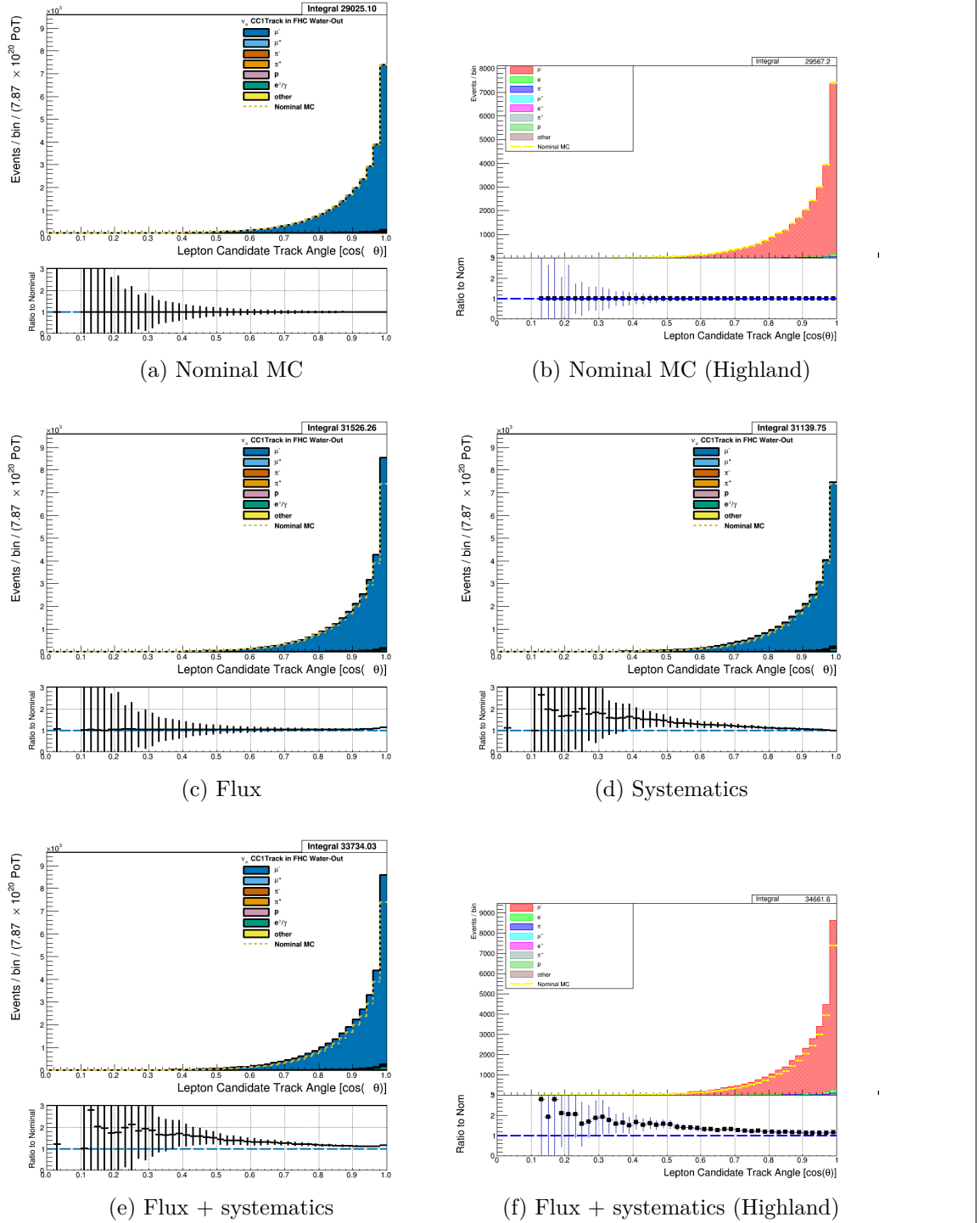


Figure 3.23: Reconstructed lepton candidate angle separated by true particle species for FHC ν_μ CC 1-Track events occurring in the PØD in water-out mode. (a) The nominal MC prediction without any weights applied. (b) The same POT-normalized plot as (a) using a subset of the water-out MC in Highland. (c) The flux tuning are applied. (d) The systematic weighting are applied. (e) Both flux and systematic weighting are applied. (f) The same POT-normalized plot as (e) using a subset of the water-out MC in Highland. There is a ~1% difference between Highland2 and BANFF⁵⁴ since a subset of the MC was used to generate Highland plots.

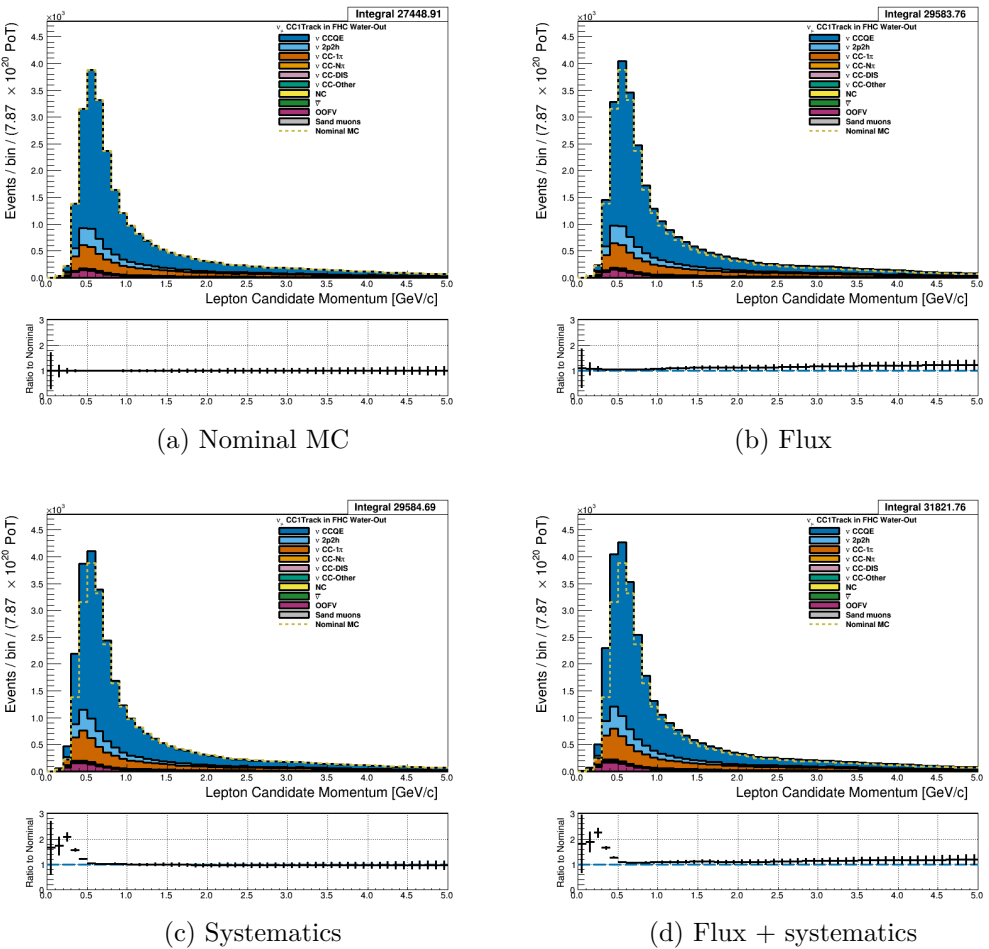


Figure 3.24: Reconstructed lepton candidate momentum separated by NEUT model interaction mode for FHC ν_μ CC 1-Track events occurring in the PØD in water-out mode. (a) The nominal MC prediction without any weights applied. (b) The flux tuning are applied. (c) The systematic weighting are applied. (d) Both flux and systematic weighting are applied.

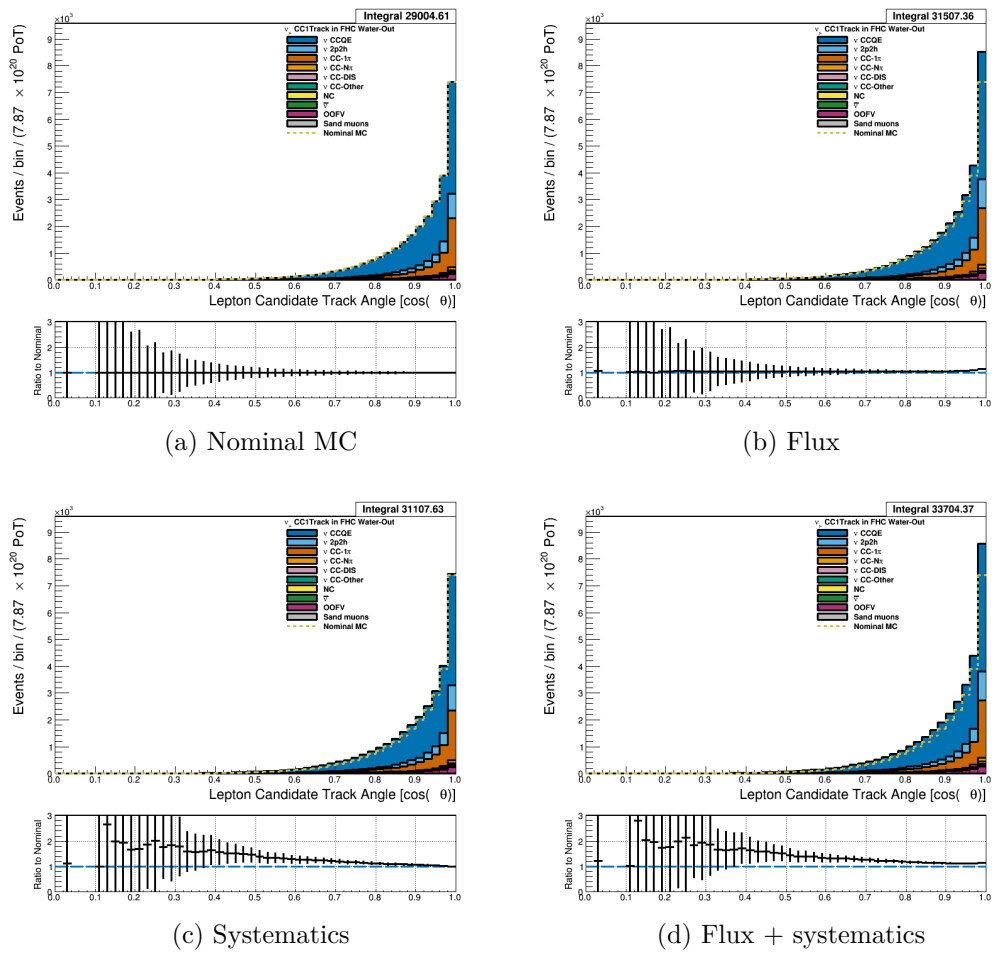


Figure 3.25: Reconstructed lepton candidate $\cos \theta$ separated by NEUT model interaction mode for FHC ν_μ CC 1-Track events occurring in the PØD in water-out mode. (a) The nominal MC prediction without any weights applied. (b) The flux tuning are applied. (c) The systematic weighting are applied. (d) Both flux and systematic weighting are applied.

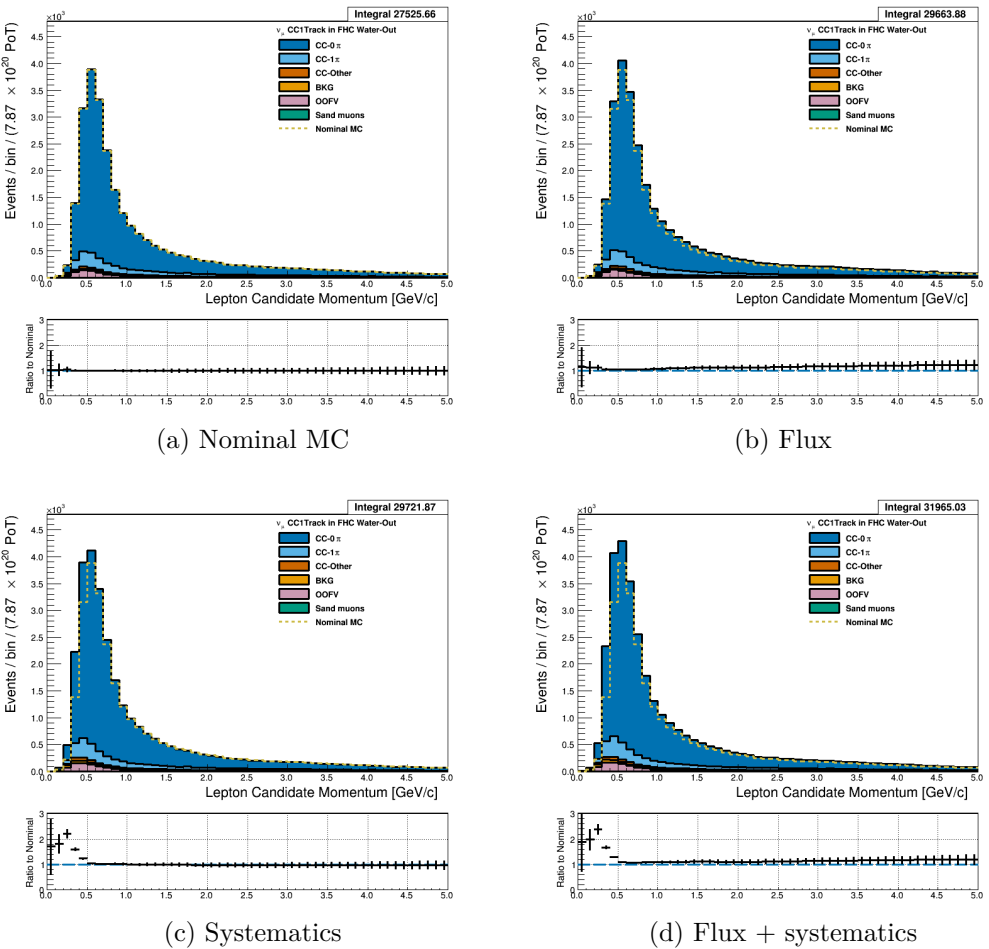


Figure 3.26: Reconstructed lepton candidate momentum separated by topology for FHC ν_μ CC 1-Track events occurring in the PØD in water-out mode. (a) The nominal MC prediction without any weights applied. (b) The flux tuning are applied. (c) The systematic weighting are applied. (d) Both flux and systematic weighting are applied.

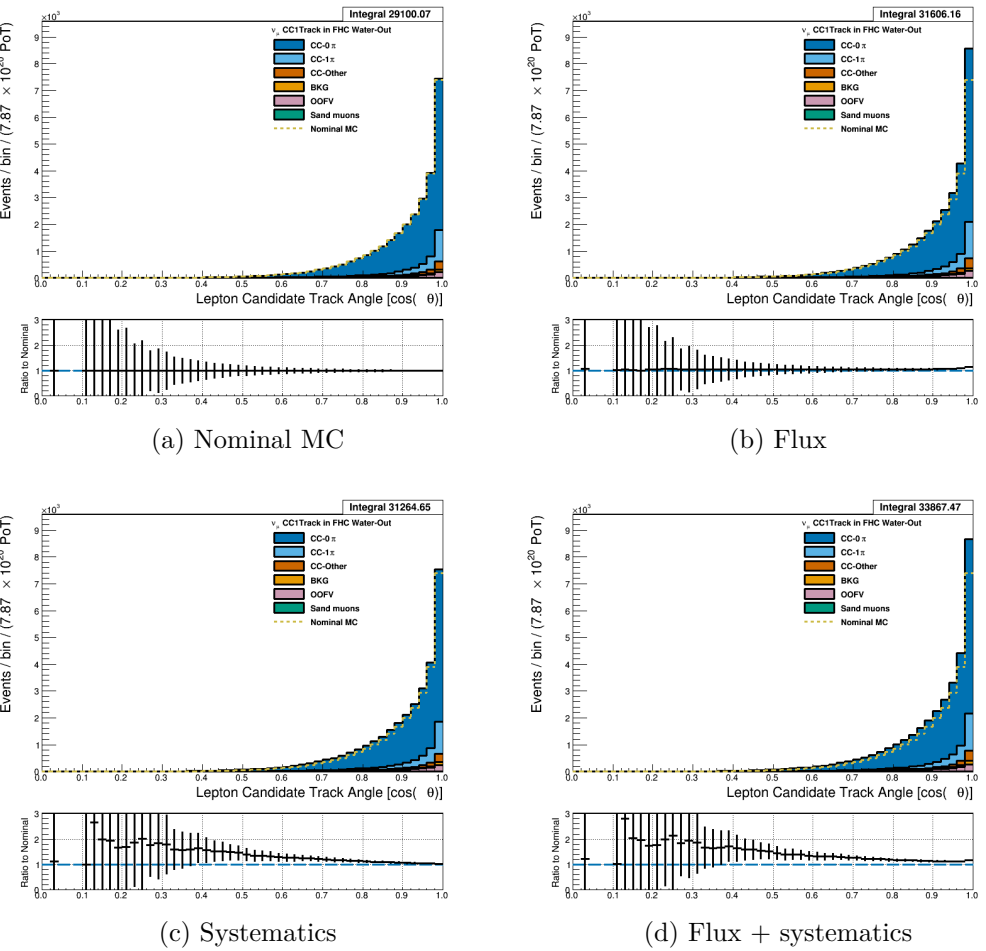


Figure 3.27: Reconstructed lepton candidate $\cos \theta$ separated by topology for FHC ν_μ CC 1-Track events occurring in the PØD in water-out mode. (a) The nominal MC prediction without any weights applied. (b) The flux tuning are applied. (c) The systematic weighting are applied. (d) Both flux and systematic weighting are applied.

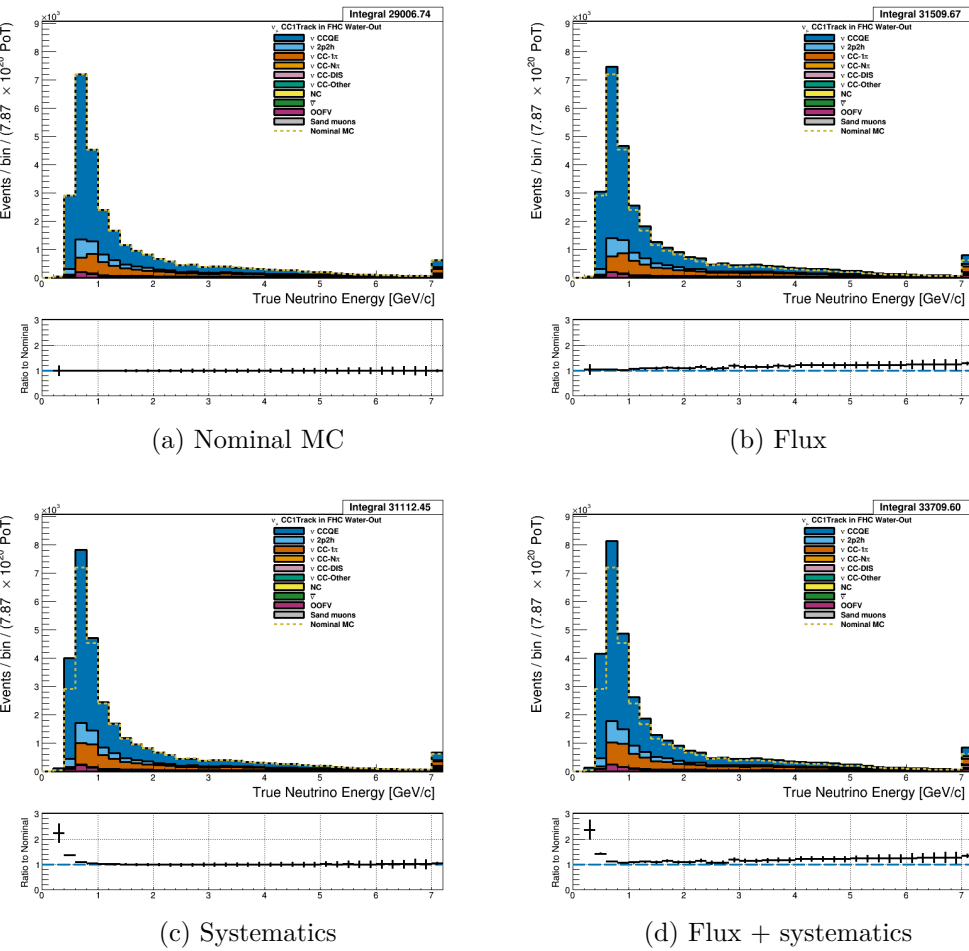


Figure 3.28: True neutrino energy associated with the lepton candidate separated by NEUT model interaction mode for FHC ν_μ CC 1-Track events occurring in the PØD in water-out mode. (a) The nominal MC prediction without any weights applied. (b) The flux tuning are applied. (c) The systematic weighting are applied. (d) Both flux and systematic weighting are applied.

524 3.4.2.2 $\bar{\nu}_\mu$ Selection in RHC Mode: Figures

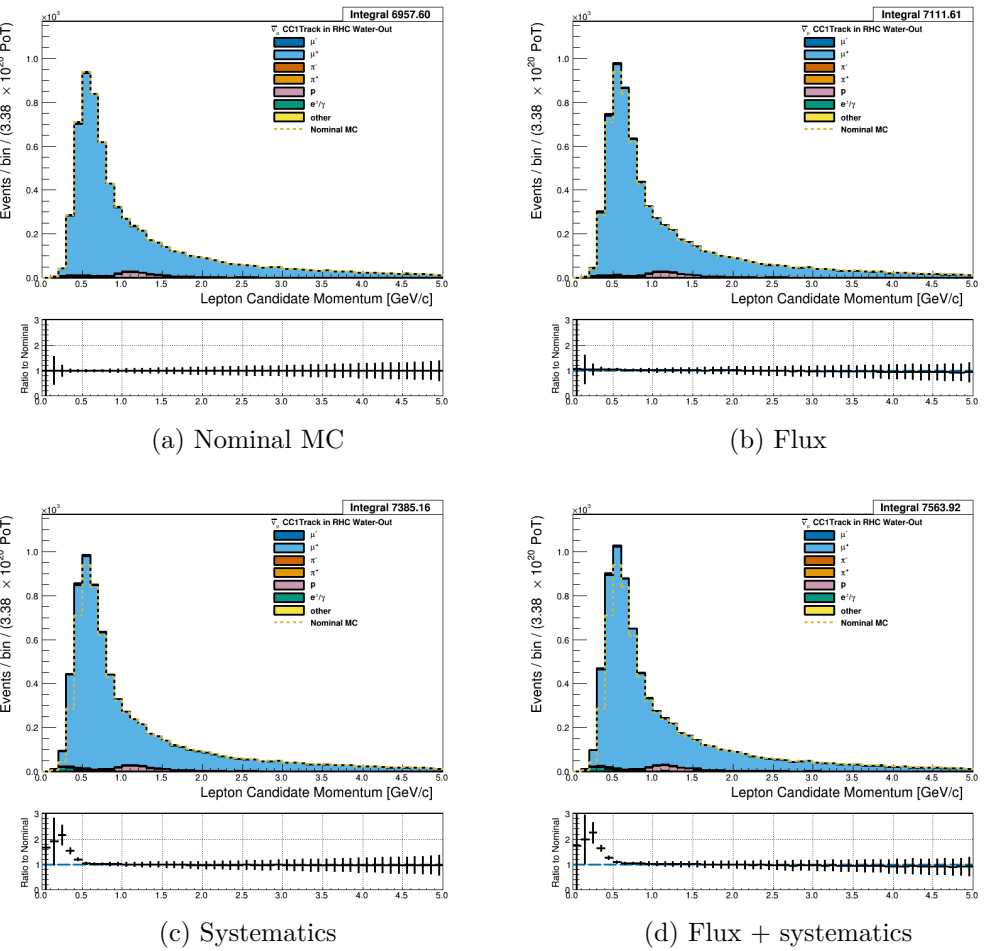


Figure 3.29: Reconstructed lepton candidate momentum separated by true particle species for RHC $\bar{\nu}_\mu$ CC 1-Track events occurring in the PØD in water-out mode. Reconstructed lepton candidate angle separated by true particle species for RHC $\bar{\nu}_\mu$ CC Inc. events occurring in the PØD in water-in mode. (a) The nominal MC prediction without any weights applied. (b) The flux tuning are applied. (c) The systematic weighting are applied. (c) Both flux and systematic weighting are applied.

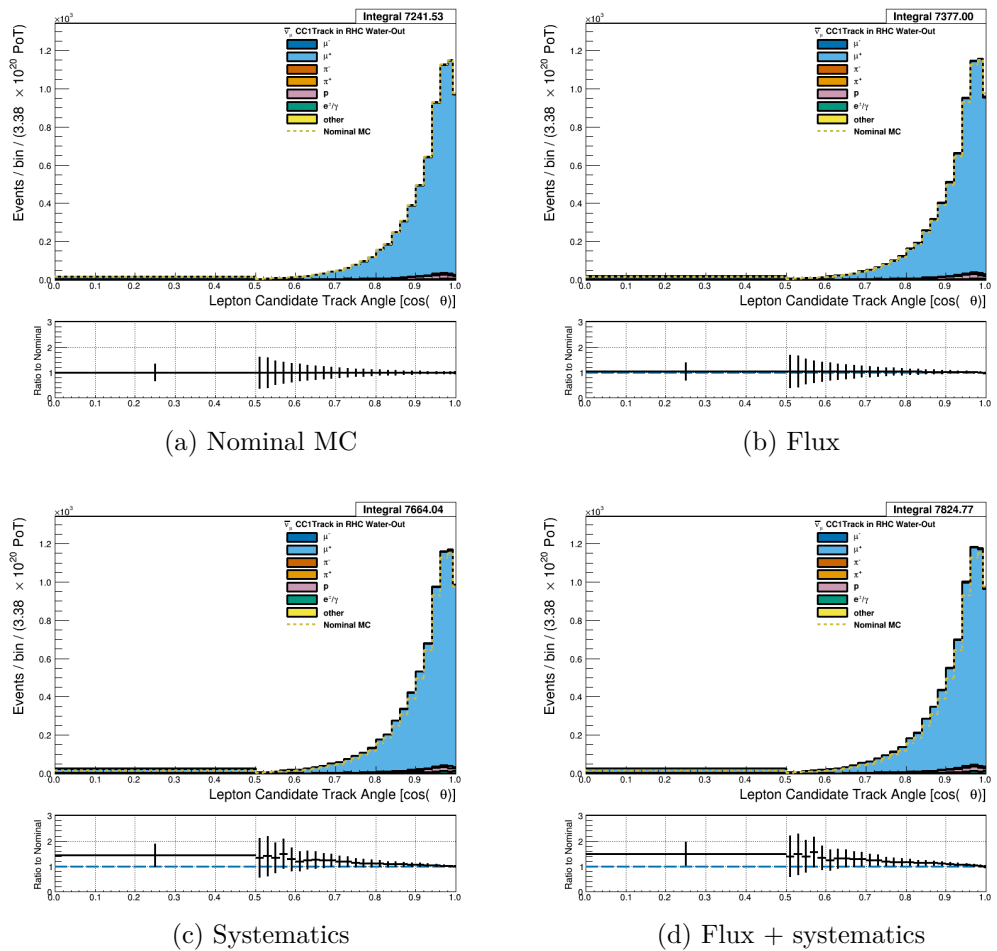


Figure 3.30: Reconstructed lepton candidate angle separated by true particle species for RHC $\bar{\nu}_\mu$ CC 1-Track events occurring in the PØD in water-out mode. (a) The nominal MC prediction without any weights applied. (b) The flux tuning are applied. (c) The systematic weighting are applied. (d) Both flux and systematic weighting are applied.

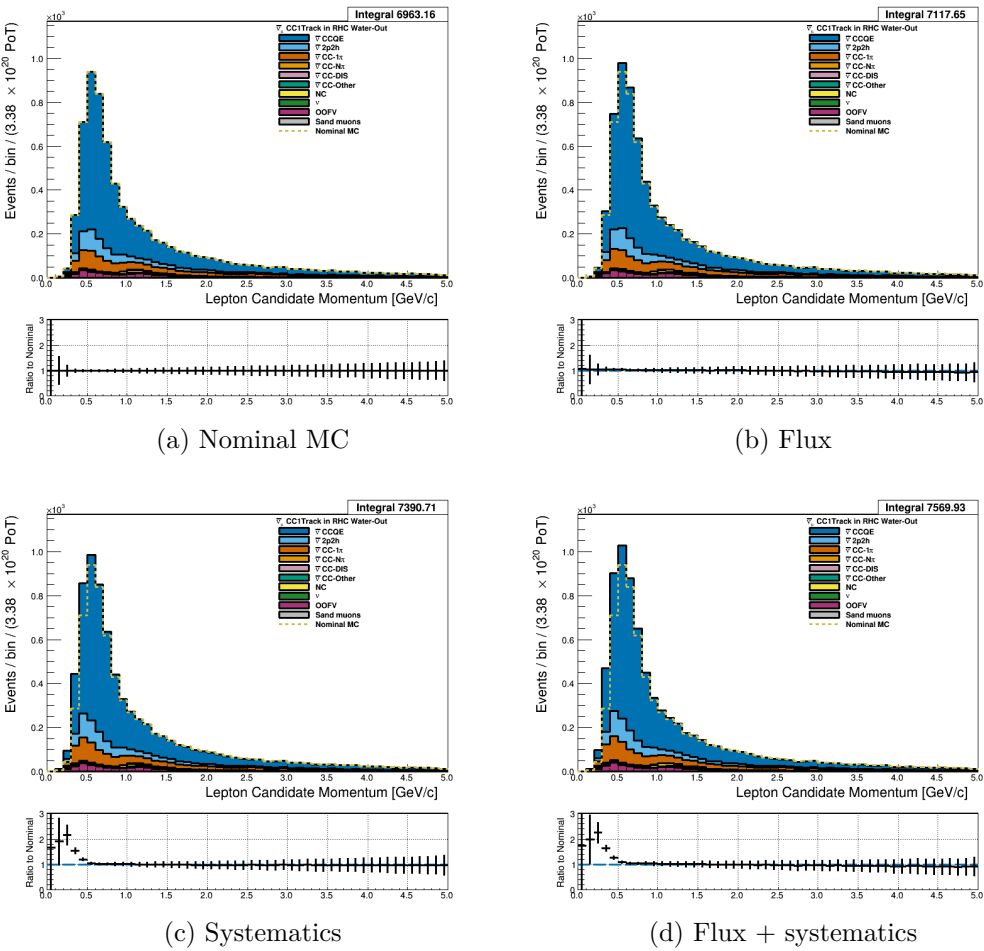


Figure 3.31: Reconstructed lepton candidate momentum separated by NEUT model interaction mode for RHC $\bar{\nu}_\mu$ CC 1-Track events occurring in the PØD in water-out mode. (a) The nominal MC prediction without any weights applied. (b) The flux tuning are applied. (c) The systematic weighting are applied. (d) Both flux and systematic weighting are applied.

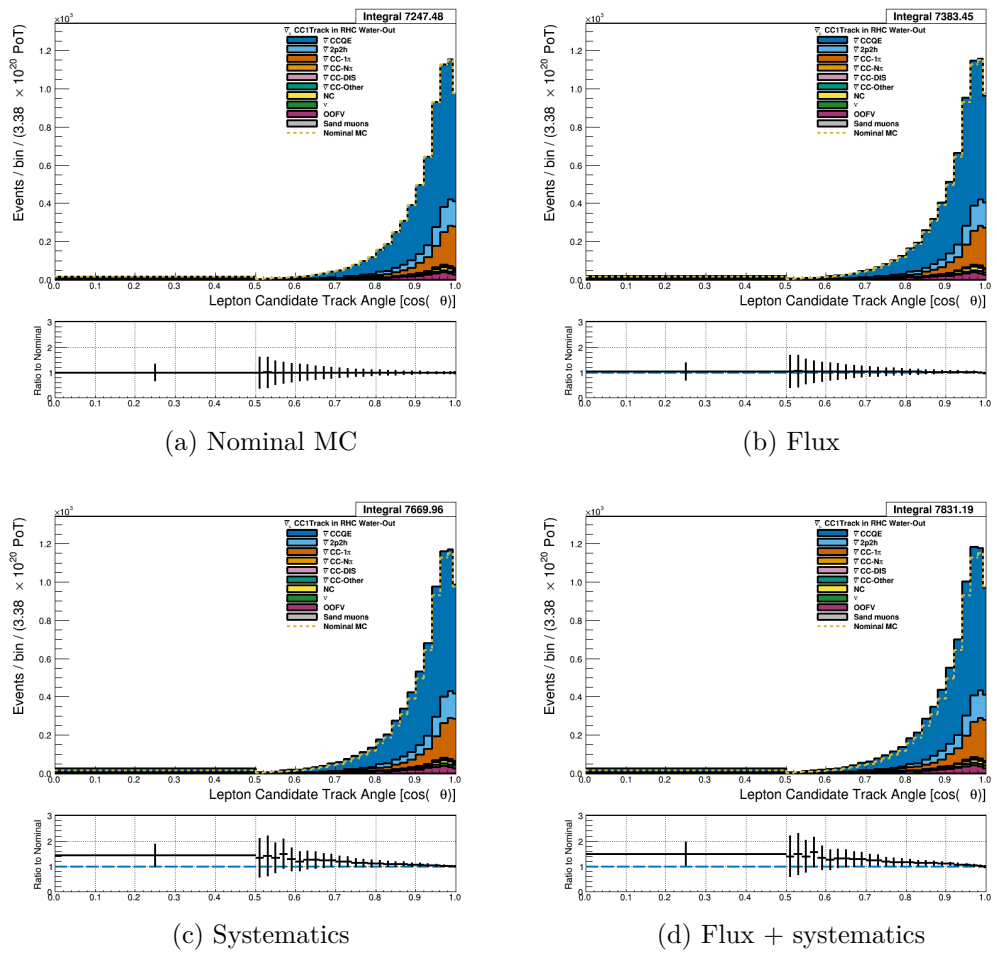


Figure 3.32: Reconstructed lepton candidate $\cos \theta$ separated by NEUT model interaction mode for RHC $\bar{\nu}_\mu$ CC 1-TracI events occurring in the P0D in water-out mode. (a) The nominal MC prediction without any weights applied. (b) The flux tuning are applied. (c) The systematic weighting are applied. (d) Both flux and systematic weighting are applied.

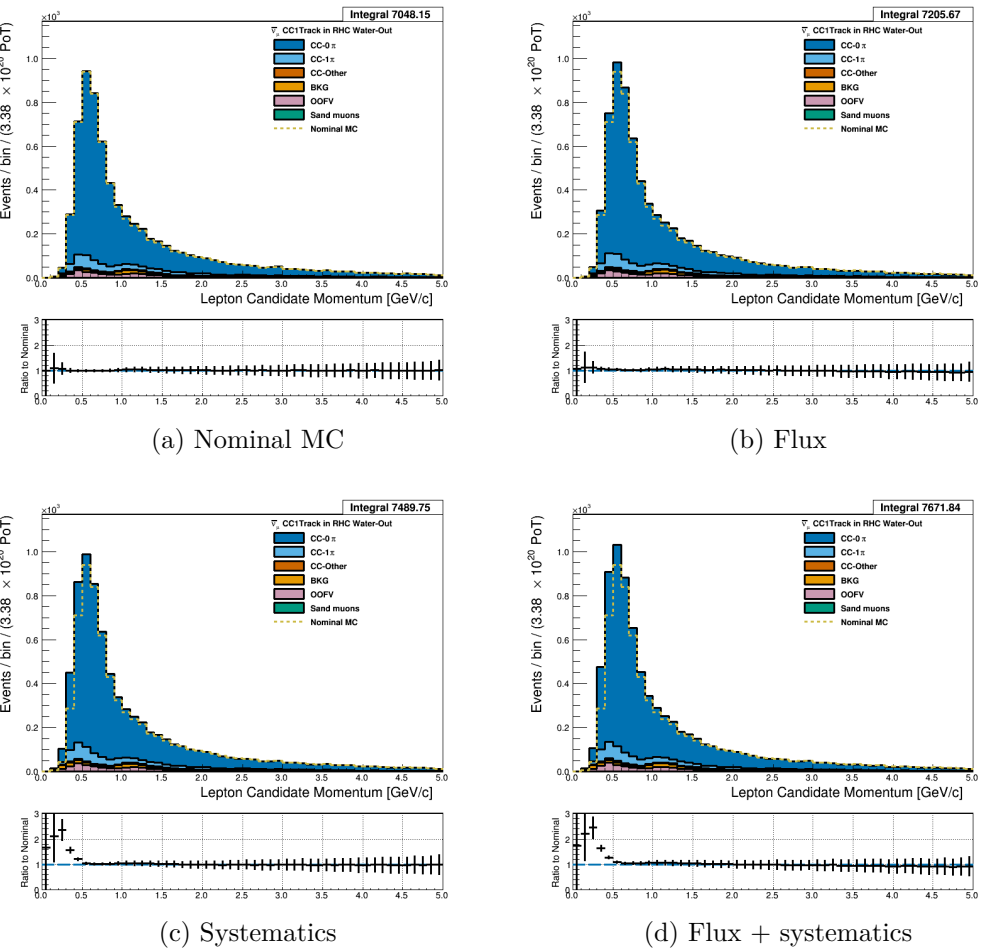


Figure 3.33: Reconstructed lepton candidate momentum separated by topology for RHC $\bar{\nu}_\mu$ CC 1-Track events occurring in the PØD in water-out mode. (a) The nominal MC prediction without any weights applied. (b) The flux tuning are applied. (c) The systematic weighting are applied. (d) Both flux and systematic weighting are applied.

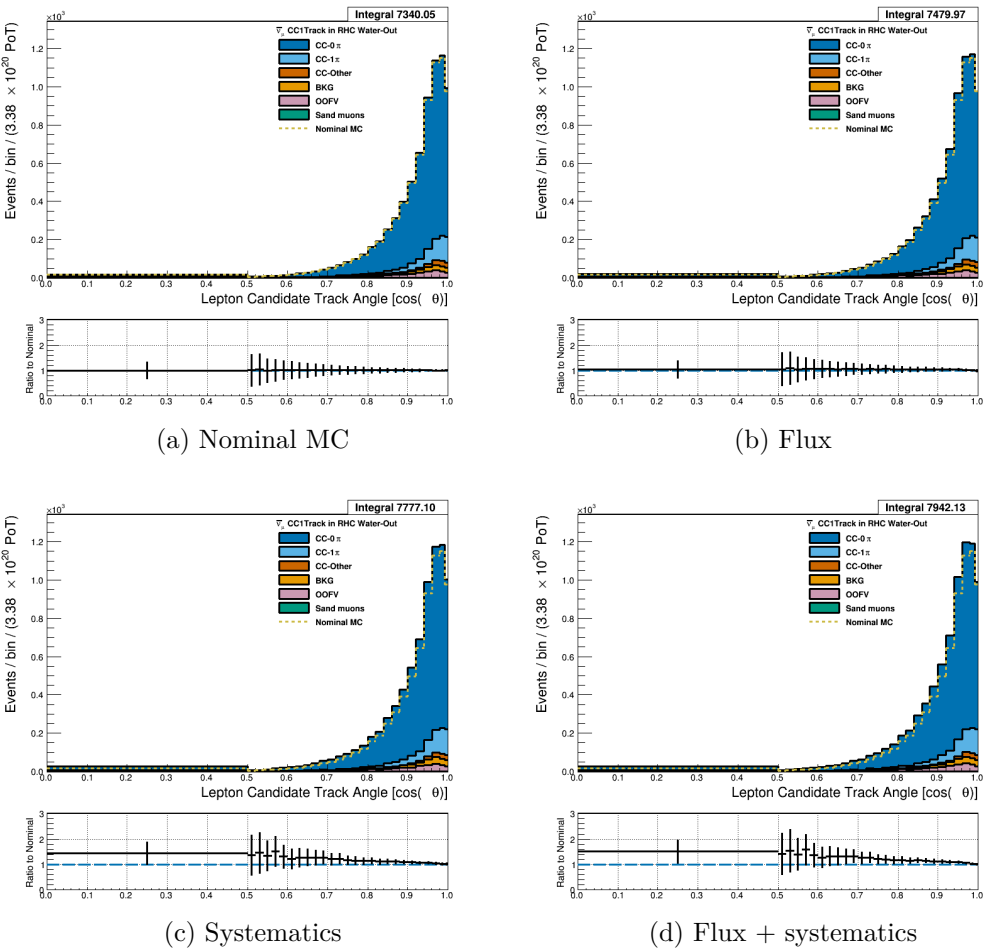


Figure 3.34: Reconstructed lepton candidate $\cos \theta$ separated by topology for RHC $\bar{\nu}_\mu$ CC 1-Track events occurring in the PØD in water-out mode. (a) The nominal MC prediction without any weights applied. (b) The flux tuning are applied. (c) The systematic weighting are applied. (d) Both flux and systematic weighting are applied.

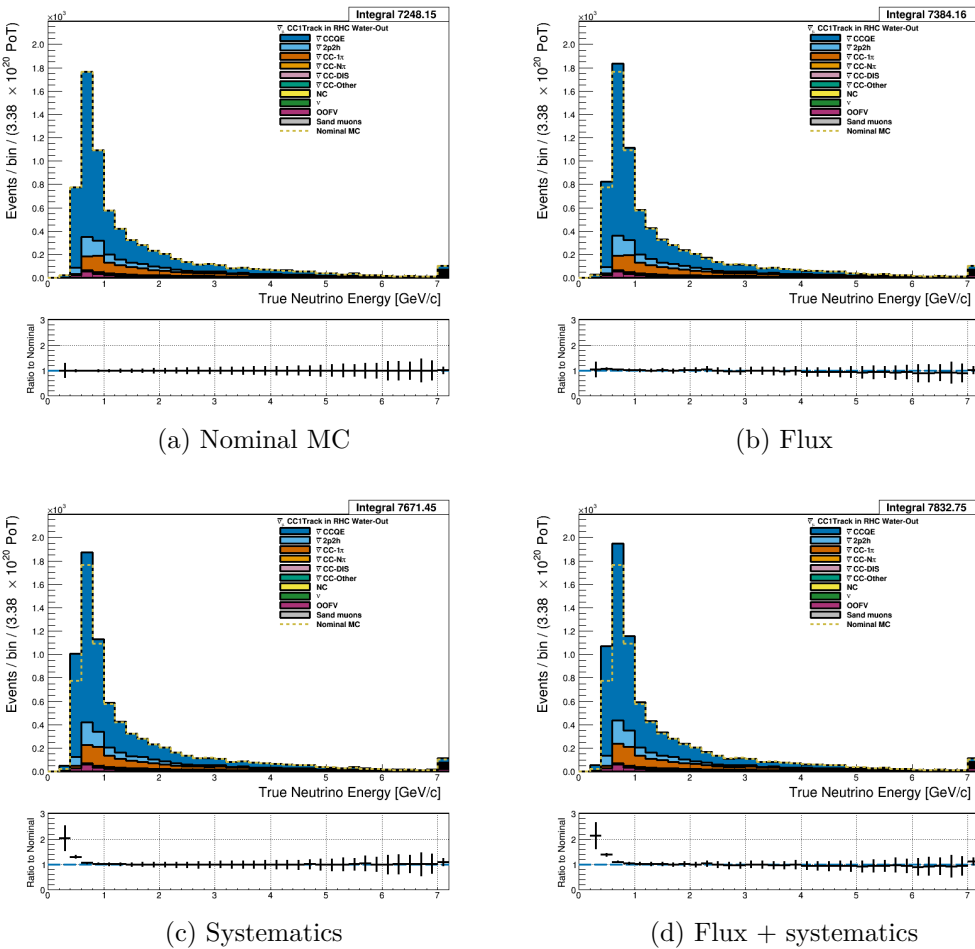


Figure 3.35: True neutrino energy associated with the lepton candidate separated by NEUT model interaction mode for RHC $\bar{\nu}_\mu$ CC 1-Track events occurring in the PØD in water-out mode. (a) The nominal MC prediction without any weights applied. (b) The flux tuning are applied. (c) The systematic weighting are applied. (d) Both flux and systematic weighting are applied.

525 **3.4.2.3 ν_μ Background Selection in RHC Mode:** Text [Add figures here](#)

526 **3.4.3 CC N-Tracks (CCnQE Enhanced)**

527 Text [Add figures here](#)

528 **3.4.3.1 ν_μ Selection in FHC Mode:** Text

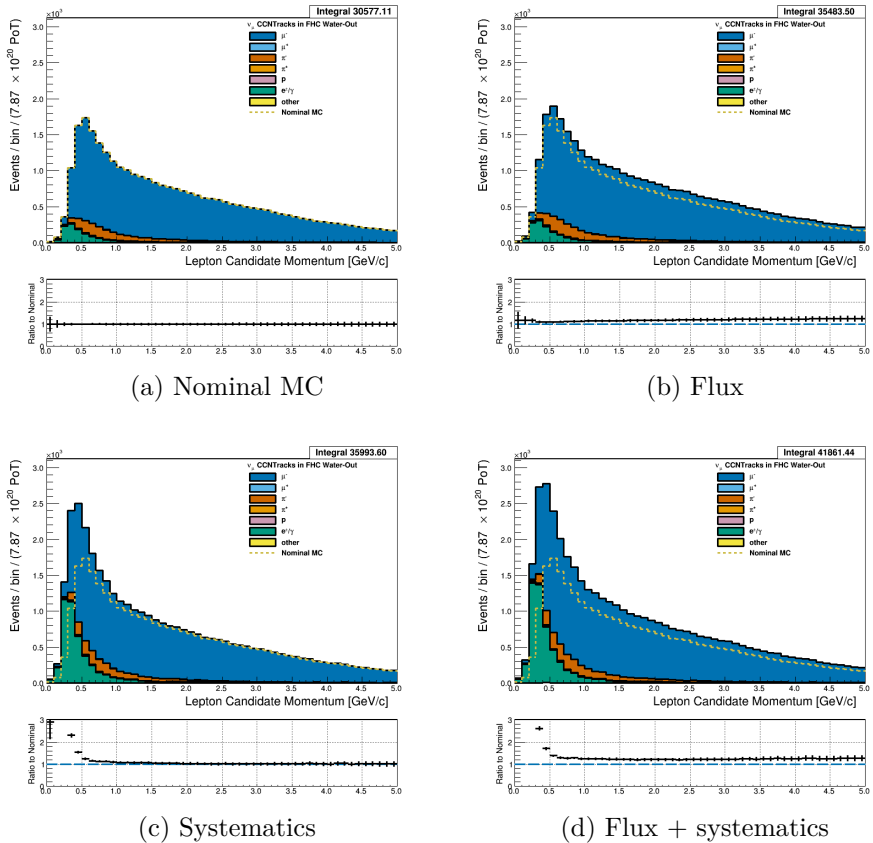


Figure 3.36: Reconstructed lepton candidate momentum separated by true particle species for FHC ν_μ CC N-Tracks events occurring in the PØD in water-out mode. (a) The nominal MC prediction without any weights applied. (b) The flux tuning are applied. (c) The systematic weighting are applied. (e) Both flux and systematic weighting are applied.

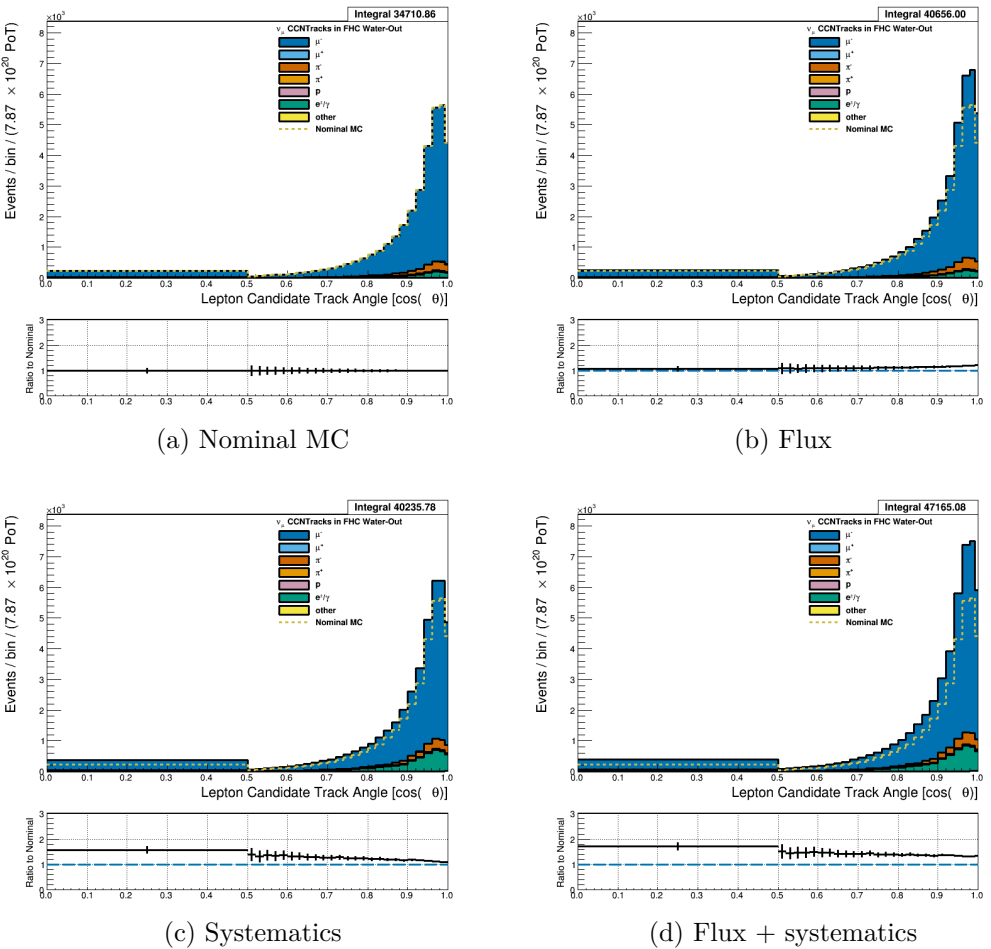


Figure 3.37: Reconstructed lepton candidate angle separated by true particle species for FHC ν_μ CC N-Tracks events occurring in the PØD in water-out mode. (a) The nominal MC prediction without any weights applied. (b) The flux tuning are applied. (c) The systematic weighting are applied. (d) Both flux and systematic weighting are applied.

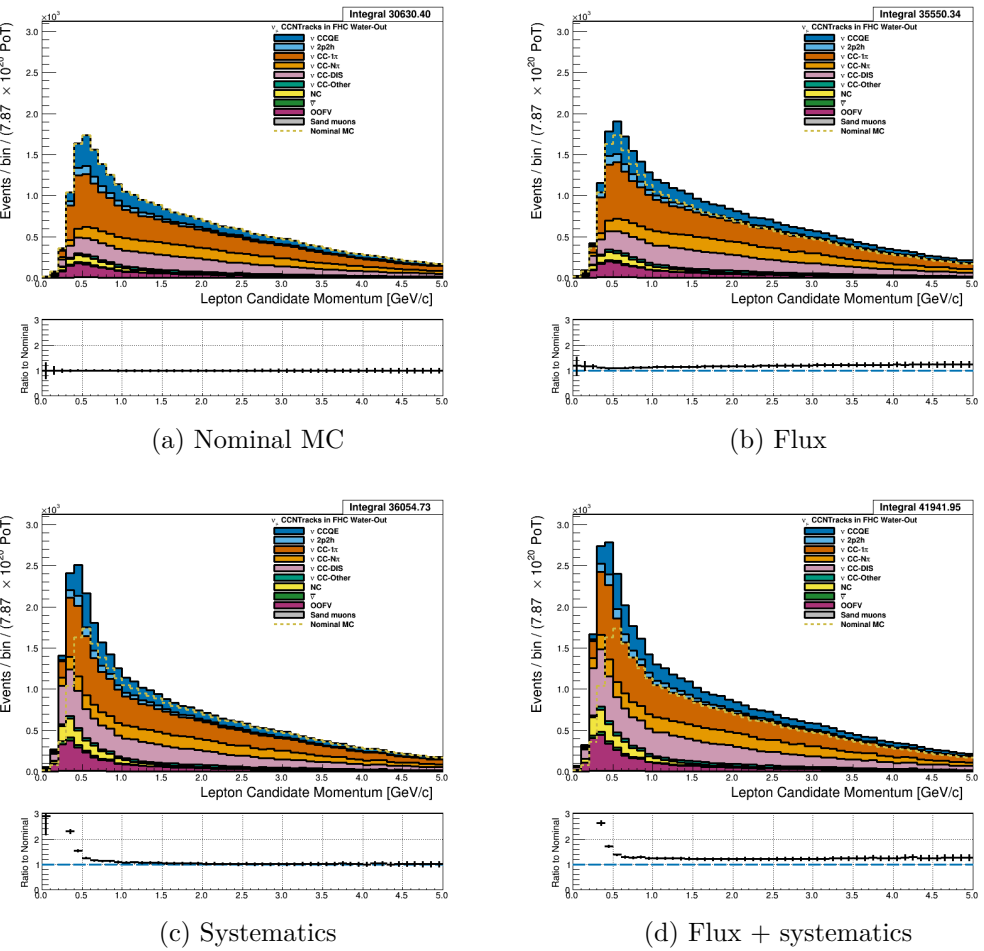


Figure 3.38: Reconstructed lepton candidate momentum separated by NEUT model interaction mode for FHC ν_μ CC N-Tracks events occurring in the PØD in water-out mode. (a) The nominal MC prediction without any weights applied. (b) The flux tuning are applied. (c) The systematic weighting are applied. (d) Both flux and systematic weighting are applied.

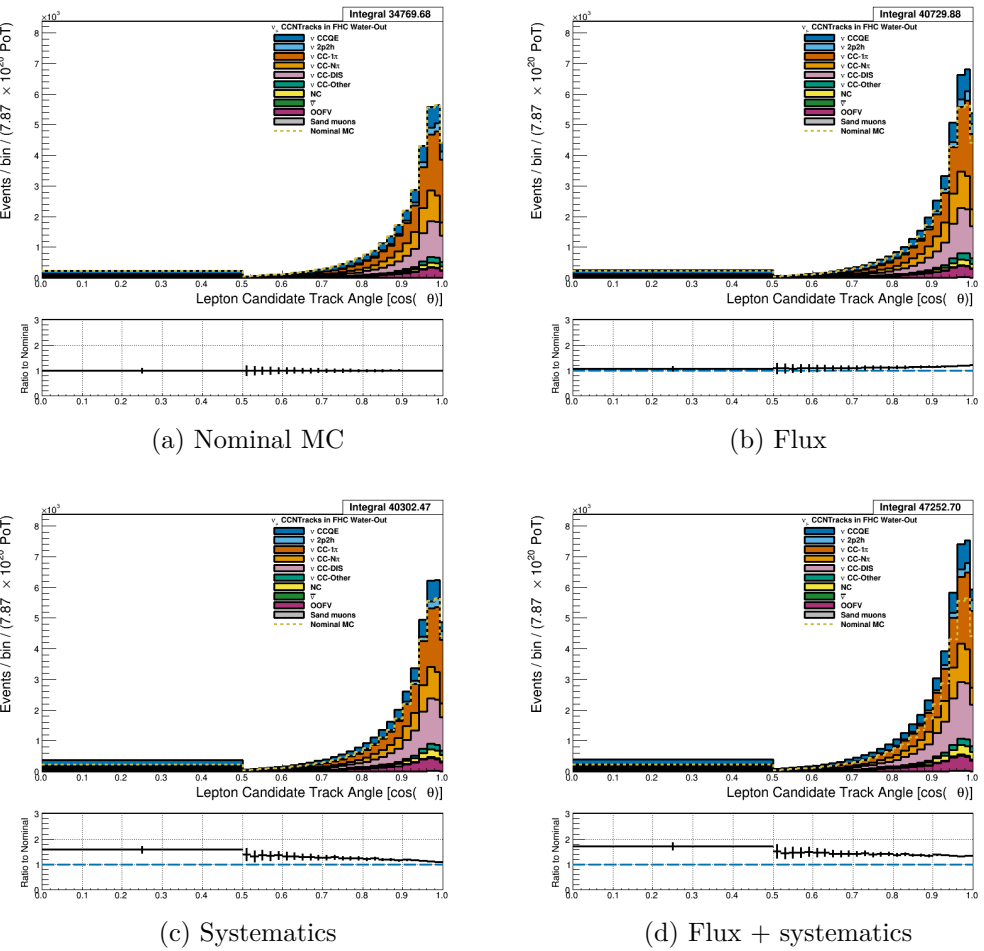


Figure 3.39: Reconstructed lepton candidate $\cos \theta$ separated by NEUT model interaction mode for FHC ν_μ CC N-Tracks events occurring in the PØD in water-out mode. (a) The nominal MC prediction without any weights applied. (b) The flux tuning are applied. (c) The systematic weighting are applied. (d) Both flux and systematic weighting are applied.

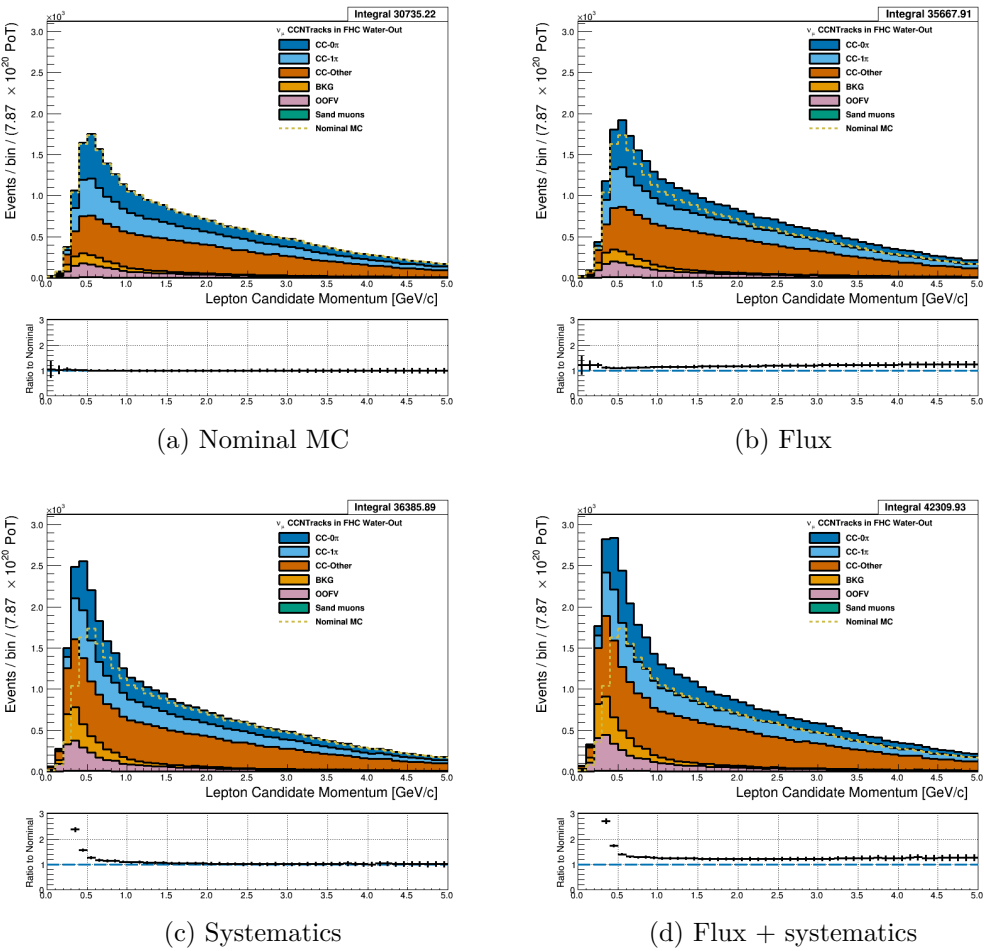


Figure 3.40: Reconstructed lepton candidate momentum separated by topology for FHC ν_μ CC N-Tracks events occurring in the PØD in water-out mode. (a) The nominal MC prediction without any weights applied. (b) The flux tuning are applied. (c) The systematic weighting are applied. (d) Both flux and systematic weighting are applied.

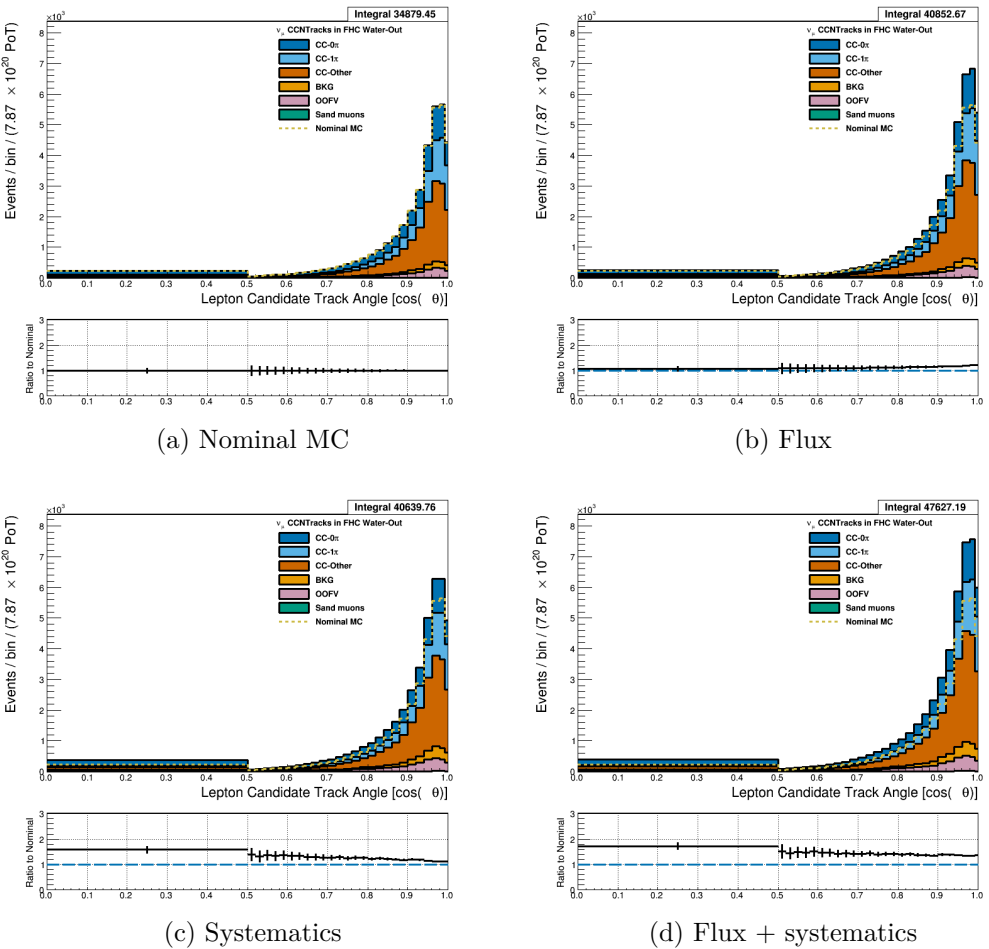


Figure 3.41: Reconstructed lepton candidate $\cos \theta$ separated by topology for FHC ν_μ CC N-Tracks events occurring in the PØD in water-out mode. (a) The nominal MC prediction without any weights applied. (b) The flux tuning are applied. (c) The systematic weighting are applied. (d) Both flux and systematic weighting are applied.

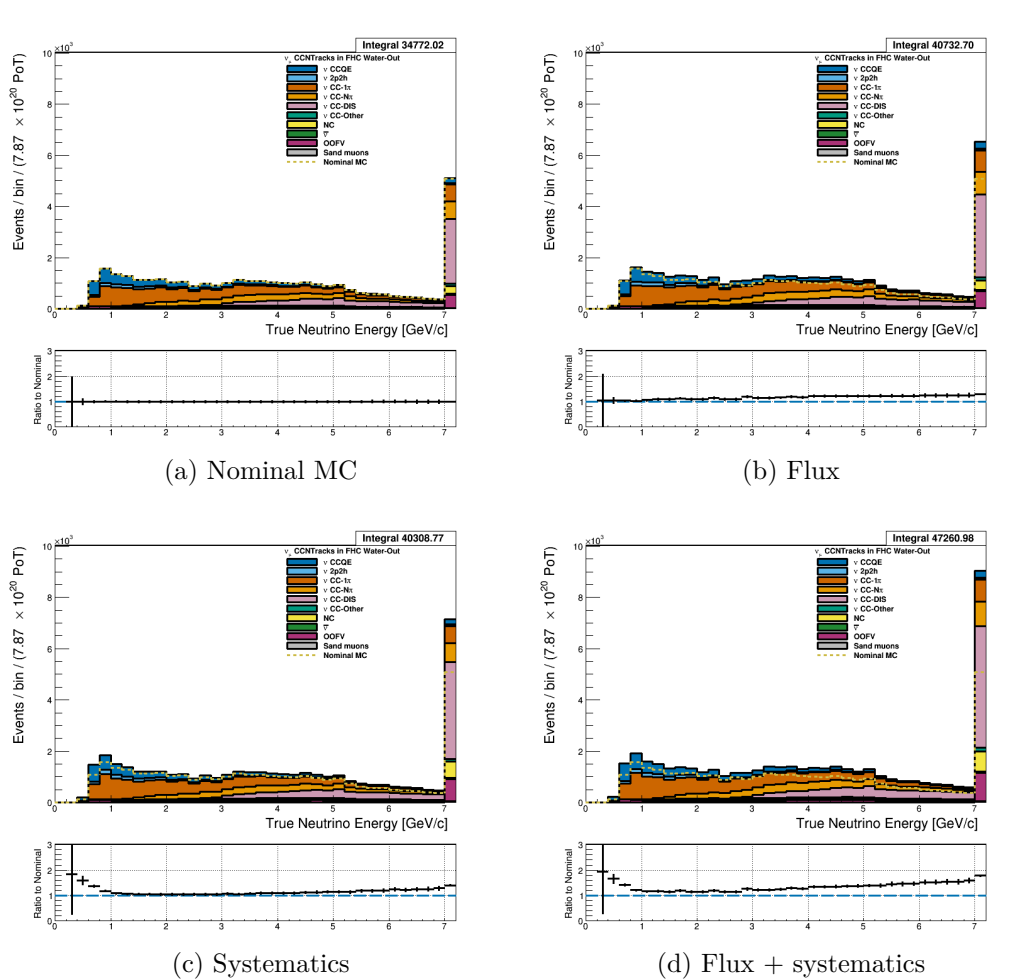


Figure 3.42: True neutrino energy associated with the lepton candidate separated by NEUT model interaction mode for FHC ν_μ CC N-Tracks events occurring in the PØD in water-out mode. (a) The nominal MC prediction without any weights applied. (b) The flux tuning are applied. (c) The systematic weighting are applied. (d) Both flux and systematic weighting are applied.

3.4.3.2 $\bar{\nu}_\mu$ Selection in RHC Mode: Text goes here

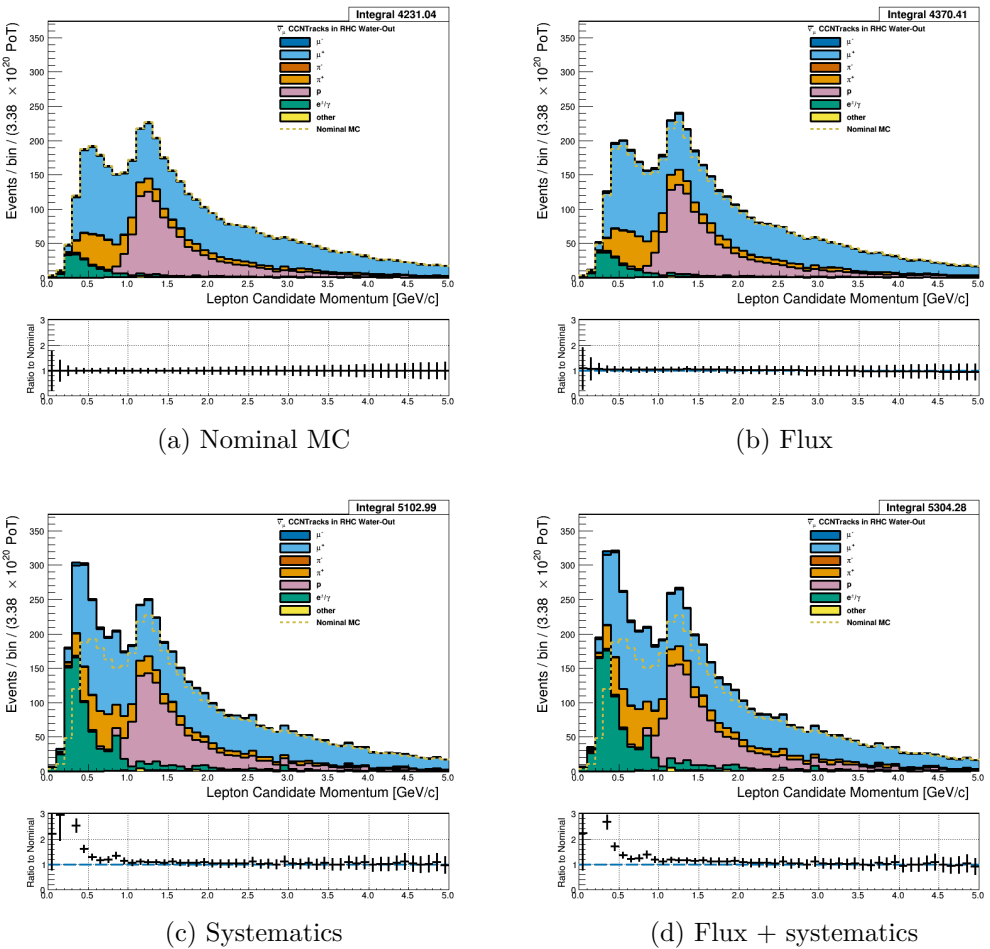


Figure 3.43: Reconstructed lepton candidate momentum separated by true particle species for RHC $\bar{\nu}_\mu$ CC N-Tracks events occurring in the PØD in water-out mode. Reconstructed lepton candidate angle separated by true particle species for RHC $\bar{\nu}_\mu$ CC N-Tracks events occurring in the PØD in water-in mode. (a) The nominal MC prediction without any weights applied. (b) The flux tuning are applied. (c) The systematic weighting are applied. (d) Both flux and systematic weighting are applied.

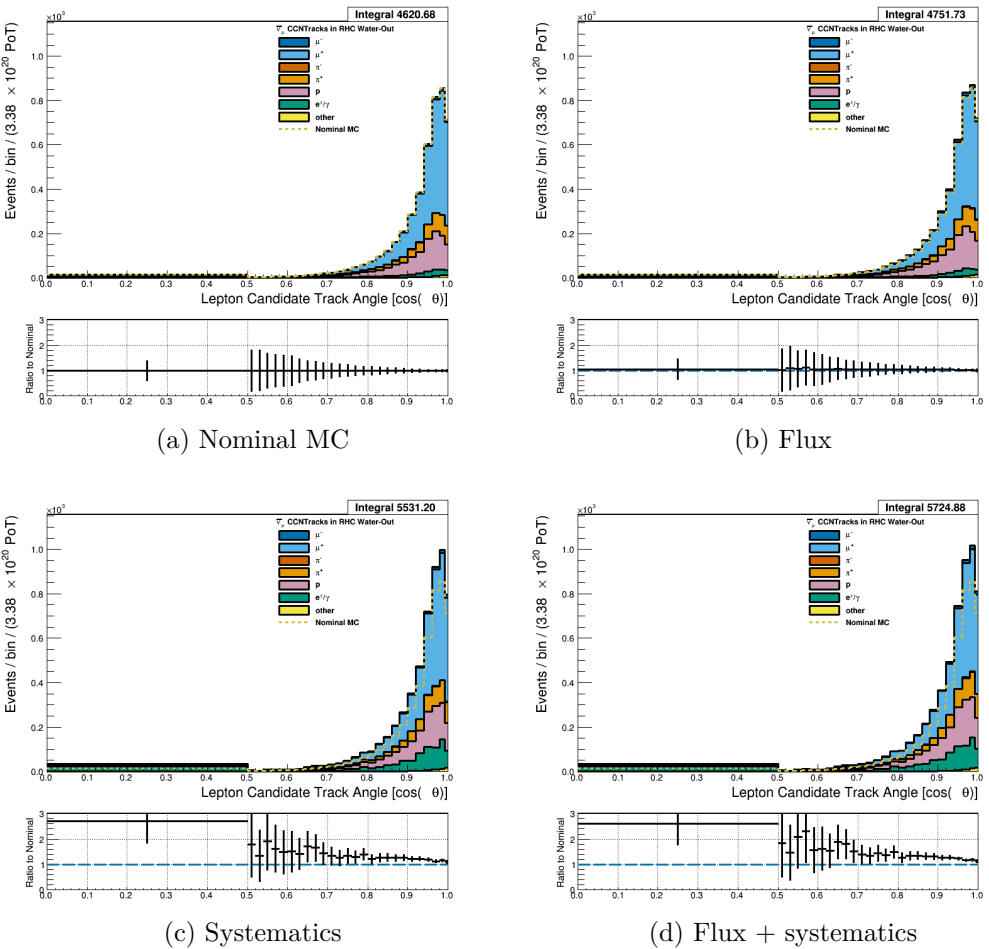


Figure 3.44: Reconstructed lepton candidate angle separated by true particle species for RHC $\bar{\nu}_\mu$ CC N-Tracks events occurring in the PØD in water-out mode. (a) The nominal MC prediction without any weights applied. (b) The flux tuning are applied. (c) The systematic weighting are applied. (d) Both flux and systematic weighting are applied.

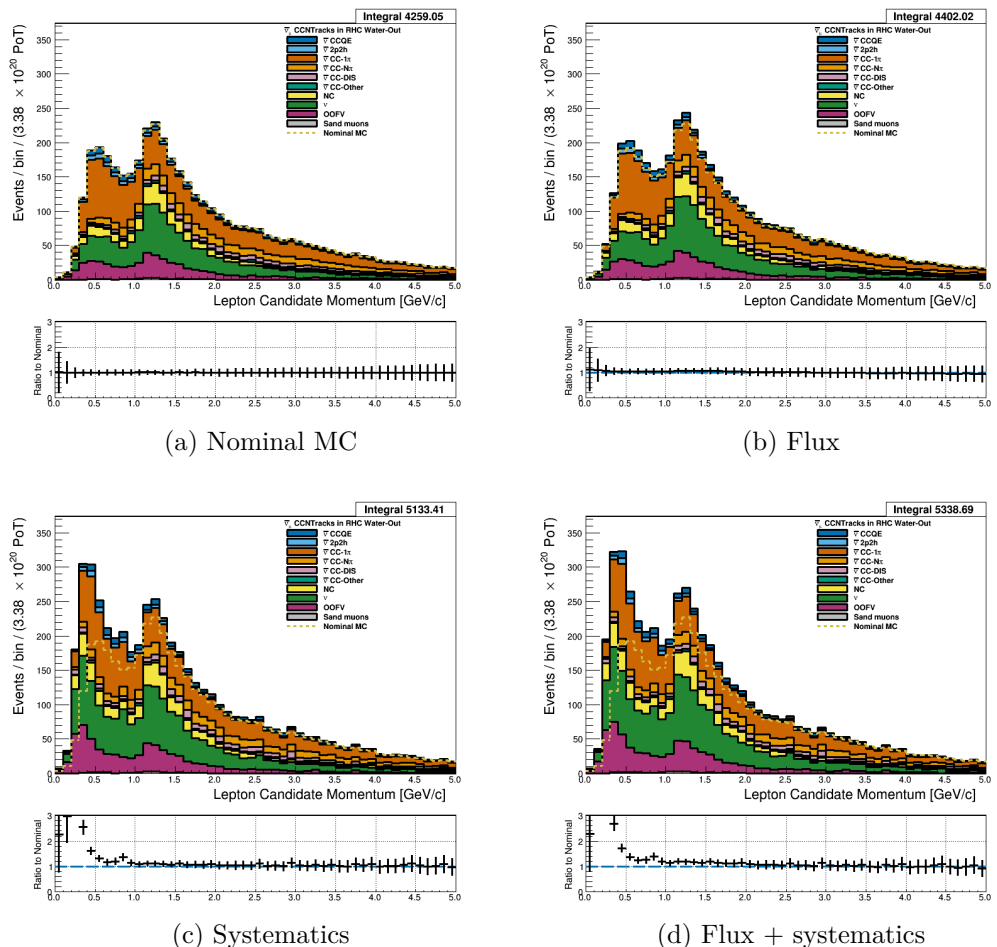


Figure 3.45: Reconstructed lepton candidate momentum separated by NEUT model interaction mode for RHC $\bar{\nu}_\mu$ CC N-Tracks events occurring in the PØD in water-out mode. (a) The nominal MC prediction without any weights applied. (b) The flux tuning are applied. (c) The systematic weighting are applied. (d) Both flux and systematic weighting are applied.

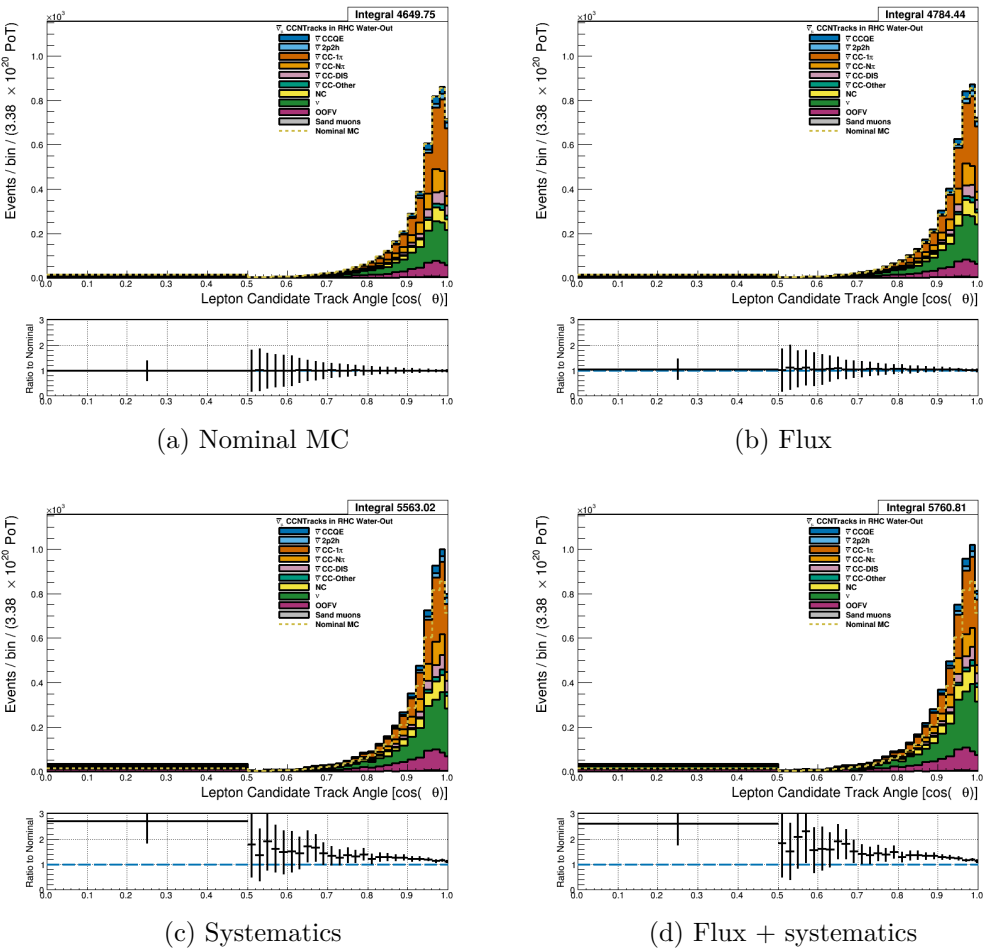


Figure 3.46: Reconstructed lepton candidate $\cos \theta$ separated by NEUT model interaction mode for RHC $\bar{\nu}_\mu$ CC N-Tracks events occurring in the PØD in water-out mode. (a) The nominal MC prediction without any weights applied. (b) The flux tuning are applied. (c) The systematic weighting are applied. (d) Both flux and systematic weighting are applied.

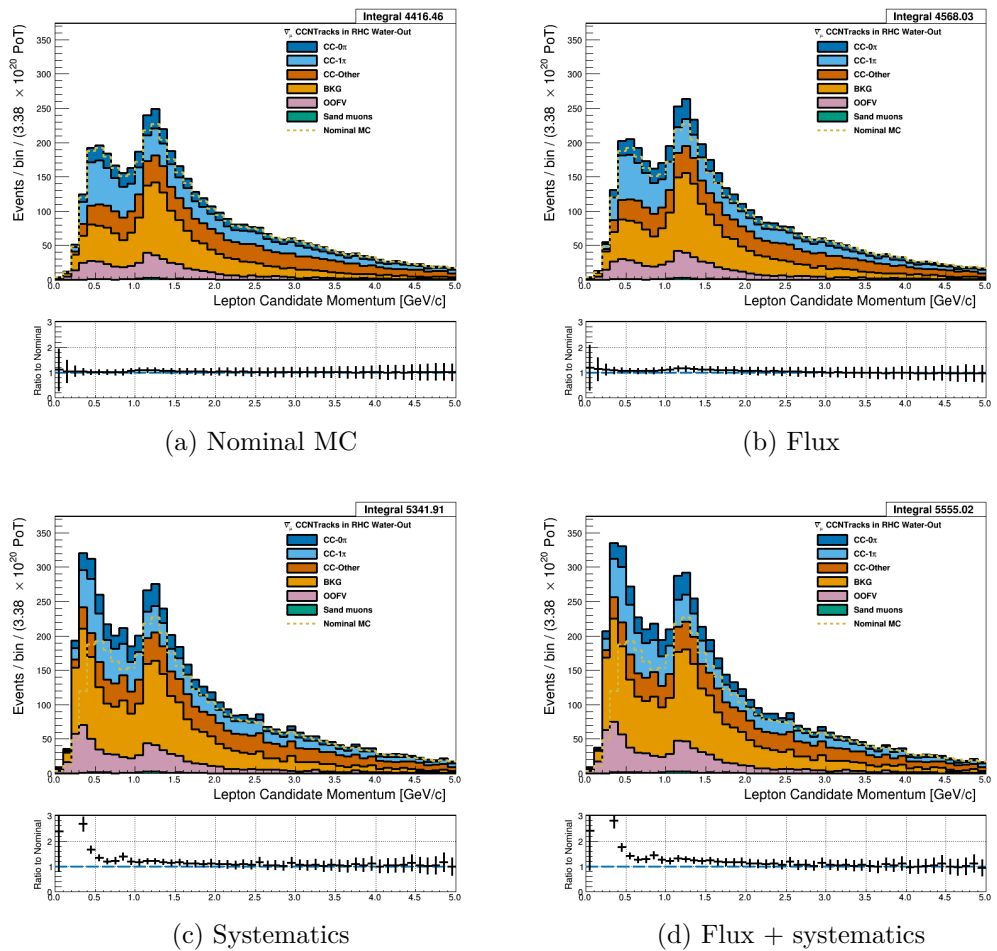


Figure 3.47: Reconstructed lepton candidate momentum separated by topology for RHC $\bar{\nu}_\mu$ CC N-Tracks events occurring in the PØD in water-out mode. (a) The nominal MC prediction without any weights applied. (b) The flux tuning are applied. (c) The systematic weighting are applied. (d) Both flux and systematic weighting are applied.

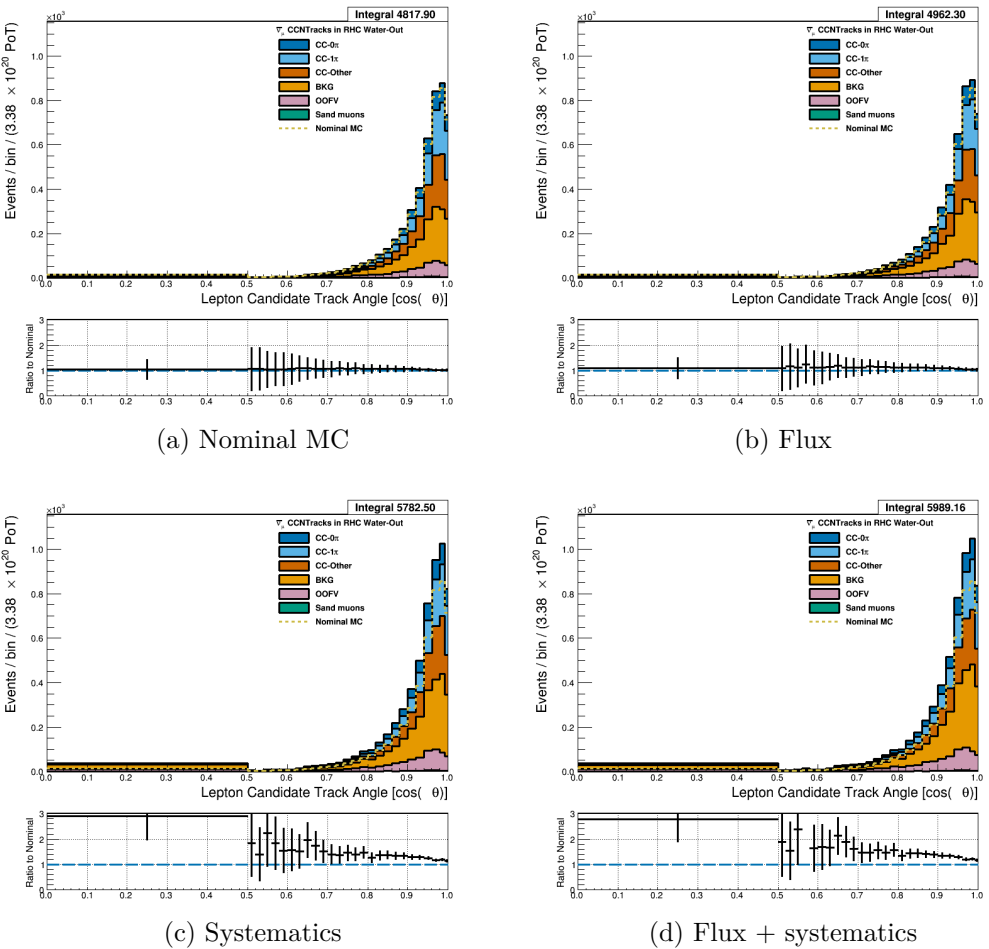


Figure 3.48: Reconstructed lepton candidate $\cos \theta$ separated by topology for RHC $\bar{\nu}_\mu$ CC N-Tracks events occurring in the PØD in water-out mode. (a) The nominal MC prediction without any weights applied. (b) The flux tuning are applied. (c) The systematic weighting are applied. (d) Both flux and systematic weighting are applied.

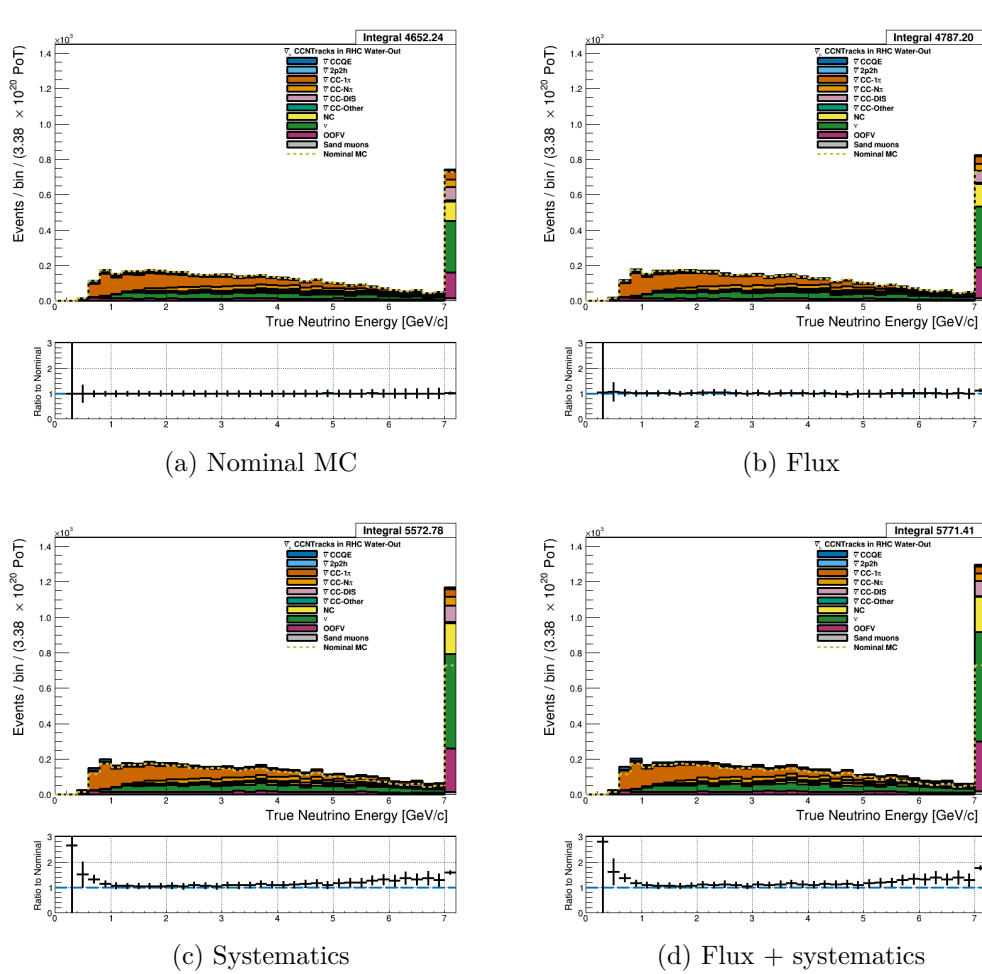


Figure 3.49: True neutrino energy associated with the lepton candidate separated by NEUT model interaction mode for RHC $\bar{\nu}_\mu$ CC N-Tracks events occurring in the PØD in water-out mode. (a) The nominal MC prediction without any weights applied. (b) The flux tuning are applied. (c) The systematic weighting are applied. (d) Both flux and systematic weighting are applied.

530 **3.4.3.3 ν_μ Background Selection in RHC Mode:** Text

531 **3.5 PØD Water-In Samples**

532 This section shows the kinematic distributions for the PØD water-in samples. These samples
 533 will demonstrate the similarities between it and water-out modes. First an examination of
 534 the CC Inclusive samples and the effects of the systematic weights will be explored. The

535 samples are then examined as CC 1-track and CC N-tracks.

536 **3.5.1 CC Inclusive**

537 The CC Inclusive sample cuts are discussed 3.2.1. Since both flux and detector systematic
538 weights are applied to all MC events in BANFF, it is important to validate the event weights.
539 Using neither set of weights is referred to as the nominal MC.

540 **3.5.1.1 ν_μ Selection in FHC Mode:** Shown in Figures 3.50 to 3.56 are the momentum
541 and $\cos\theta$ distributions for ν_μ CC Inclusive events in FHC mode. There are three pairs of
542 P, θ figures with the same truth information break down accompanied by one of neutrino
543 energy. The truth information categories are lepton candidate particle, NEUT reaction, and
544 topology. Each figure consists of a set of four sub-figures which illustrate the application of
545 flux and detector systematic weights.

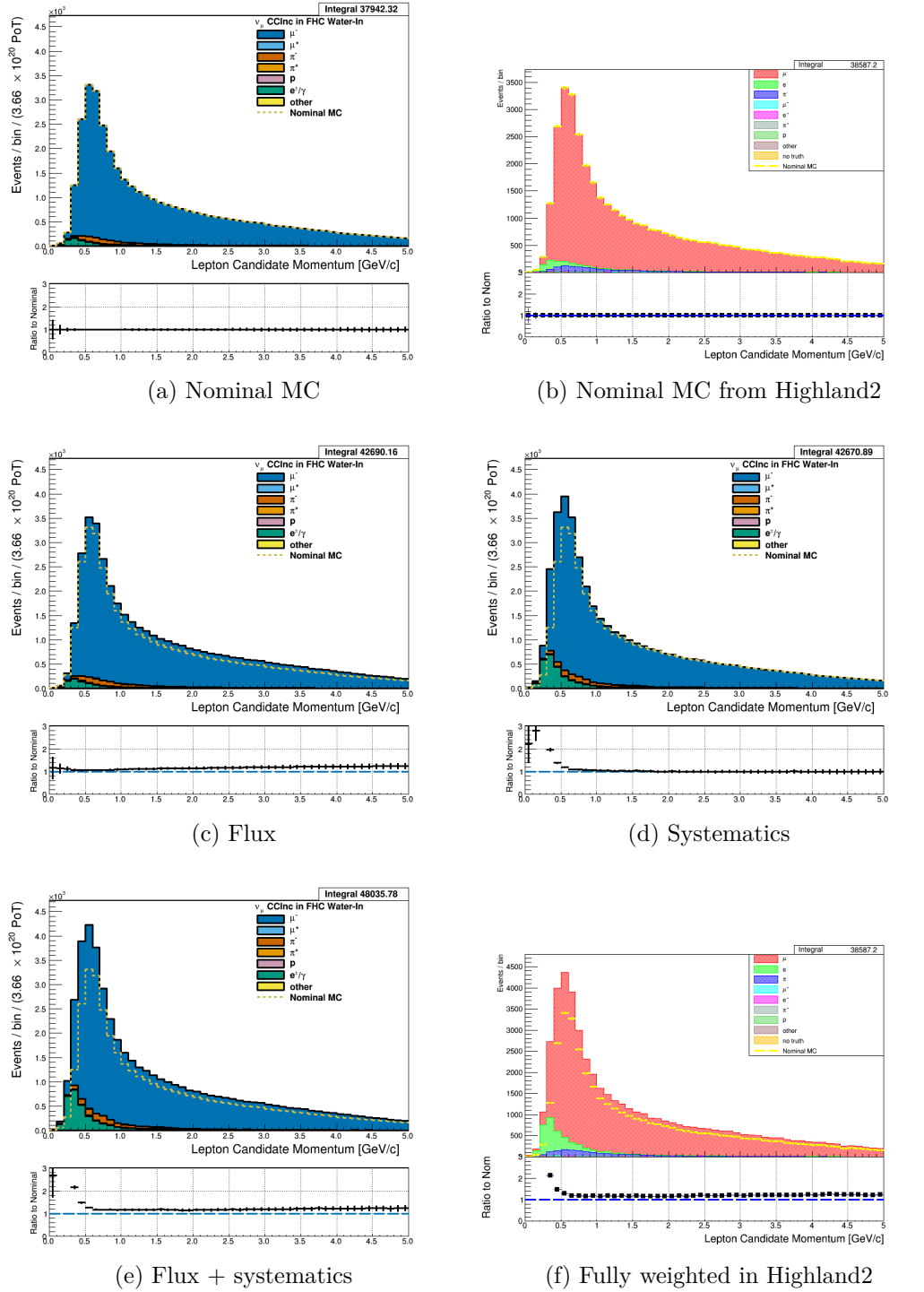


Figure 3.50: Reconstructed lepton candidate momentum separated by true particle species for FHC ν_μ CC Inc. events occurring in the PØD in water-in mode. (a) The nominal MC prediction without any weights applied. (b) Highland2 comparison for (a) without any weights applied using the “NOW” draw option. (c) The flux tuning are applied. (d) The systematic weighting are applied. (e) Both flux and systematic weighting are applied. (f) Highland2 comparison for (e).

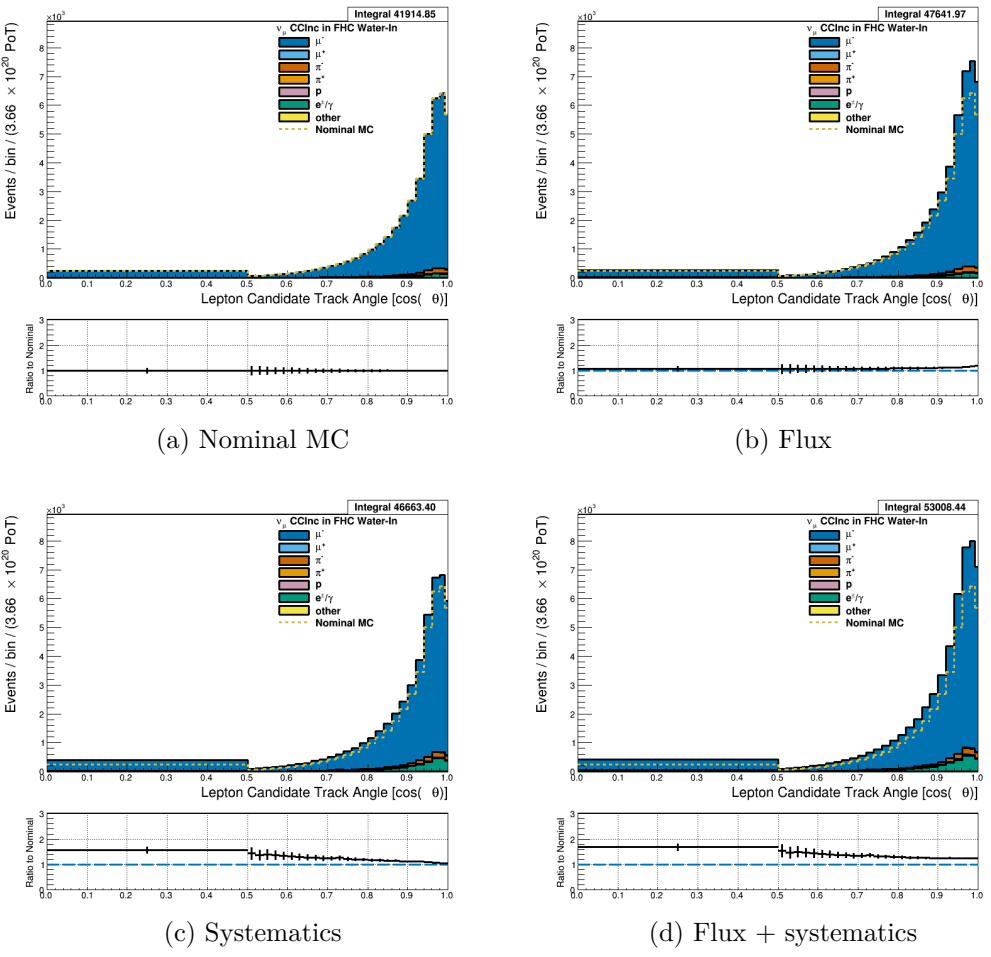


Figure 3.51: Reconstructed lepton candidate angle separated by true particle species for FHC ν_μ CC Inc. events occurring in the PØD in water-in mode. (a) The nominal MC prediction without any weights applied. (b) The flux tuning are applied. (c) The systematic weighting are applied. (d) Both flux and systematic weighting are applied.

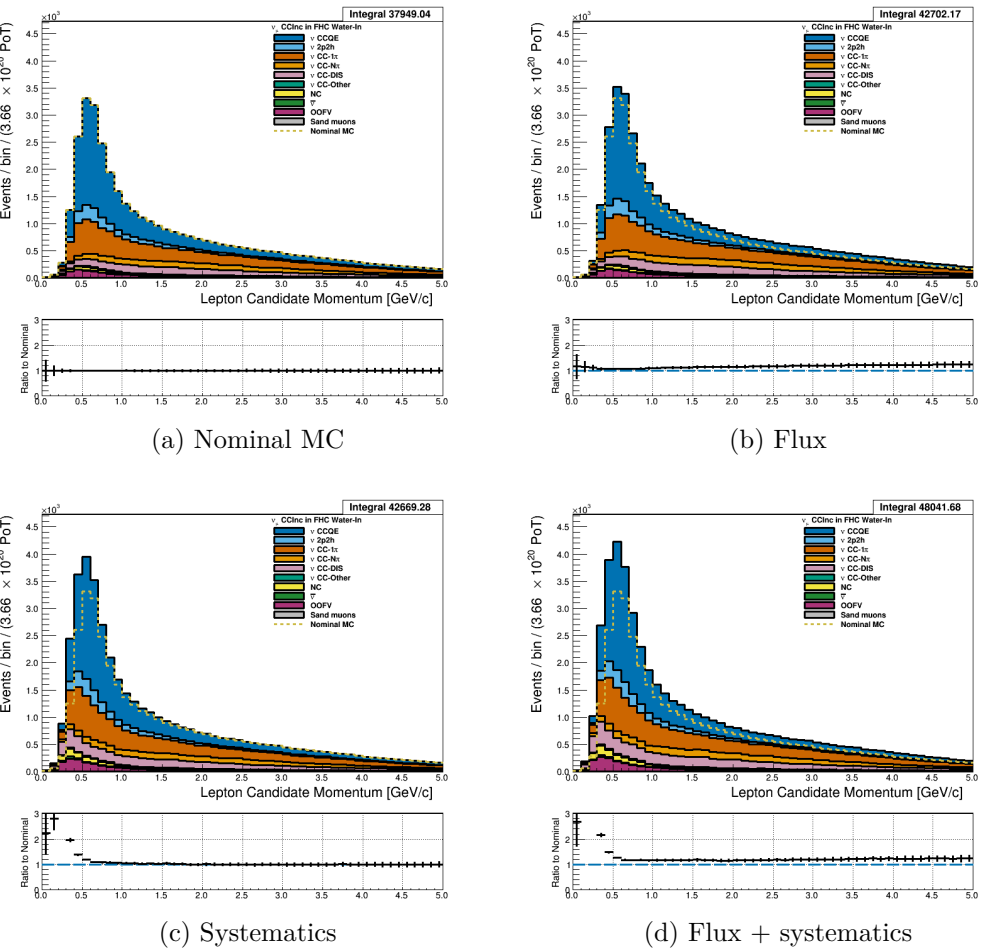


Figure 3.52: Reconstructed lepton candidate momentum separated by NEUT model interaction mode for FHC ν_μ CC Inc. events occurring in the PØD in water-in mode. (a) The nominal MC prediction without any weights applied. (b) The flux tuning are applied. (c) The systematic weighting are applied. (d) Both flux and systematic weighting are applied.

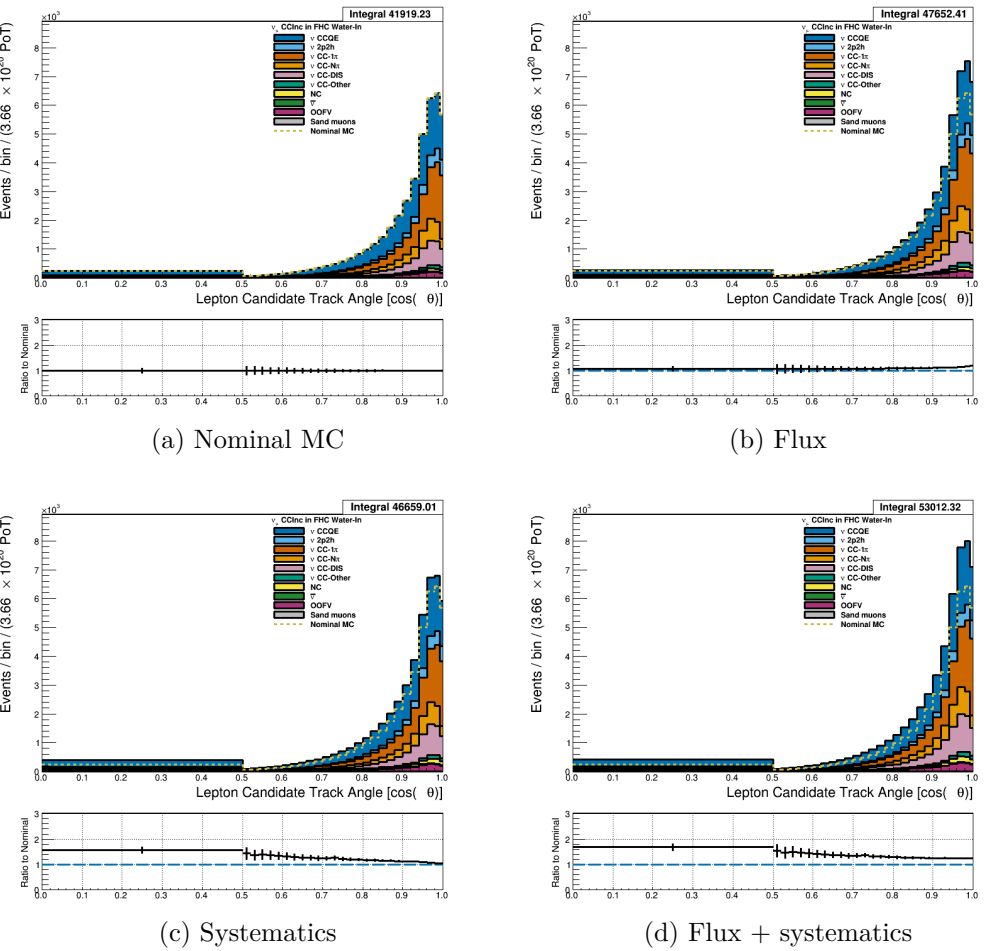


Figure 3.53: Reconstructed lepton candidate $\cos \theta$ separated by NEUT model interaction mode for FHC ν_μ CC Inc. events occurring in the PØD in water-in mode. (a) The nominal MC prediction without any weights applied. (b) The flux tuning are applied. (c) The systematic weighting are applied. (d) Both flux and systematic weighting are applied.

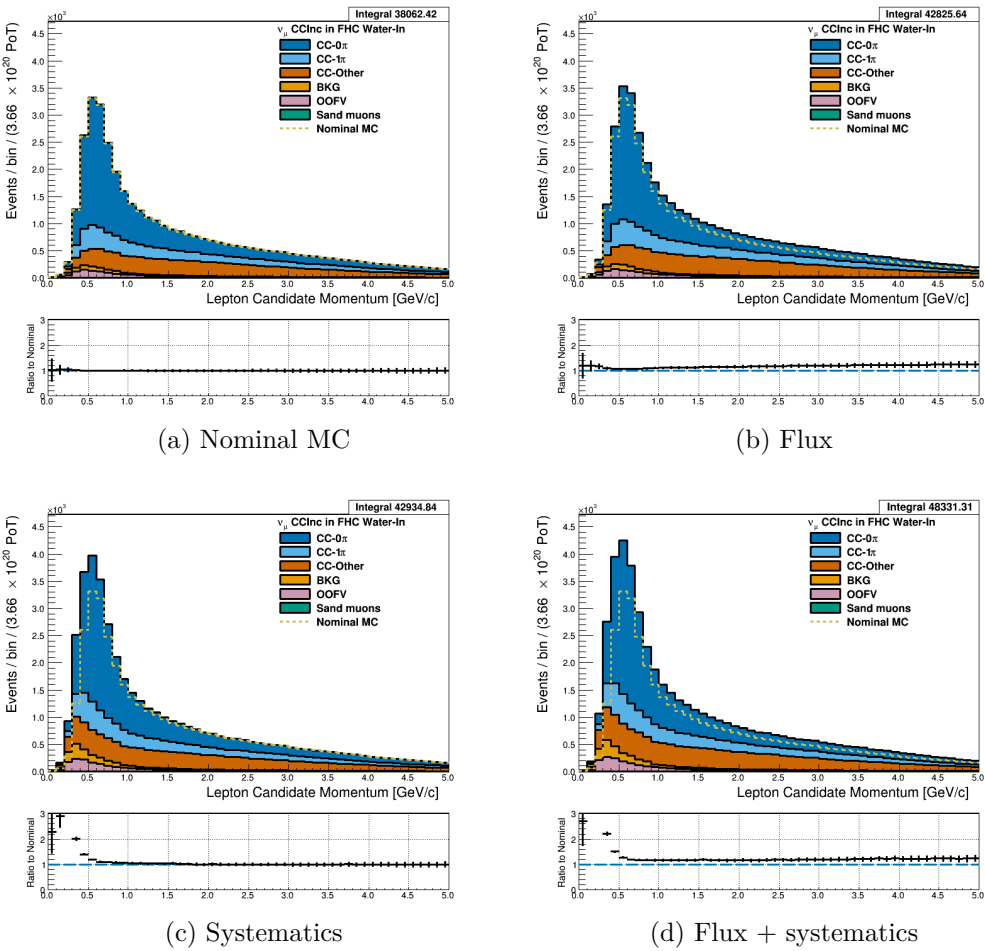


Figure 3.54: Reconstructed lepton candidate momentum separated by topology for FHC ν_μ CC Inc. events occurring in the PØD in water-in mode. (a) The nominal MC prediction without any weights applied. (b) The flux tuning are applied. (c) The systematic weighting are applied. (d) Both flux and systematic weighting are applied.

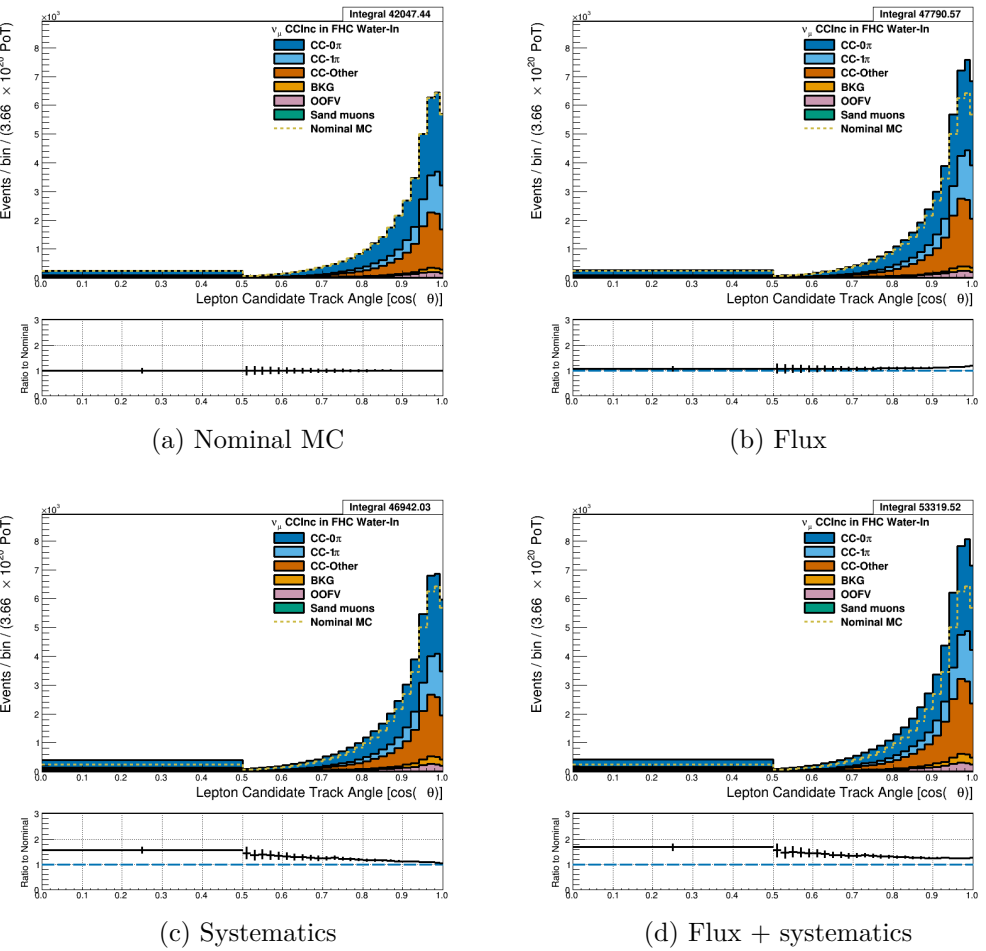


Figure 3.55: Reconstructed lepton candidate $\cos \theta$ separated by topology for FHC ν_μ CC Inc. events occurring in the PØD in water-in mode. (a) The nominal MC prediction without any weights applied. (b) The flux tuning are applied. (c) The systematic weighting are applied. (d) Both flux and systematic weighting are applied.

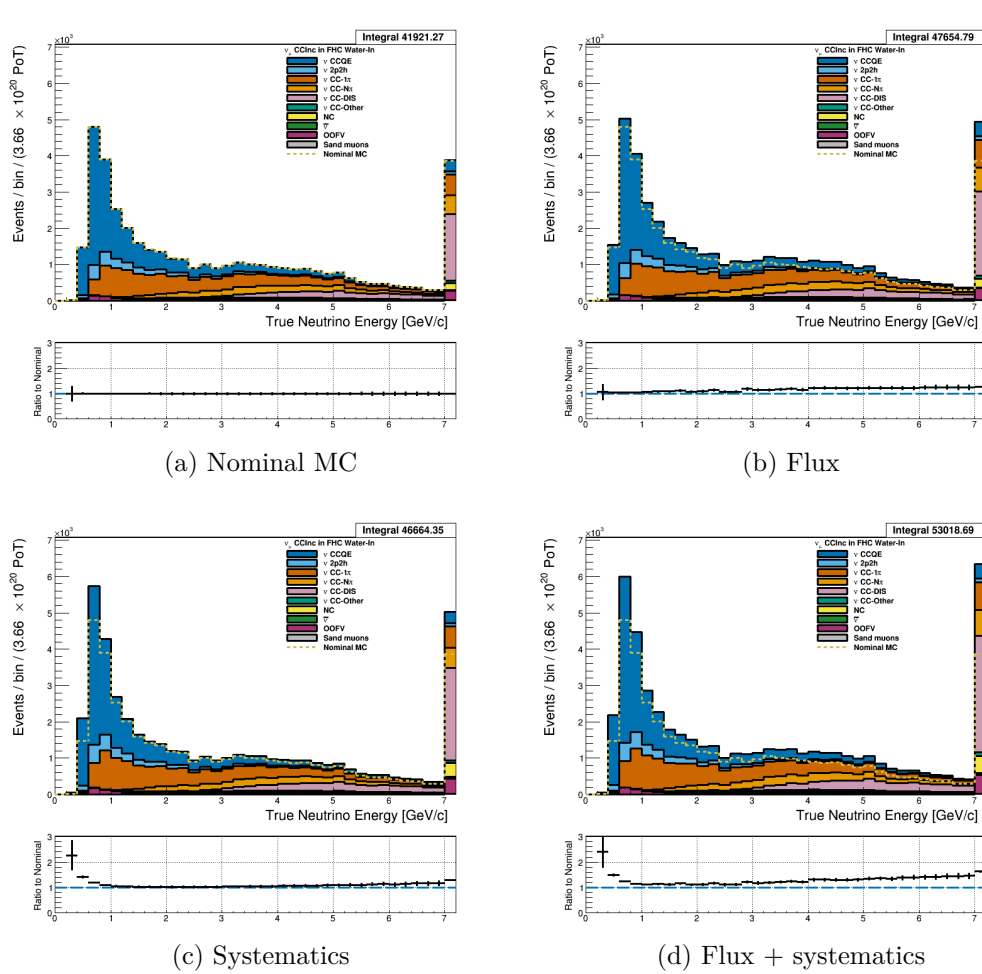


Figure 3.56: True neutrino energy associated with the lepton candidate separated by NEUT model interaction mode for FHC ν_μ CC Inc. events occurring in the PØD in water-out mode. (a) The nominal MC prediction without any weights applied. (b) The flux tuning are applied. (c) The systematic weighting are applied. (d) Both flux and systematic weighting are applied.

3.5.1.2 $\bar{\nu}_\mu$ Selection in RHC Mode: Shown in Figures 3.57 to 3.63 for $\bar{\nu}_\mu$ CC Inclusive events in RHC mode. There are three pairs of P, θ figures with the same truth information break down accompanied by one of neutrino energy. The truth information categories are lepton candidate particle, NEUT reaction, and topology. Each figure consists of a set of four sub-figures which illustrate the application of flux and detector systematic weights.

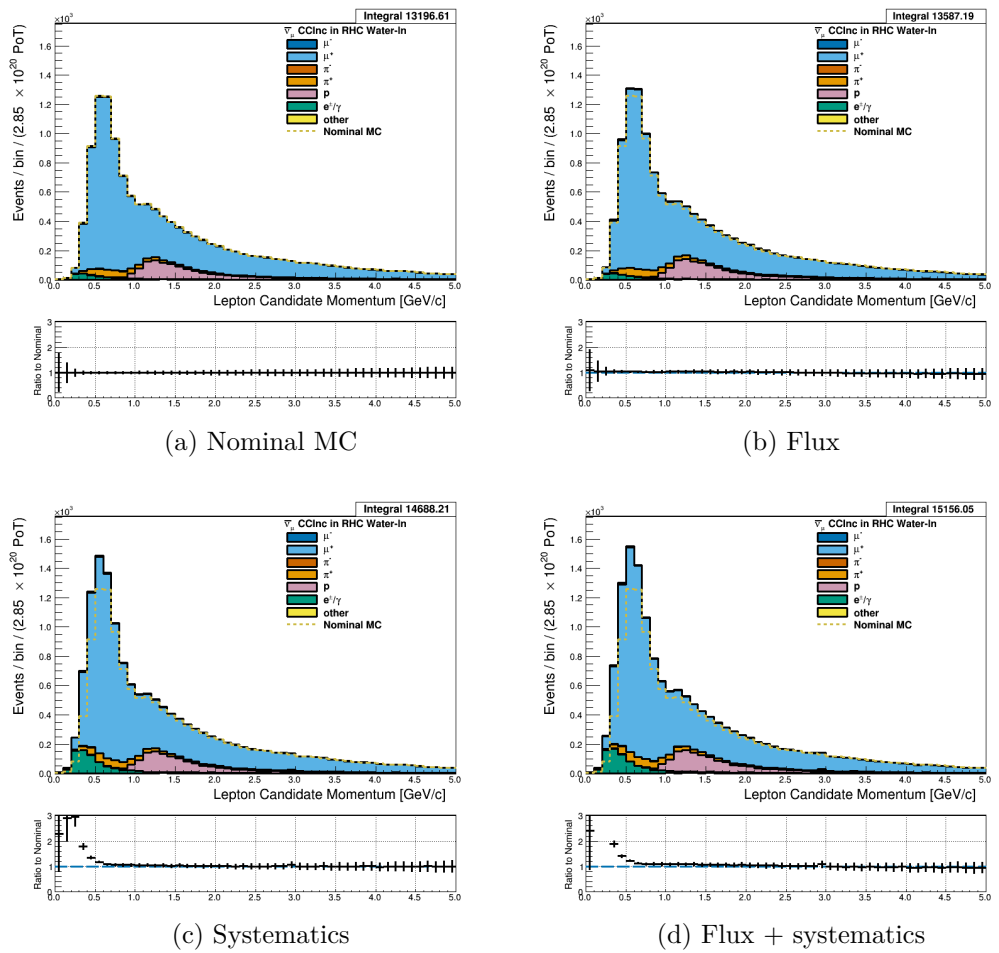


Figure 3.57: Reconstructed lepton candidate momentum separated by true particle species for RHC $\bar{\nu}_\mu$ CC Inc. events occurring in the PØD in water-out mode. (a) The nominal MC prediction without any weights applied. (b) The flux tuning are applied. (c) The systematic weighting are applied. (d) Both flux and systematic weighting are applied.

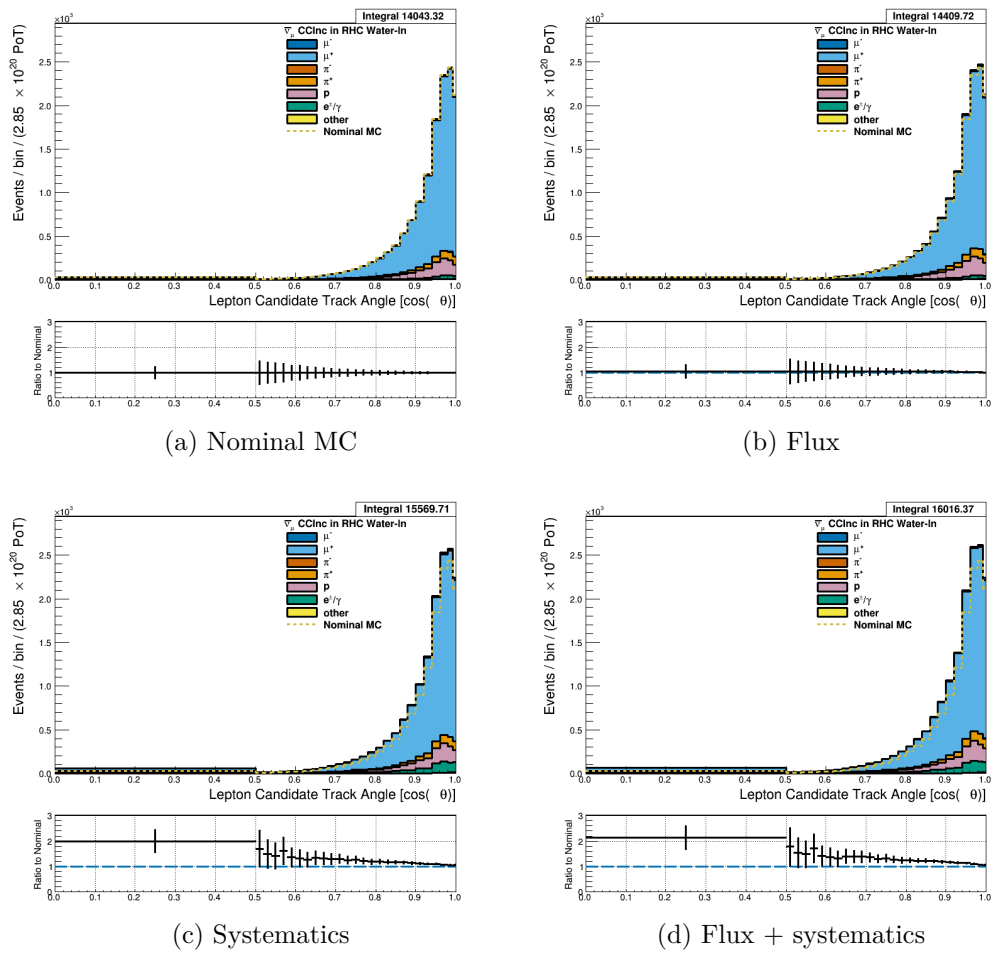


Figure 3.58: Reconstructed lepton candidate angle separated by true particle species for RHC $\bar{\nu}_\mu$ CC Inc. events occurring in the PØD in water-in mode. (a) The nominal MC prediction without any weights applied. (b) The flux tuning are applied. (c) The systematic weighting are applied. (d) Both flux and systematic weighting are applied.

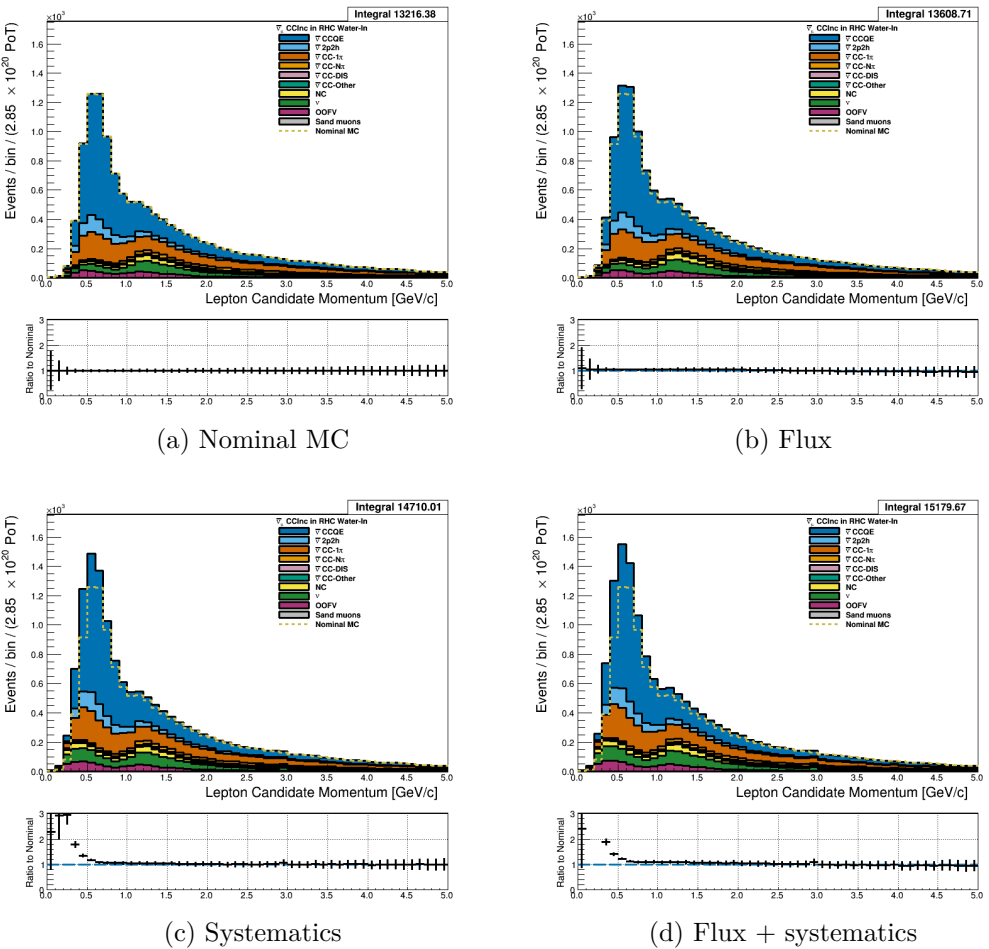


Figure 3.59: Reconstructed lepton candidate momentum separated by NEUT model interaction mode for RHC $\bar{\nu}_\mu$ CC Inc. events occurring in the PØD in water-out mode. (a) The nominal MC prediction without any weights applied. (b) The flux tuning are applied. (c) The systematic weighting are applied. (d) Both flux and systematic weighting are applied.

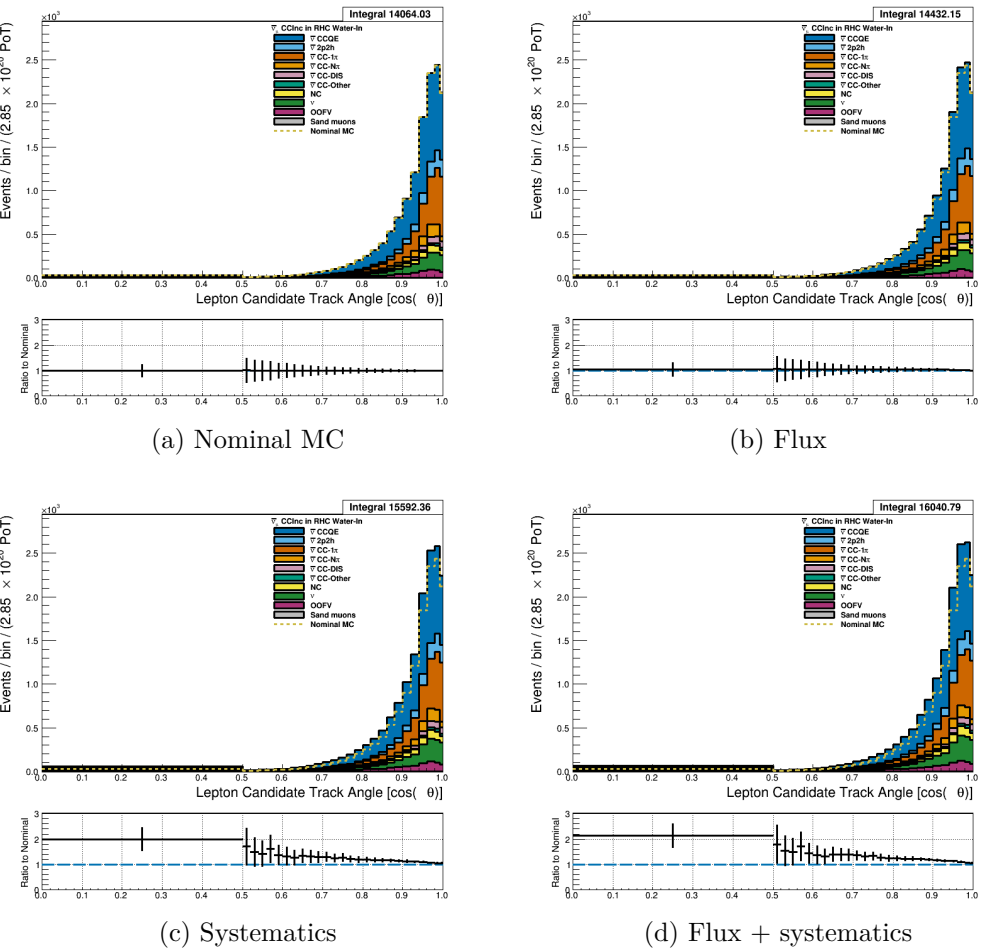


Figure 3.60: Reconstructed lepton candidate $\cos \theta$ separated by NEUT model interaction mode for RHC $\bar{\nu}_\mu$ CC Inc. events occurring in the PØD in water-out mode. (a) The nominal MC prediction without any weights applied. (b) The flux tuning are applied. (c) The systematic weighting are applied. (d) Both flux and systematic weighting are applied.

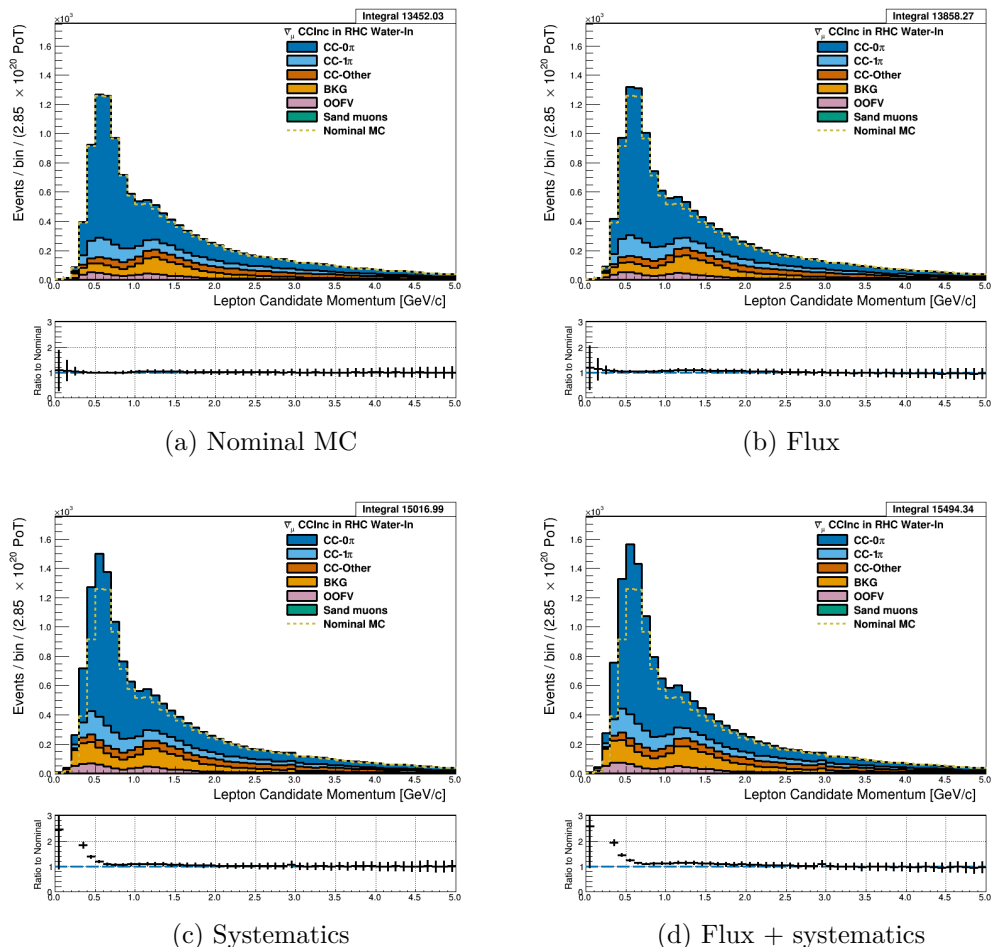


Figure 3.61: Reconstructed lepton candidate momentum separated by topology for RHC $\bar{\nu}_\mu$ CC Inc. events occurring in the PØD in water-out mode. (a) The nominal MC prediction without any weights applied. (b) The flux tuning are applied. (c) The systematic weighting are applied. (d) Both flux and systematic weighting are applied.

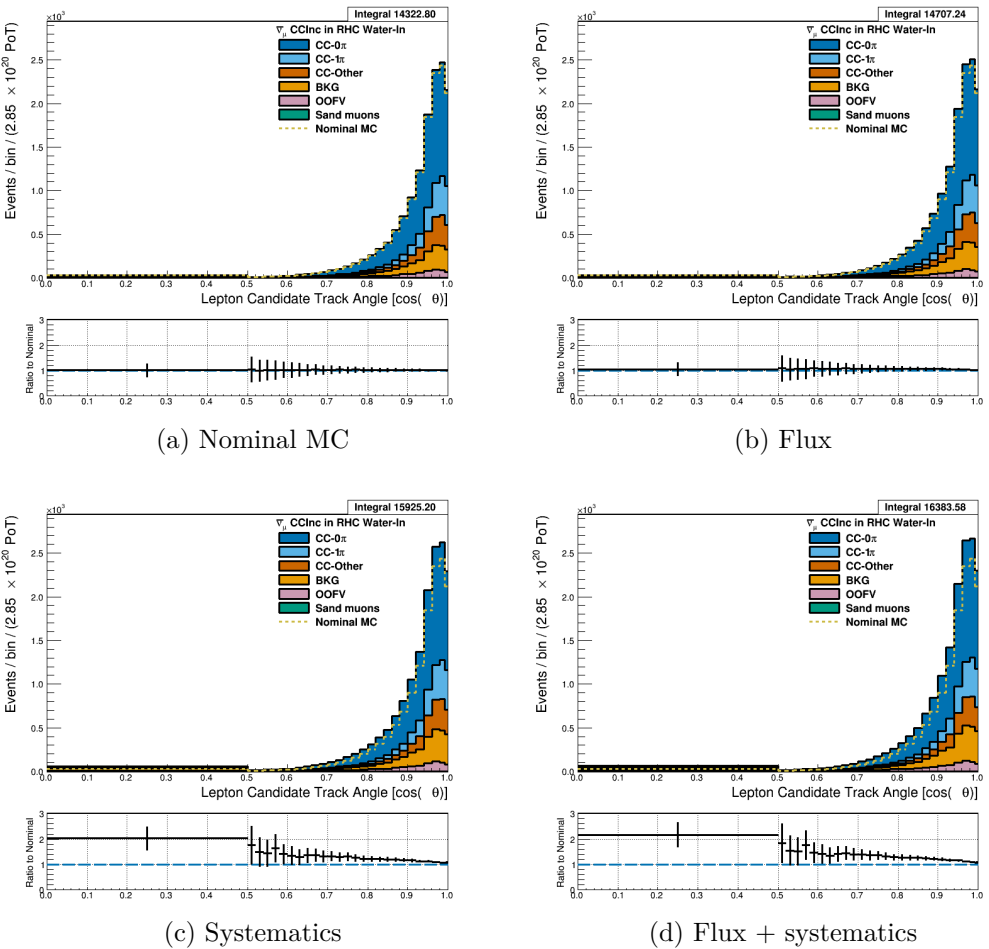


Figure 3.62: Reconstructed lepton candidate $\cos \theta$ separated by topology for RHC $\bar{\nu}_\mu$ CC Inc. events occurring in the PØD in water-out mode. (a) The nominal MC prediction without any weights applied. (b) The flux tuning are applied. (c) The systematic weighting are applied. (d) Both flux and systematic weighting are applied.

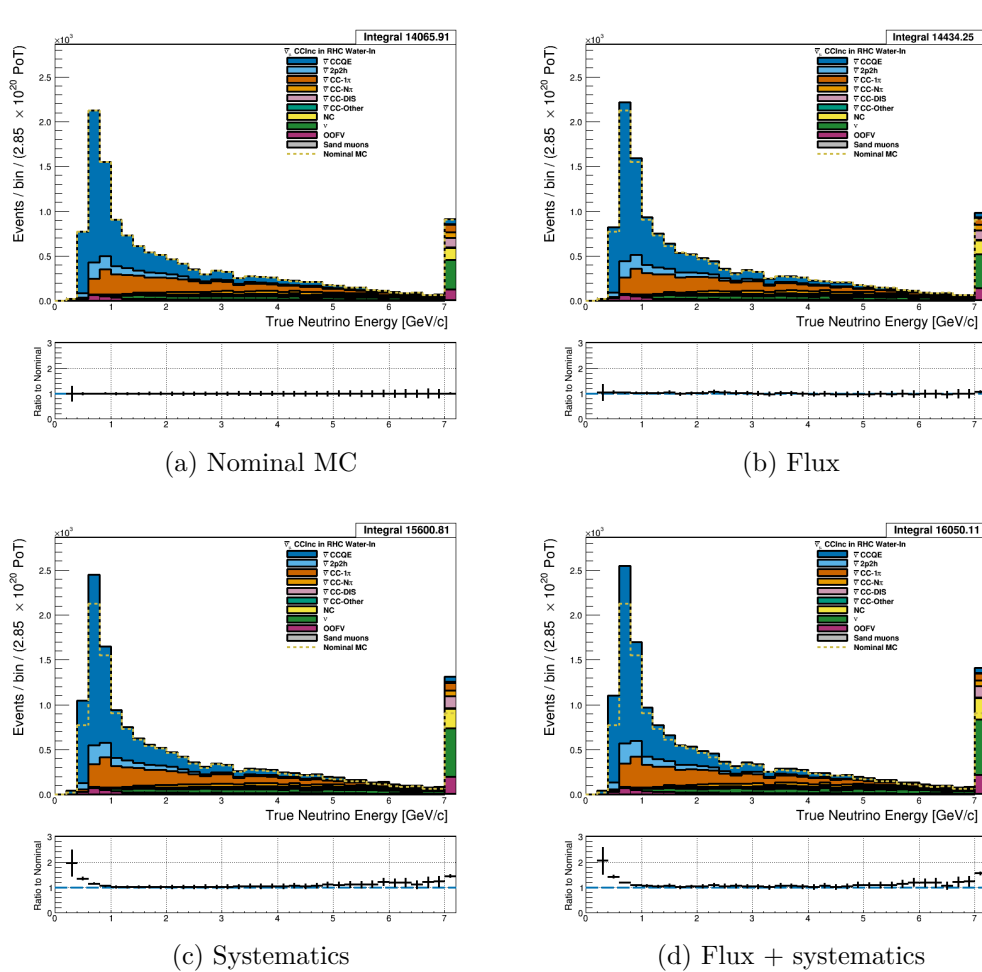


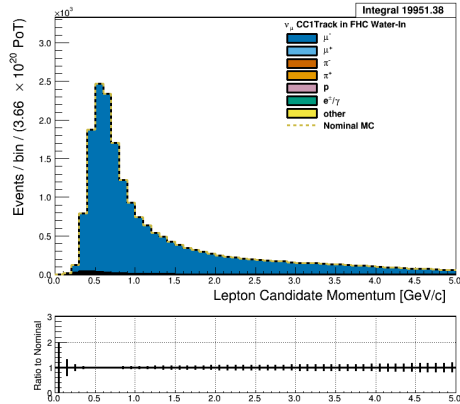
Figure 3.63: True neutrino energy associated with the lepton candidate separated by NEUT model interaction mode for RHC $\bar{\nu}_\mu$ CC Inc. events occurring in the PØD in water-out mode. (a) The nominal MC prediction without any weights applied. (b) The flux tuning are applied. (c) The systematic weighting are applied. (d) Both flux and systematic weighting are applied.

551 **3.5.1.3 ν_μ Background Selection in RHC Mode:** Add figures here

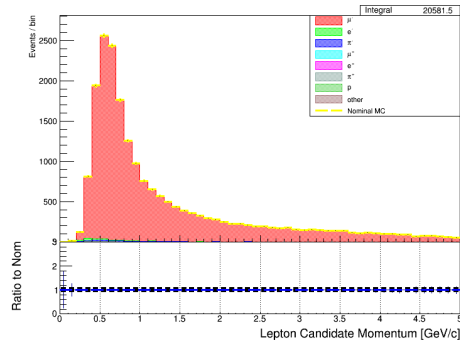
552 **3.5.2 CC 1-Track (CCQE Enhanced)**

553 Text

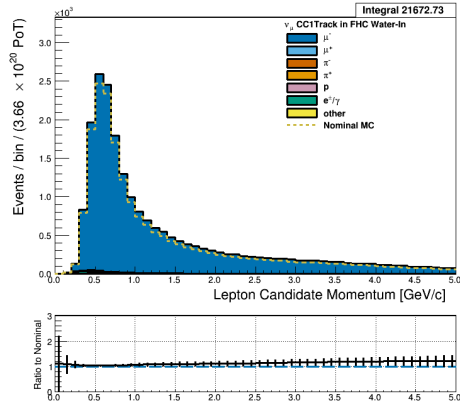
554 **3.5.2.1 ν_μ Selection in FHC Mode:** Text



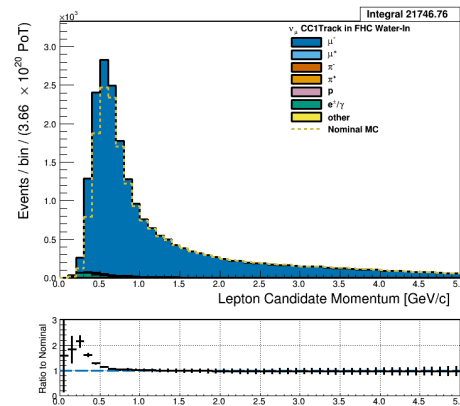
(a) Nominal MC



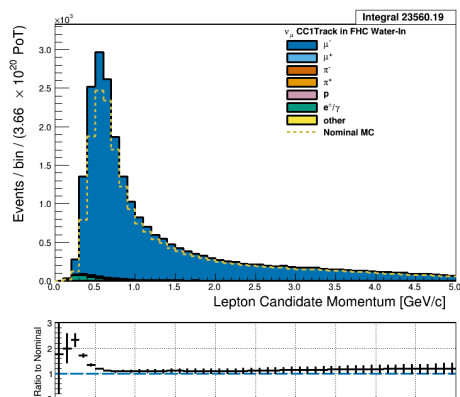
(b) Nominal MC from Highland2



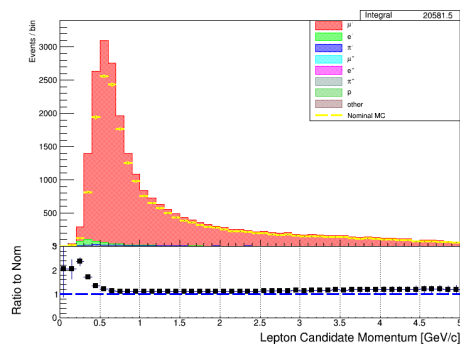
(c) Flux



(d) Systematics



(e) Flux + systematics



(f) Fully weighted in Highland2

Figure 3.64: Reconstructed lepton candidate momentum separated by true particle species for FHC ν_μ CC 1-Track events occurring in the PØD in water-in mode. (a) The nominal MC prediction without any weights applied. (b) Highland2 comparison for (a) without any weights applied using the “NOW” draw option. (c) The flux tuning are applied. (d) The systematic weighting are applied. (e) Both flux and systematic weighting are applied. (f) Highland2 comparison for (e).

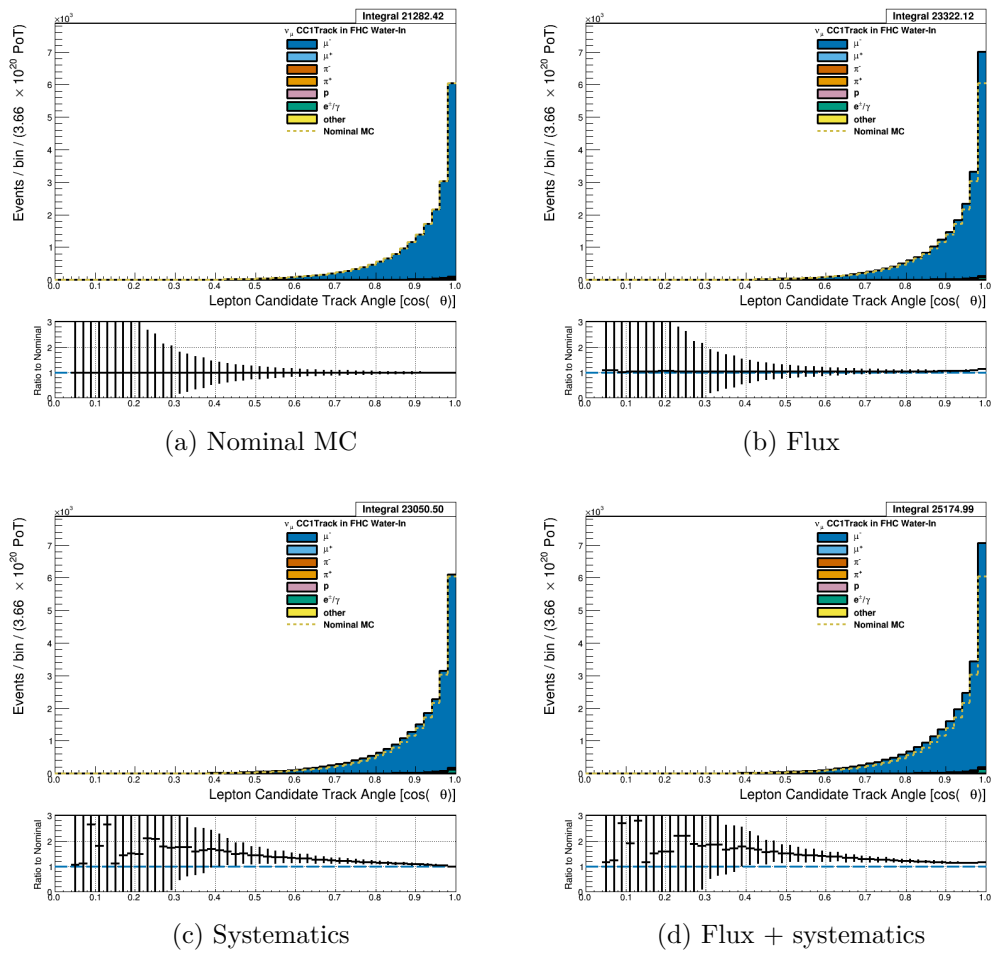


Figure 3.65: Reconstructed lepton candidate angle separated by true particle species for FHC ν_μ CC 1-Track events occurring in the PØD in water-in mode. (a) The nominal MC prediction without any weights applied. (b) The flux tuning are applied. (c) The systematic weighting are applied. (d) Both flux and systematic weighting are applied.

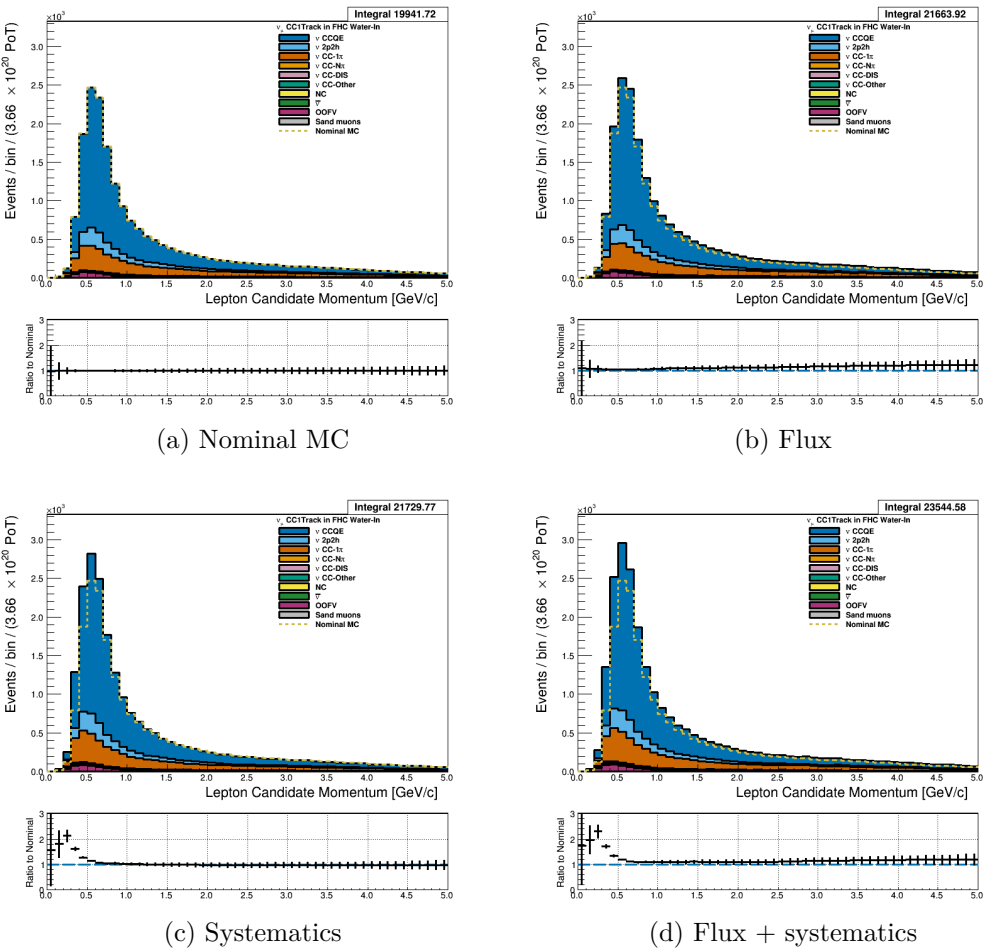


Figure 3.66: Reconstructed lepton candidate momentum separated by NEUT model interaction mode for FHC ν_μ CC 1-Track events occurring in the PØD in water-in mode. (a) The nominal MC prediction without any weights applied. (b) The flux tuning are applied. (c) The systematic weighting are applied. (d) Both flux and systematic weighting are applied.

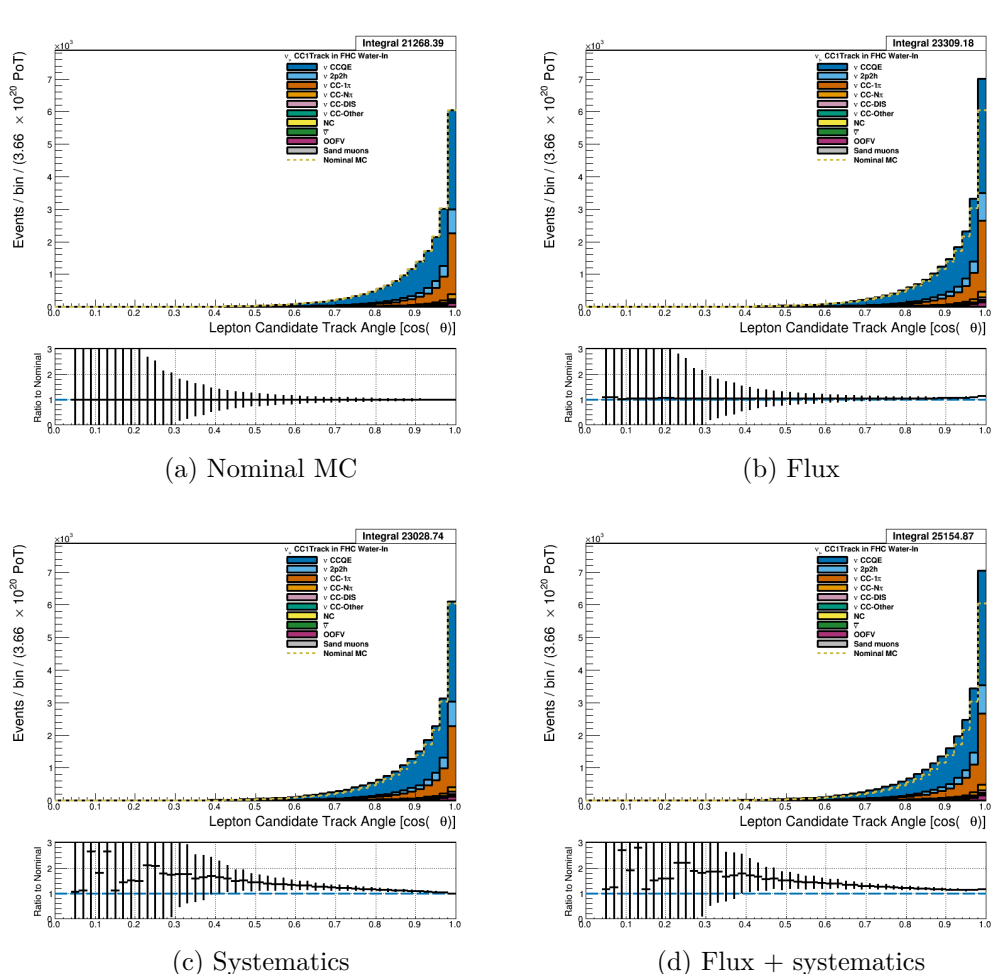


Figure 3.67: Reconstructed lepton candidate $\cos \theta$ separated by NEUT model interaction mode for FHC ν_μ CC 1-Track events occurring in the PØD in water-in mode. (a) The nominal MC prediction without any weights applied. (b) The flux tuning are applied. (c) The systematic weighting are applied. (d) Both flux and systematic weighting are applied.

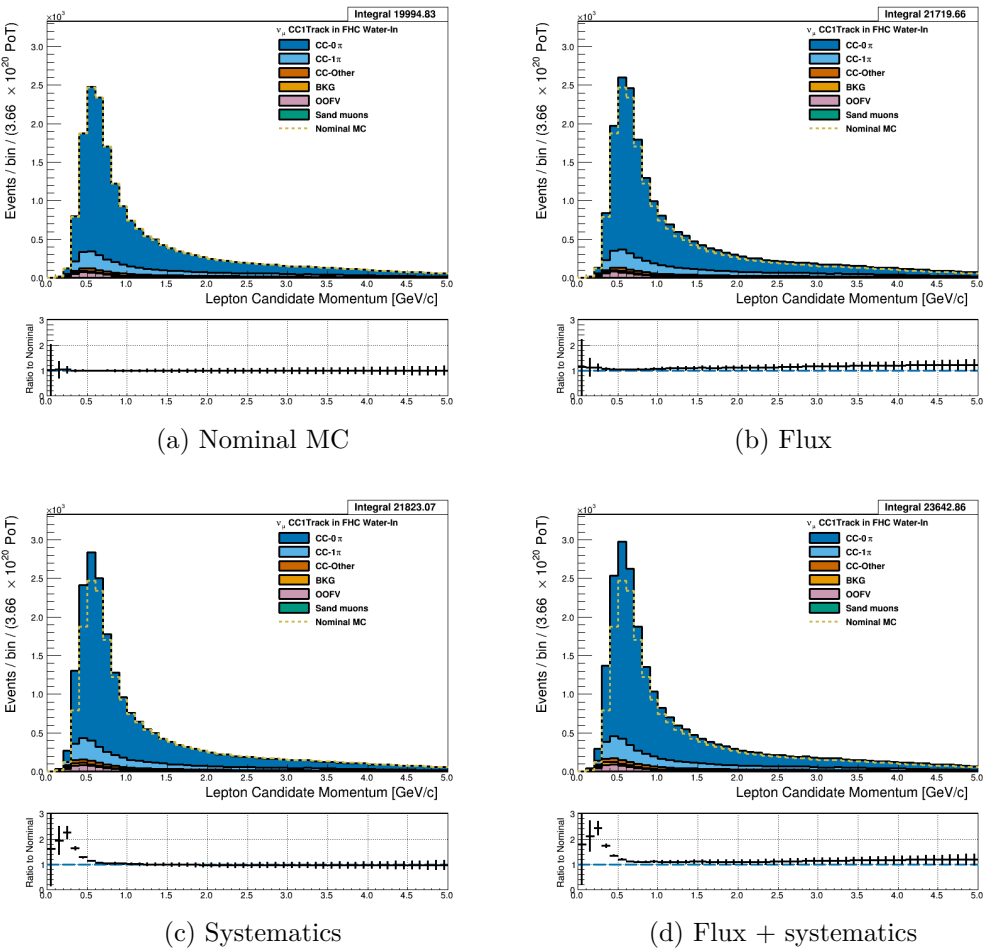


Figure 3.68: Reconstructed lepton candidate momentum separated by topology for FHC ν_μ CC 1-Track events occurring in the PØD in water-in mode. (a) The nominal MC prediction without any weights applied. (b) The flux tuning are applied. (c) The systematic weighting are applied. (d) Both flux and systematic weighting are applied.

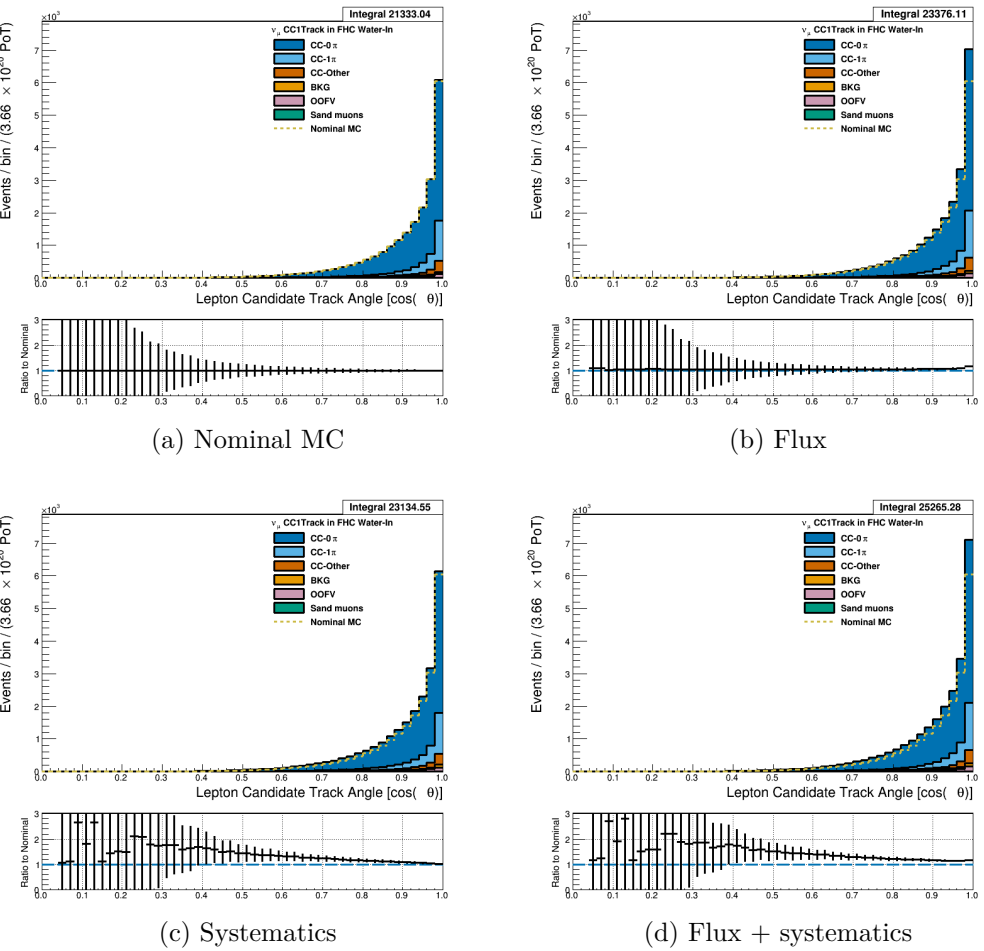


Figure 3.69: Reconstructed lepton candidate $\cos \theta$ separated by topology for FHC ν_μ CC 1-Track events occurring in the PØD in water-in mode. (a) The nominal MC prediction without any weights applied. (b) The flux tuning are applied. (c) The systematic weighting are applied. (d) Both flux and systematic weighting are applied.

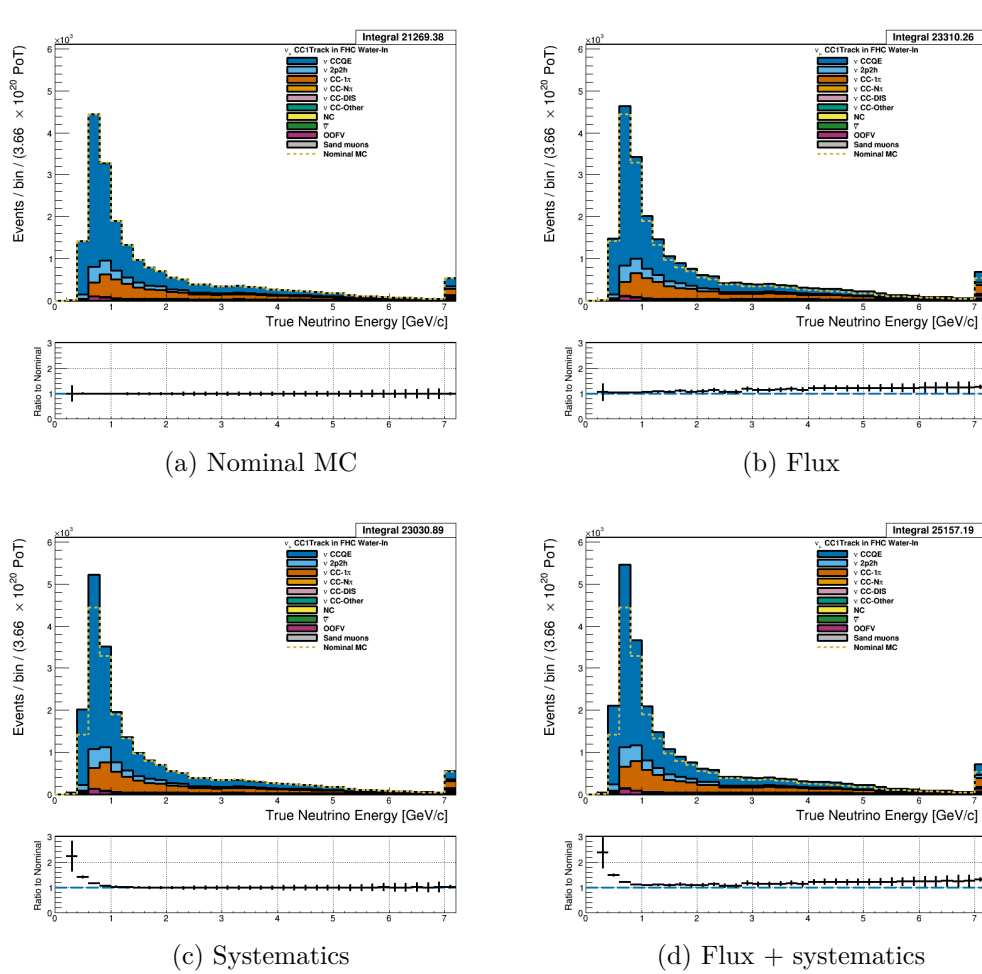


Figure 3.70: True neutrino energy associated with the lepton candidate separated by NEUT model interaction mode for FHC ν_μ CC 1-Track events occurring in the PØD in water-out mode. (a) The nominal MC prediction without any weights applied. (b) The flux tuning are applied. (c) The systematic weighting are applied. (d) Both flux and systematic weighting are applied.

3.5.2.2 $\bar{\nu}_\mu$ Selection in RHC Mode: Text

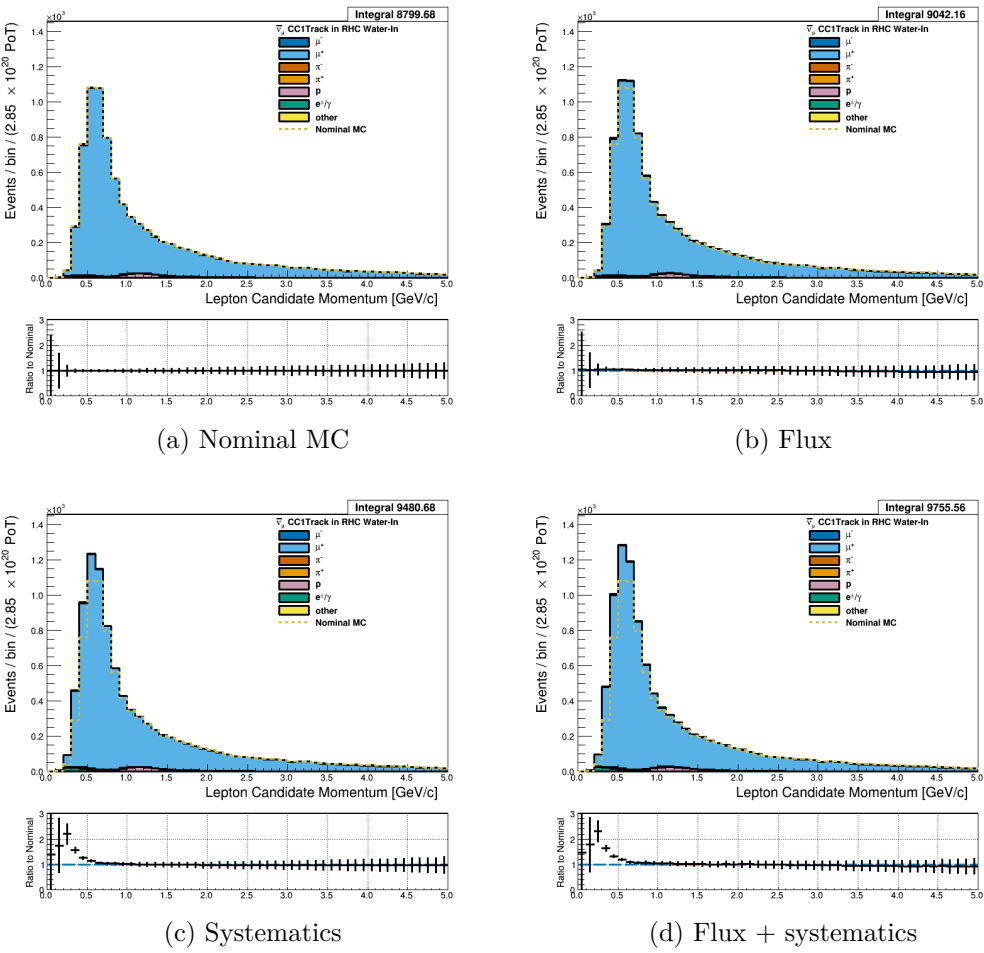


Figure 3.71: Reconstructed lepton candidate momentum separated by true particle species for RHC $\bar{\nu}_\mu$ CC 1-Track events occurring in the PØD in water-out mode. (a) The nominal MC prediction without any weights applied. (b) The flux tuning are applied. (c) The systematic weighting are applied. (d) Both flux and systematic weighting are applied.

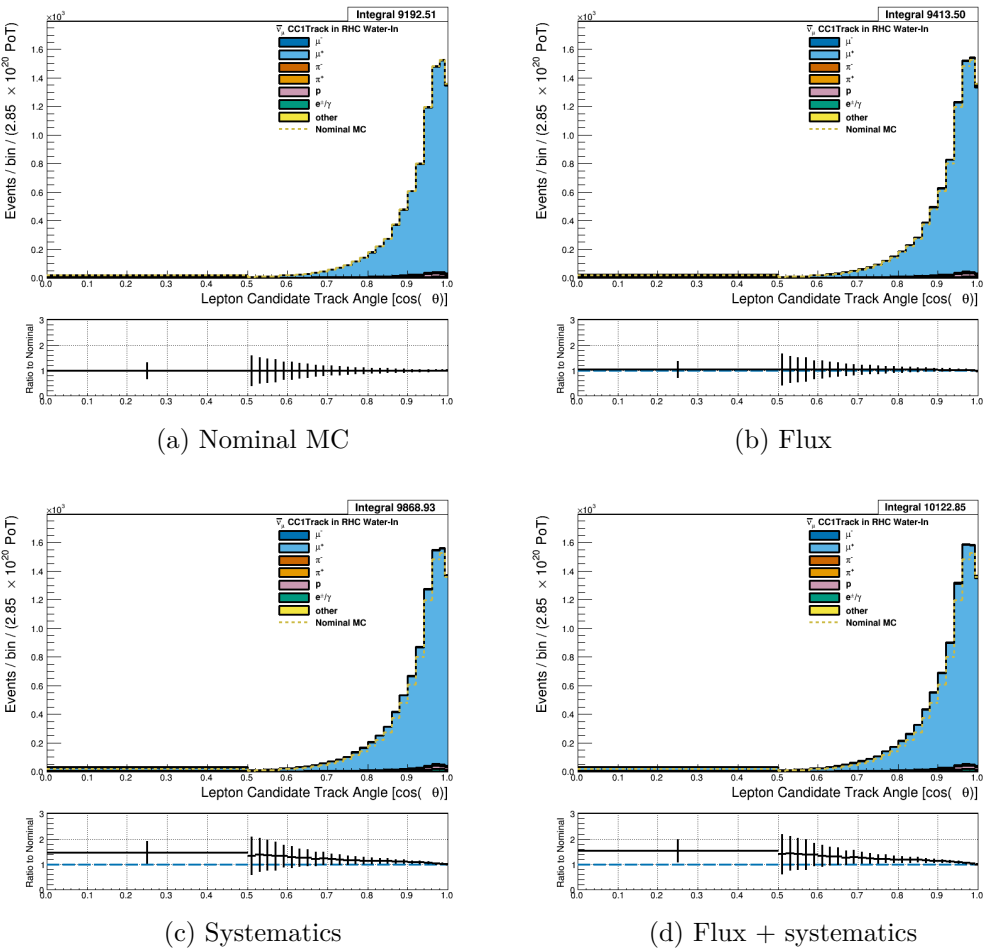


Figure 3.72: Reconstructed lepton candidate angle separated by true particle species for RHC $\bar{\nu}_\mu$ CC 1-Track events occurring in the PØD in water-in mode. (a) The nominal MC prediction without any weights applied. (b) The flux tuning are applied. (c) The systematic weighting are applied. (d) Both flux and systematic weighting are applied.

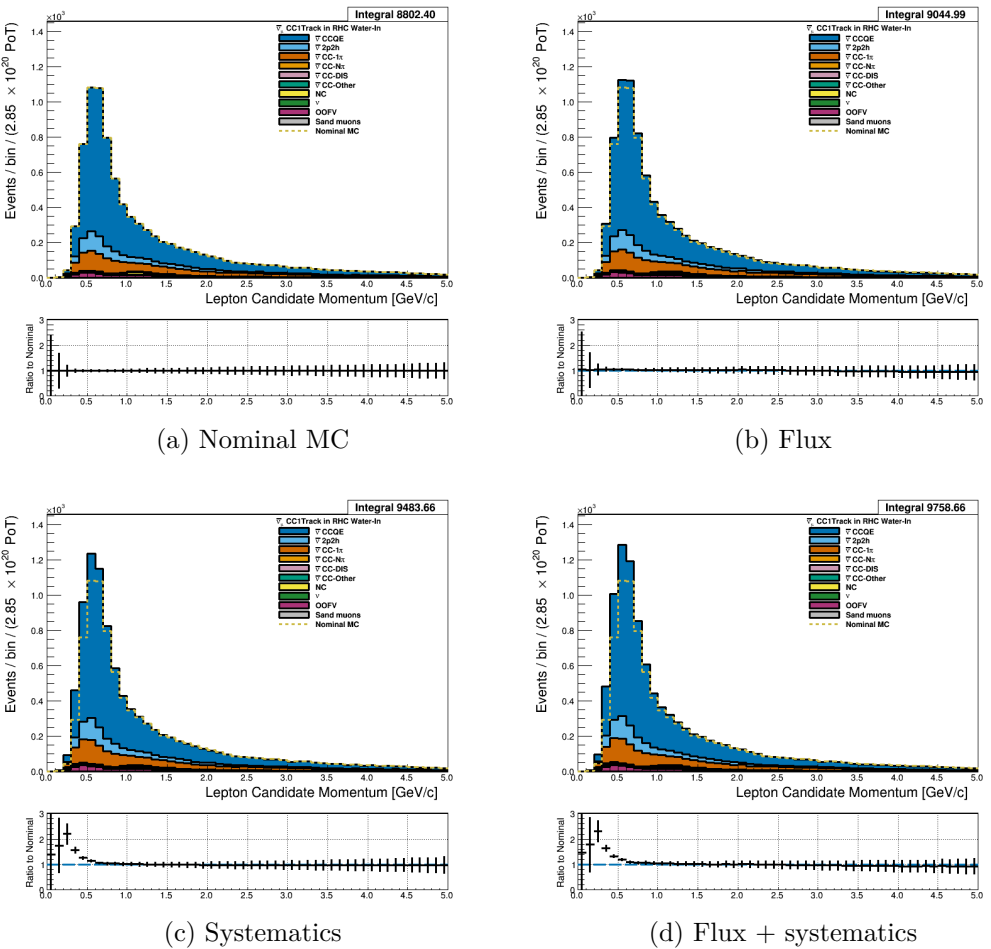


Figure 3.73: Reconstructed lepton candidate momentum separated by NEUT model interaction mode for RHC $\bar{\nu}_\mu$ CC 1-Track events occurring in the PØD in water-out mode. (a) The nominal MC prediction without any weights applied. (b) The flux tuning are applied. (c) The systematic weighting are applied. (d) Both flux and systematic weighting are applied.

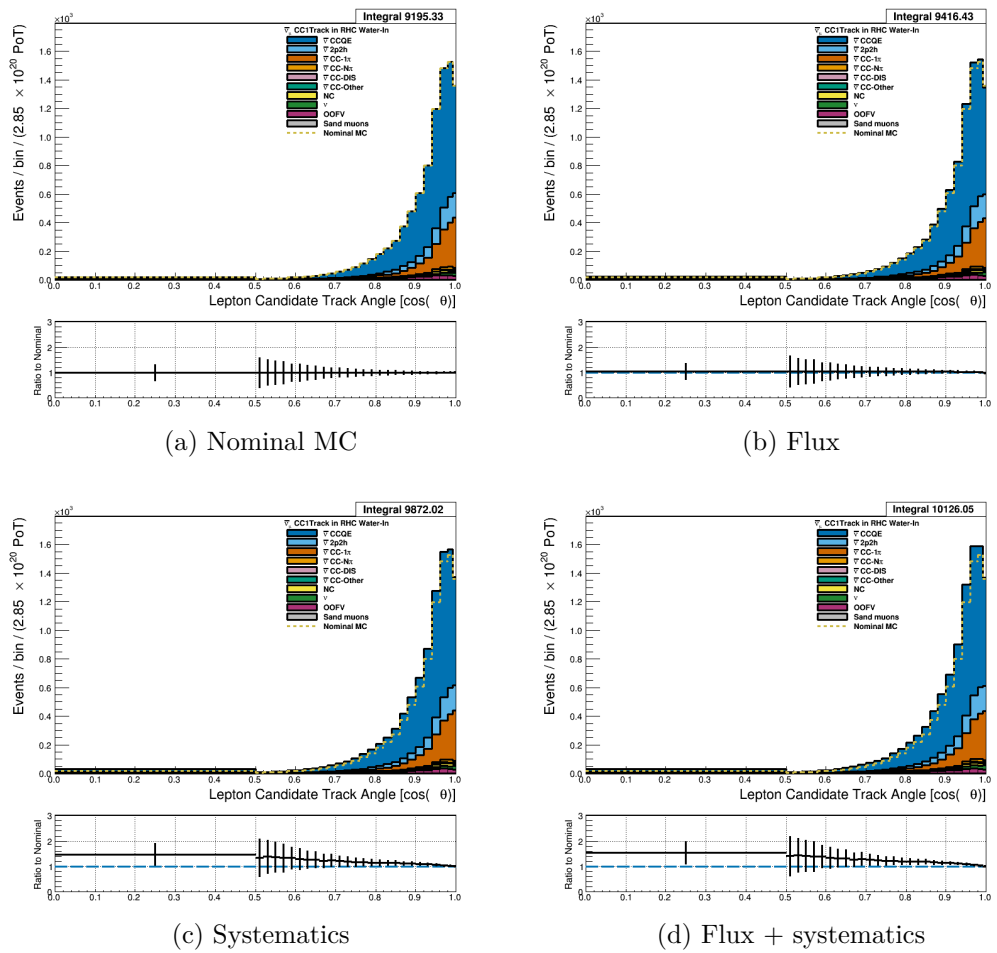


Figure 3.74: Reconstructed lepton candidate $\cos \theta$ separated by NEUT model interaction mode for RHC $\bar{\nu}_\mu$ CC 1-Track events occurring in the PØD in water-out mode. (a) The nominal MC prediction without any weights applied. (b) The flux tuning are applied. (c) The systematic weighting are applied. (d) Both flux and systematic weighting are applied.

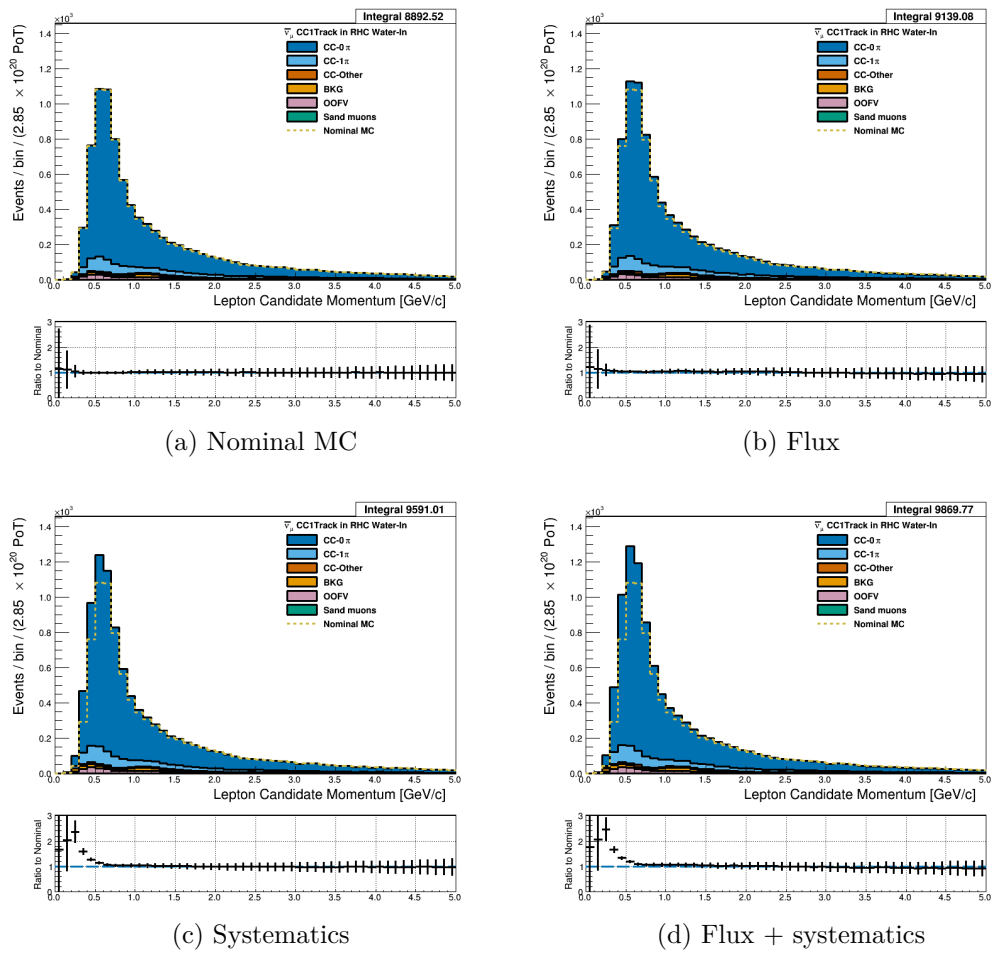


Figure 3.75: Reconstructed lepton candidate momentum separated by topology for RHC $\bar{\nu}_\mu$ CC 1-Track events occurring in the PØD in water-out mode. (a) The nominal MC prediction without any weights applied. (b) The flux tuning are applied. (c) The systematic weighting are applied. (d) Both flux and systematic weighting are applied.

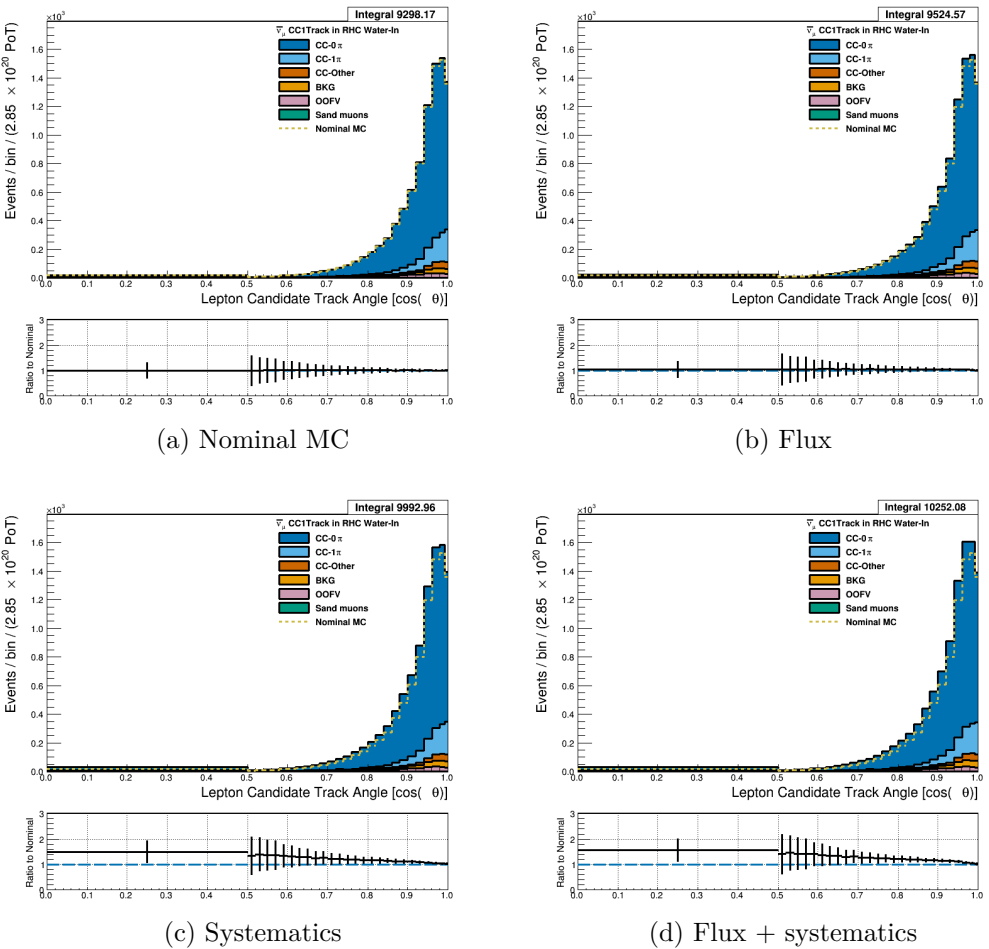


Figure 3.76: Reconstructed lepton candidate $\cos \theta$ separated by topology for RHC $\bar{\nu}_\mu$ CC 1-Track events occurring in the PØD in water-out mode. (a) The nominal MC prediction without any weights applied. (b) The flux tuning are applied. (c) The systematic weighting are applied. (d) Both flux and systematic weighting are applied.

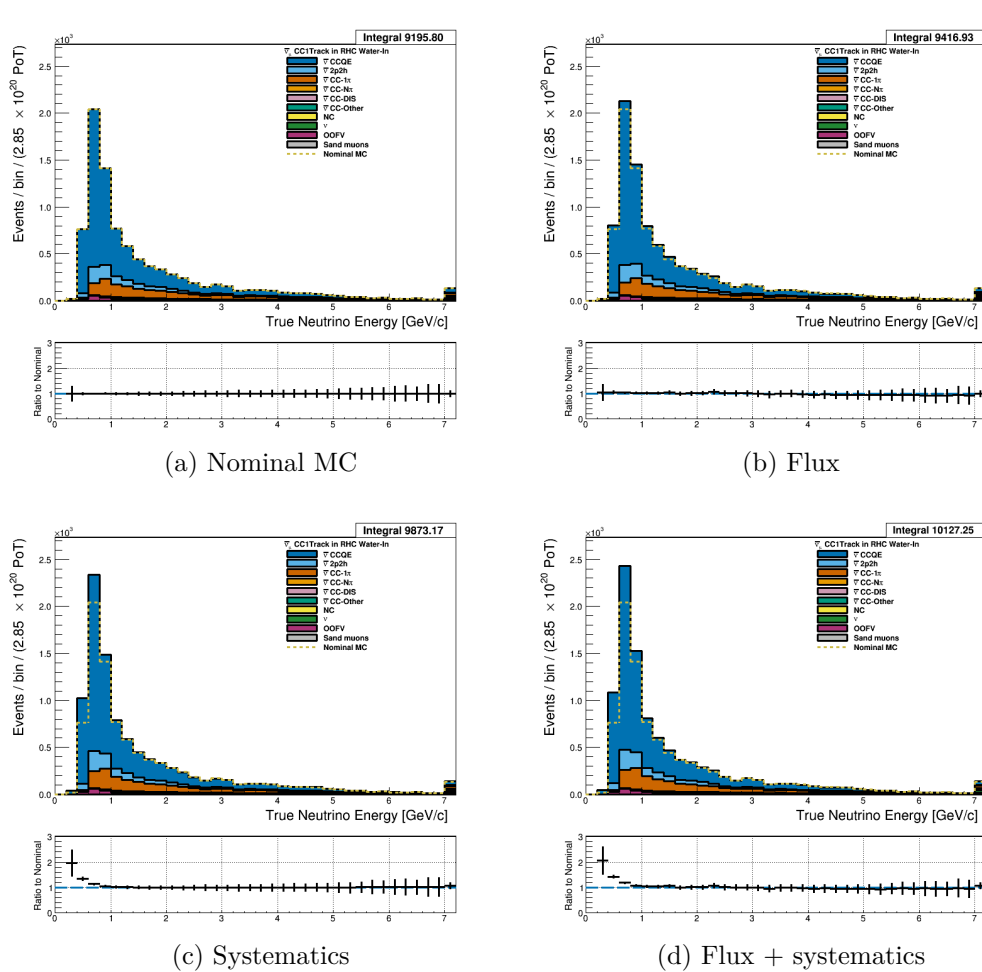


Figure 3.77: True neutrino energy associated with the lepton candidate separated by NEUT model interaction mode for RHC $\bar{\nu}_\mu$ CC 1-Track events occurring in the PØD in water-out mode. (a) The nominal MC prediction without any weights applied. (b) The flux tuning are applied. (c) The systematic weighting are applied. (d) Both flux and systematic weighting are applied.

556 **3.5.2.3 ν_μ Background Selection in RHC Mode:** Text

557 **3.5.3 CC N-Tracks (CCnQE Enhanced)**

558 Text

559 **3.5.3.1 ν_μ Selection in FHC Mode:** Text

560 **3.5.3.2 $\bar{\nu}_\mu$ Selection in RHC Mode:** Text

561 **3.5.3.3 ν_μ Background Selection in RHC Mode:** Text

562 **3.5.4 Differences Between Water-Out and Water-In Samples**

563 **4 PØD-Only BANFF Parameterization**

564 **4.1 PØD Samples Fit Binning**

565 The PØD ND280 BANFF fit uses the samples described in 3. The bin edges are tabulated
566 below.

- 567 • FHC ν_μ CC 1-Track bin edges:

568 p [GeV/c]: 0, 0.3, 0.4, 0.5, 0.6, 0.7, 0.8, 1, 1.25, 1.5, 2, 3, 4, 5.5, 30

569 $\cos\theta$: -1, 0.7, 0.8 , 0.88, 0.94, 0.96, 0.975, 0.99, 1

- 570 • FHC ν_μ CC N-Tracks bin edges:

571 p [GeV/c]: 0, 0.4, 0.5, 0.6, 0.7, 0.8, 1, 1.2, 1.5, 1.8, 2.2, 2.7, 3.5, 5, 10, 30

572 $\cos\theta$: -1, 0.65, 0.77, 0.85, 0.9, 0.94, 0.97, 0.99, 1

- 573 • RHC $\bar{\nu}_\mu$ CC 1-Track bin edges:

574 p [GeV/c]: 0, 0.4, 0.5, 0.6, 0.7, 0.8, 1, 1.25, 1.5, 2, 3, 30

575 $\cos\theta$: -1, 0.82, 0.87, 0.9, 0.93, 0.95, 0.97, 0.99, 1

- 576 • RHC $\bar{\nu}_\mu$ CC N-Tracks bin edges:

577 p [GeV/c]: 0, 0.5, 0.9, 1.25, 1.6, 2, 3, 8, 30

578 $\cos\theta$: -1, 0.8, 0.89, 0.95, 0.97, 0.99, 1

- 579 • RHC ν_μ CC 1-Track bin edges:

580 p [GeV/c]: 0, 0.4, 0.6, 0.8, 1.1, 2, 10

581 $\cos\theta$: -1, 0.78, 0.84, 0.89, 0.92, 0.95, 0.97, 0.98, 0.99, 1

- 582 • RHC ν_μ CC N-Tracks bin edges:

583 p [GeV/c]:0, 0.4, 0.6, 0.8, 1, 1.5, 2, 3, 10

584 $\cos\theta$: -1, 0.7, 0.8, 0.85, 0.9, 0.94, 0.965, 0.98, 0.99, 1

585 4.1.1 Fit Binning Determination

586 The fit binning is designed to optimized to ensure at least 1 predicted Monte Carlo (MC)
587 event in each bin when scaled to the collected data POT. The fit bins must also account
588 for detector smearing effects. In order to mitigate smearing and event migration, the recon-
589 structed kinematics were examined to their MC truth value using only correctly identified
590 leptons in one-dimensional kinematic slices. Since the MC provides about $10\times$ the data
591 statistics, the statistical uncertainty for each bin should be negligible for high statistics re-
592 gions. The kinematics are scanned across their full relevant spaces in order to understand the
593 needed width for a fit bin. The first fit bin is always defined from the kinematic maximum.

594 For the momentum bins, the momentum resolution is compared to MC truth . The
595 momentum resolution is defined as

$$R(r, t) = \frac{r - t}{t},$$

596 where r is the reconstructed momentum and t is the true value. The momentum was scanned
597 in finite bin widths with the mean and standard deviation of the resolution R extracted. The
598 mean and standard deviation are used as a proxy for the true bias and true resolution, re-
599 spectively. In addition, a bootstrapping algorithm was employed to understand the accuracy
600 of the sample estimates. Bootstrapping in this context is sampling over all relevant values
601 of true momentum and randomly replacing the values. For each scanned bin, at least 1000
602 bootstrapping sampling with replacement was performed. In the case of large variances in
603 the bootstrapping samples, additional 10000 sampling with replacement were performed.
604 The results for analyzing the FHC ν_μ CC 1-Track selection is shown in Figure 4.1 on page

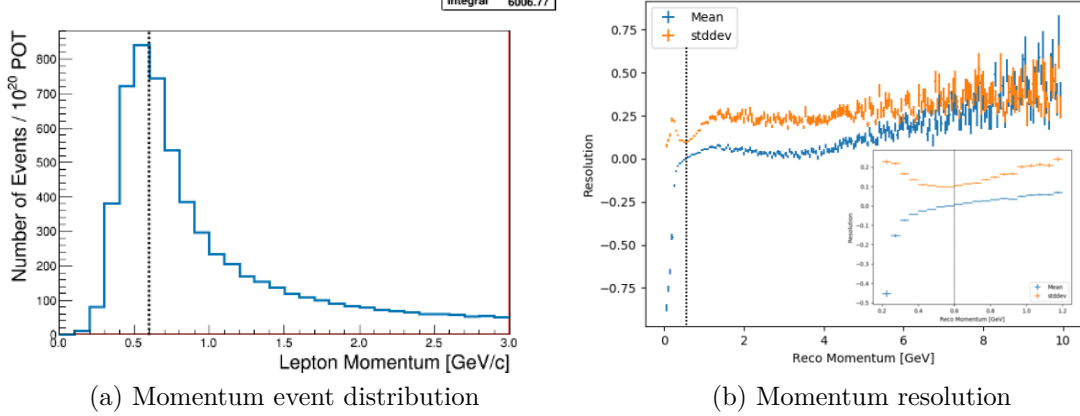


Figure 4.1: The momentum event distribution and uncertainty for FHC ν_μ CC 1-Track events is shown above. Only correctly identified muons are shown. (a) The number of events per unit momentum is scaled to 10^{20} POT which is the approximate scale for all the samples in this analysis. A dashed line indicates the maximum of the peak. (b) The resolution of the momentum measurement is shown for a wide region of momenta. In the inset is the resolution zoomed near the momentum distribution maximum. Like in (a), a dashed line shows the momentum maximum.

113.

The angle bins are treated in an almost identical manner. While the fit bins and physics parameterized in $\cos \theta$, the angle with respect to the z-axis, the detector smearing is a function of the angle θ . In addition, since the angle can be nearly zero for the most forward-going tracks, the resolution was not used to characterize the angular uncertainties. Instead, the difference between the true and reconstructed angle were analyzed as shown in . The mean and standard deviation were studied. Bootstrapping was again used to quantify the accuracy of the mean and standard deviation.

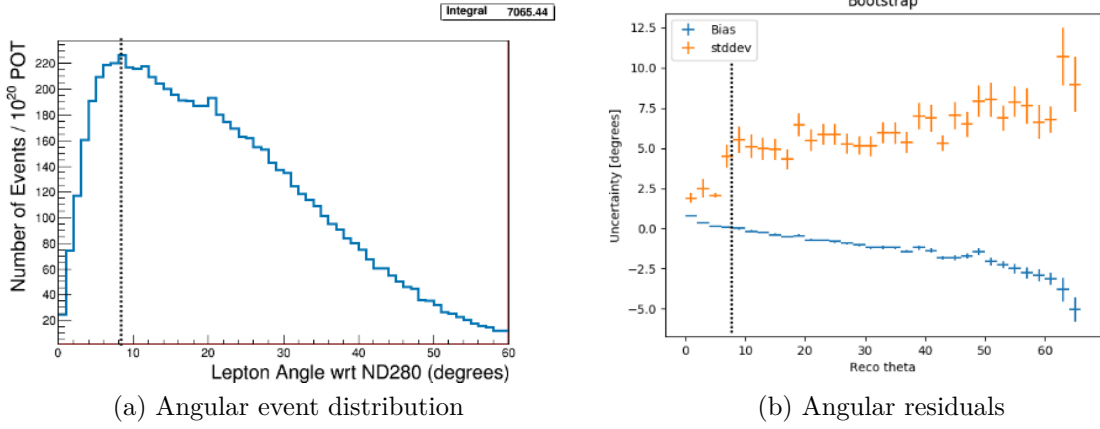


Figure 4.2: The angular event distribution and uncertainty for FHC ν_μ CC 1-Track events is shown above. Only correctly identified muons are shown. (a) The number of angular events is scaled to 10^{20} POT which is the approximate scale for all the samples in this analysis. A dashed line indicates the maximum of the peak. (b) The residual of the angular measurement is shown up to where there are sufficient statistics. Like in (a), a dashed line shows the momentum maximum.

613 **5 Detector Systematics**

614 Text goes here

615 **6 Fitter Validation**

616 Fitter validation

617

7 Fitter Results

618

Fitter results

619 **8 Discussion**

620 Discussion

621 **References**

- 622 [1] K. Abe et al. The T2K Experiment. *Nucl. Instrum. Meth.*, A659:106–135, 2011. 24
- 623 [2] S. Baker and R. D. Cousins. Clarification of the use of Chi-Square and Likelihood
624 Functions in Fits to Histograms. *Nucl. Instrum. Meth.*, A221:437–442, 1983. 16
- 625 [3] S. Bienstock et al. Assessing the effect of cross-section model uncertainties on the T2K
626 oscillation analyses with simulated data studies using the BANFF, MaCh3, P-Theta
627 and VALOR frameworks, May 2018. T2K-TN-331 v5. 14
- 628 [4] S. Bienstock and Others. Constraining the Flux and Cross Section Models with Data
629 from the ND280 Detector using FGD1 and FGD2 for the 2017 Joint Oscillation Analysis,
630 August 2017. T2K-TN-324 v3. 14, 21
- 631 [5] S. Bolognesi and Others. Niwg model and uncertainties for 2017 oscillation analysis,
632 April 2017. T2K-TN-315 v5. 21
- 633 [6] T. Campbell. Measurement of the ν_μ cc- 0π double differential cross section on water in
634 the pød, February 2018. T2K-TN-328. 23
- 635 [7] T. Campbell and Others. Analysis of ν_μ charged current inclusive events in the pød in
636 runs 1+2+3+4, Mar 2014. T2K-TN-80 v4. 23, 25, 26
- 637 [8] R. Das and Others. Measurement of induced charged current cross section on water
638 using the pød and tpc, November 2014. T2K-TN-100. 23
- 639 [9] K. Gilje. Geometry and mass of the π^0 detector in the nd280 basket, Apr 2012. T2K-
640 TN-73 v3.1. 26

- 641 [10] M. Hartz and Others. Constraining the flux and cross section models with data from
642 the nd280 detector for the 2014/15 oscillation analysis, May 2015. T2K-TN-220 v4. 14,
643 16
- 644 [11] M. Hartz and Others. Constraining the Flux and Cross Section Models with Data from
645 the ND280 Detector using FGD1 and FGD2 for the 2016 Joint Oscillation Analysis,
646 June 2016. T2K-TN-230 v3. 14
- 647 [12] A. Hillairet and Others. Nd280 reconstruction, Nov 2011. T2K-TN-72 v1. 26
- 648 [13] T. Koga. Comparison between banff post fit results and on-axis detectors, 2017. 10
- 649 [14] K. Mahn and Others. Implementation of new cross section parameters for the 2017
650 oscillation analysis, 2017. T2K-TN-307. 21
- 651 [15] G. Wikström and A. Finch. Global kalman vertexing in nd280, Feb 2018. T2K-TN-46
652 v3. 25
- 653 [16] T. Yuan and Others. Double differential measurement of the flux averaged ν_μ cc0pi
654 cross section on water, Aug 2016. T2K-TN-258 v4.6.1. 23, 25

655 **Nomenclature**

- 656 BANFF The **beam and near detector task force** is the group responsible for providing near
657 detector constraints on cross section and flux model parameters.
- 658 CC- 0π A **charged current zero pion selection** is an exclusive selection that selects neutrino
659 interaction topologies only one MIP-like particle.
- 660 CC-Inclusive A **charged current event selection** that selects all neutrino interaction topolo-
661 gies with an outgoing charged lepton.
- 662 FD The **far detector** refers to the particle detector in a long baseline neutrino oscilla-
663 tion experiment that is located far away from the neutrino production source where
664 oscillated neutrinos are observed.
- 665 FGD A **fine grain detector** is a detector made of closely spaced, small scintillating bars
666 designed to provide precise resolution of charged particle tracks
- 667 FHC The **forward horn current beam configuration** that focuses positively charged particles
668 into the particle decay pipe. This configuration produces a very pure ν_μ neutrino beam
- 669 HMNT The **highest momentum negatively-charged track** in the bunch
- 670 HMPT The **highest momentum positively-charged track** in the bunch
- 671 MIP A **minimum ionizing particle**
- 672 ND280 The **Near Detector** of T2K which is **280** meters away from the neutrino source.
- 673 ND The **near detector** refers to the particle detector in a long baseline neutrino oscillation
674 experiment that is located close to the neutrino production source before neutrino
675 oscillations occur.

676 CECal The Central **ECal** detector which is a part of the PØD inside ND280

677 PØD The π^0 detector (**pi-Q** detector)

678 PØDule A collection of two active scintillator bar layers inside the PØD

679 RHC The **reverse horn current** beam configuration that focuses negatively charged particles
680 into the particle decay pipe. This configuration produces a $\bar{\nu}_\mu$ enriched neutrino beam
681 with a significant ν_μ contribution.

682 FV The **fiducial volume** of a detector is the region where the detector response is well
683 understood

684 TPC A **time projection chamber** is a device that detects and tracks charged particles with
685 the application of strong electric fields

686 Tracker The region of ND280 consisting of two FGDs and TPCs

687 Global The **Global reconstruction module** responsible for making joined tracks between the
688 subdetectors inside ND280

689 USECal The **Upstream ECal** which is a part of the PØD inside ND280